The production and characterisation of cell-laden microparticles for bone tissue engineering

Luetchford, Kim

Award date:
2016

Awarding institution:
University of Bath

The production and characterisation of cell-laden microparticles for bone tissue engineering

Kimberley Anne Luetchford

A thesis submitted for the degree of Doctor of Philosophy

University of Bath

Department of Pharmacy and Pharmacology

March 2016

Table of Contents

Abstract

This work examines the use of a small number of naturally-derived materials as scaffolds, specifically for bone tissue engineering. Damaged bone is typically replaced with grafts, and second only to blood, bone is the most transplanted tissue [1]. The ability to produce autologous grafts from patients' own cells using an engineered scaffold would therefore be extremely valuable. This thesis reports the design and use of microparticle cell carriers for bone tissue engineering applications, as potential injectable or mouldable units.

The suitability of silk fibroin (SF) and gelatin (G) blends as biomaterials was tested in two-dimensional cultures, using 3T3 fibroblasts and rat MSCs (rMSCs). The blends (25:75, 50:50 and 75:25) were shown to be biocompatible and with appropriate mechanical properties for bone tissue engineering with Young's moduli between 36 and 59 MPa. The SF/G blends supported the osteodifferentiation of rMSCs at levels equivalent to tissue culture plastic. Although SF alone did not strongly support cell attachment, the cells that did adhere showed high levels of osteodifferentiation, measured by osteopontin expression. The inclusion of gelatin significantly improved cell attachment while retaining the ability of the SF/G blends to support osteodifferentiation. Novel microparticles were created from the same SF/G blends in a reproducible, controllable manner using a flow focussing device assembled from commercially available fittings. Cell behaviour on the 3D scaffolds mimicked the results observed on 2D films: cell adhesion was significantly improved by the addition of gelatin with the seeding efficiency of 3T3 fibroblasts increasing from 25% on SF microparticles to 69 – 81% on the blended microparticles. Osteogenic differentiation of rMSCs was observed on SF/G 25:75 microparticles in both basal and osteogenic medium, and osteopontin expression was shown to be slightly higher than for rMSCs grown on commercially available Cultispher-S microparticles. Although attempts were made to mould the particles into larger 3D structure, successful preliminary results could not be repeated.

Adapting the flow focussing device from liquid-liquid to a liquid-air system allowed the rapid production of oxidised alginate microparticles, blended with extracellular matrix proteins, and with encapsulated cells. These microparticle scaffolds were also shown to support cell viability (75% of rMSCs were viable after 7 days) and osteogenic differentiation. With the potential to easily encapsulate different proteins or ECM extracts, alginate-blended microparticles are potentially useful tools for culture of different cell types. Finally, the culture of microparticles within a hollow fibre bioreactor, with the hollow fibre mimicking blood capillaries, was shown to improve cell viability compared to a non-perfused control: 20 times more 3T3 fibroblasts were harvested from the bioreactor than from the control. This showed the potential for using the hollow fibre bioreactor to rapidly produce large, viable, tissue engineered constructs in vitro.

Acknowledgements

Firstly, I would like to thank my supervisors, Dr Paul De Bank and Prof. Julian Chaudhuri, for all their help, support, advice and of course, optimism. “There’s no reason it shouldn’t work!” will be ringing in my ears for some time yet. Secondly, I would like to acknowledge the Medical Research Council for the funding that has made it possible for me to take on a PhD.

The staff in the Microscopy and Analysis Suite, Ursula Potter, Adrian Rogers and John Mitchels, provided invaluable technical support and I am very grateful to them for it. The technical staff in both Pharmacy and Pharmacology and Chemical Engineering have always been generous with their time and without them keeping things running behind the scenes, my PhD would have been a great deal harder.

My time at Bath would not have been the same without the many friends I have made in the Department of Pharmacy and Pharmacology and my thanks go to all of you, old and new. Especially to Natalie and Mike, Jo, Helen, Amit, Liz, Alex, Nour, and Christopher, thank you.

Abbreviations & Nomenclature

2D	Two-dimensional
3D	Three-dimensional
AFM	Atomic force microscopy
ALP	Alkaline phosphatase
αMEM	Minimum Essential Medium Eagle, alpha modification
ANOVA	Analysis of Variance
BCA	Bicinchoninic acid
BMP-2	Bone morphogenic protein 2
DAPI	4',6-Diamidino-2-phenylindole
dH_2O	Distilled water
DMEM	Dulbecco's Modified Eagle Medium
DNA	Deoxyribonucleic acid
ECM	Extracellular matrix
EDC	1-Ethyl-3-(3-dimethylaminopropyl)carbodiimide
EDTA	Ethylenediaminetetraacetic acid
EDX	Energy dispersive X-ray spectroscopy
ELISA	Enzyme linked immunosorbent assay
Ex/Em	Excitation/Emission
FACS	Fluorescent activated cell sorting
FBS	Foetal bovine serum
FITC	Fluorescein isothiocyanate
H&E	Haematoxylin and Eosin
HFIP	Hexafluoroisopropanol
hMSC	Human mesenchymal stem cell

HMDS	Hexamethyldisilazane
HUVEC	Human umbilical vein endothelial cells
IBMX	3-Isobutyl-1-methylxanthine
IPA	2-Propanol
LV	Low viscosity
MEM	Minimum Essential Medium Eagle
MSBF	Modified simulated body fluid
MSC	Mesenchymal stem cell
MTS	3-(4,5-Dimethylthiazol-2-yl)-5-(3-carboxymethoxyphenyl)-2-(4-sulfophenyl)-2H-tetrazolium
MV	Medium viscosity
NBT/BCIP	Nitro-blue tetrazolium/5-bromo-4-chloro-3'-indolyphosphate
ODM	Osteogenic differentiation media
PE	Phycoerythrin
PBS	Phosphate buffered saline
PCR	Polymerase chain reaction
PEEK	Polyether ether ketone
PEG	Polyethylene glycol
PGA	Polyglycolic acid
PLA	Polylactic acid
PLGA	Polylactide-co-glycolide
PSM	Porcine skeletal muscle
PVDF	Polyvinylidene fluoride
Q_{inner}	Flow rate, inner
Q_{outer}	Flow rate, outer
REDV	Arginine - glutamic acid - aspartic acid - valine

RGD	Arginine - glycine - aspartic acid
rMSC	Rat mesenchymal stem cell
RPM	Revolutions per minute
RUNX2	Runt-related transcription factor 2
SD	Standard deviation
SDS	Sodium dodecyl sulphate
SDS-PAGE	Sodium dodecyl sulphate-polyacrylamide gel electrophoresis
SEM	Scanning electron microscopy
SF	Silk fibroin
SF/G	Silk fibroin/gelatin
SIS	Small intestinal submucosa
TCP	Tissue culture plastic
TGF-β1	Transforming growth factor, beta 1
UV	Ultraviolet

List of Figures

List of Tables

List of Equations

Chapter 1

Introduction

Within the field of tissue engineering, there is a lack of consensus about which materials are the most appropriate for cell scaffolds. In reality, since there is a wide range of target organs for tissue engineering products, it is unlikely that one material could fulfil all the requirements for all potential applications and thus investigation into a range of materials is justified. One of the primary decisions to make in choosing a scaffold material is between the use of synthetic and naturally-derived materials. It is now widely understood that cells grown in two-dimensional systems differ in morphology and behaviour to their *in vivo* counterparts. Investigation into three-dimensional scaffolds is therefore timely and important to produce physiologically relevant tissue engineering products.

While the composition of synthetic polymers can be finely controlled, materials of this type typically lack innate cell recognition sites which leads to poor cell attachment. On the other hand, naturally-derived polymers such as collagen are rich in cell attachment sites. Rather than attempting to best mimic the natural extracellular matrix (ECM) using synthetic materials, it seems logical to use materials that actually form the ECM in the first place, or at least those that closely resemble them. For example, collagen makes up 25% of the protein mass of most mammals, while alginate is a hydrophobic polysaccharide resembling hyaluronic acid (an important ECM glycosaminoglycan) in structure [2].

A second key decision is the design and construction of the scaffold itself. While it is possible to create scaffolds in a particular shape or of a specific size from the start, a more flexible approach is to build scaffolds from the bottom up, using small units such as microparticles. This allows for different scaffold materials or cell types to be built into the final product, mimicking the heterogeneity of endogenous tissues. Small scaffold units also have potential for use as injectable scaffolds, which could be delivered without the need for invasive surgery.

1.1. Thesis outline

Chapter 2 is a literature review of research into the requirements of scaffolds for use in tissue engineering and candidate materials for scaffold production. It covers scaffold design, cell sources, the formation of tissue engineering constructs, and the use of biomaterial scaffolds for the delivery of growth factors or other relevant biochemical signalling

molecules. At the end of this chapter, the aims and objectives of this thesis are set out. The third chapter reports the materials and methods used in the research carried out in this project.

The following chapters report results from the research performed. Chapter 4 describes the characterisation of silk fibroin and silk fibroin/gelatin blends as osteodifferentiation-supporting biomaterials, while Chapter 5 describes the translation of this work into a three-dimensional context. The work exploring decellularised materials and their use with alginate is reported in Chapter 6. The final results chapter, Chapter 7, describes the design and use of a custom hollow fibre bioreactor for the culture of cell laden microparticles and the production of a viable tissue construct.

Chapter 8, the final chapter, draws conclusions from the results described within this thesis, and includes suggestions for future work.

Chapter 2

Tissue engineering: natural materials, microparticles and bioreactors for the bottom up development of tissue constructs

Tissue engineering is a multidisciplinary field that combines biological and engineering perspectives to create functional substitutes for diseased or damaged tissue, or model tissues for *in vitro* testing. The field of regenerative medicine is more focussed on harnessing the body's ability to heal itself, with the help of therapeutic cells or growth factors where appropriate. The main focus of these fields are diseases or injuries where often the only treatment is whole organ transplant.

Organ transplants are overwhelmingly successful (97% of living donor kidney transplants function well after 1 year [3]) but problems arise when suitable donor organs are not available, which is a frequent issue. Additionally, the use of allograft organs always carries the risk of immune rejection. Tissue engineering aims to overcome these problems by building new organs or tissues essentially from scratch, using the patient's own cells and therefore removing both the need for a suitable donor and the use of immunosuppressant therapies post-transplant.

Figure 2.01 illustrates the simplified stages in this process. The first step consists of cell harvest though the cell type will vary with the intended product. The next stage is the expansion of cells in culture to produce a therapeutically relevant quantity, though again this is application dependent. For cells that are capable of significant proliferation *in vivo*, 10^6-10^7 cells may be sufficient, but for fully differentiated cells, or to produce a construct with a cell density equivalent to native tissue (~10^8 cells/cm^3) the number may easily reach 10^{10} [4, 5]. These numbers render traditional two-dimensional flask-based culture deeply impractical both in terms of the space the flasks would require and the time it would take to manually culture them. Alternative cell expansion systems such as stirred tank bioreactors or packed bed systems must therefore be considered. Once a suitable number of cells is obtained, the cells are seeded onto or encapsulated within a scaffold. The scaffold must be appropriate to the target tissue in terms of its structure, strength, flexibility and biodegradability.

This review will focus on ideal scaffold properties and candidate materials, with particular reference to microparticle scaffolds. Other key considerations of the tissue engineering process, such as potential cell sources and bioreactor systems, will also be discussed.

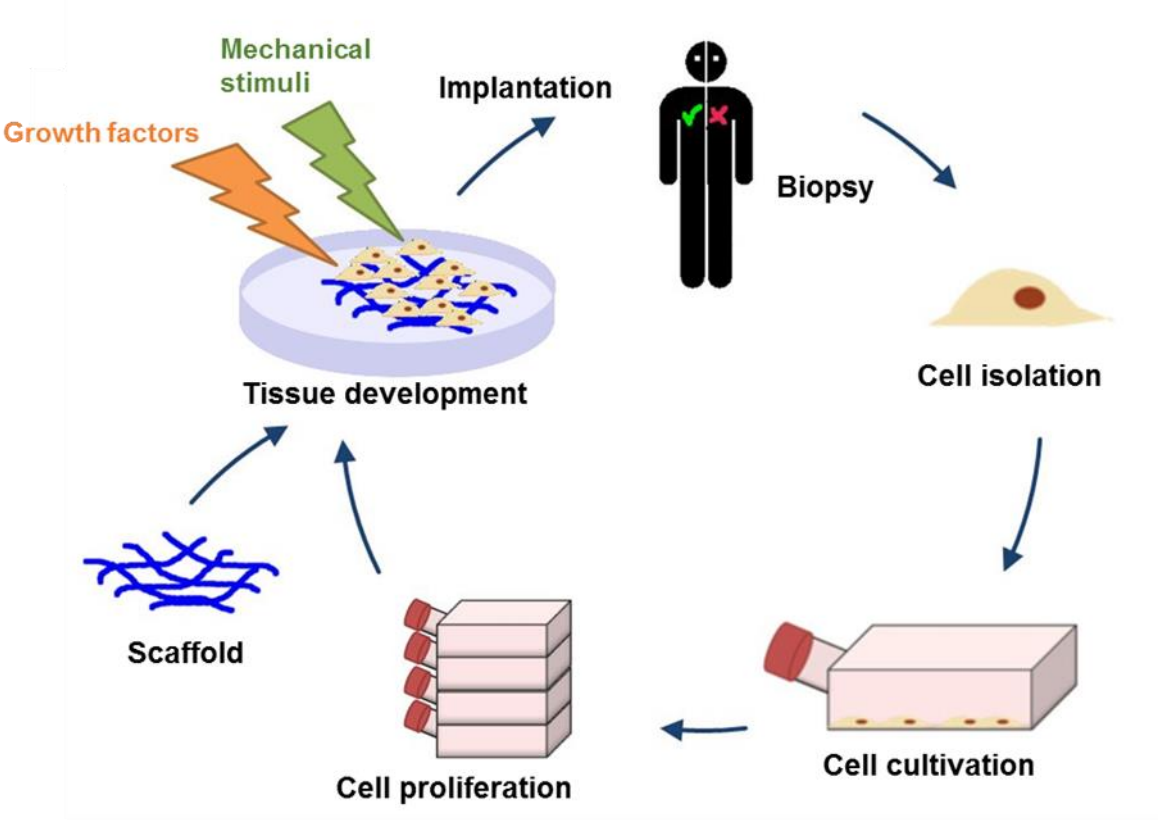

Figure 2.01: Schematic of the key stages necessary to create an autologous transplant. Cells are harvested from a patient, isolated and expanded in culture before maturation on an appropriate scaffold, primed with chemical and mechanical stimuli. The tissue or organ construct is implanted into the patient to repair their damaged or diseased tissue. © HIA/ Wikimedia Commons [6].

2.1. Cell sources for bone tissue engineering

The choice of cell for a given tissue engineering application is determined primarily by the target tissue, followed by the availability of each cell type. These criteria also affect the choice between autologous or allogeneic cells. The cells chosen must be available in a sufficient quantity or capable of substantial proliferation while maintaining their phenotype. The cells must remain biologically functional, and be able to lay down new extracellular matrix and interact with the scaffold and neighbouring cells through the release of cytokines or growth factors [7].

While the use of mature primary cells may seem an attractive prospect for autologous transplant, primary cells often de-differentiate *ex vivo* and have limited potential for proliferation. For example, articular chondrocytes have a tendency to produce fibrocartilage instead of hyaline cartilage during cultivation [8]. There are also cell types, such as spinal cord neurons, which are not suitable for patient harvest due to the loss of function at the donor site. Autologous bone grafts are possible but limited by the amount or volume of bone

that can be removed from a donor site (e.g. the iliac crest). Primary cells therefore have limited use in tissue engineering.

Immortalized cell lines typically have much greater proliferative potential than primary cells and are useful tools for *in vitro* experiments and investigations. However, their proliferative nature is often due to the fact they are derived from tumours, or have been genetically modified to allow their continued proliferation. They are unsuitable for transplantation into patients but remain a valuable resource for research.

Embryonic stem cells (ESCs), derived from the inner cell mass of blastocysts, are a pluripotent cell source, capable of differentiation to all mature cell types. Cultured *in vitro*, hESCs were traditionally grown on top of a feeder layer of mouse fibroblasts to maintain their capacity for self-renewal, but it was found cells cultured in this way expressed a non-human protein [9]. These cells would therefore be susceptible to immunogenic attack after implantation. Animal-product or xeno- free conditions have since been established for the culture of hESCs [10, 11]. The ESCs would need to be matched to individual patients to avoid immunogenic rejection and differentiation tightly controlled to prevent the formation of teratocarcinomas. However, it is the moral and ethical debate on the destruction of embryos to produce ESCs that is most likely to hinder their use as a potential cell source for therapeutic applications [7, 12].

A more promising candidate cell type for bone tissue engineering is the adult mesenchymal stem cell (MSC). These cells are found in many adult tissues, where they exist in an undifferentiated state, capable of undergoing multi-lineage differentiation in order to repair damaged and aging tissues. They may differentiate into connective tissue cells, including bone, cartilage, muscle and fat [13]. Bone marrow was the first known source of MSCs, though obtaining bone marrow samples for clinical use necessitates an invasive procedure performed under general anaesthetic [14]. In the case of an autologous transplant, this results in further pain for the patient with the risk of donor site morbidity. Cell numbers obtained from bone marrow may also be low, and so other cell sources were investigated. Of particular interest are adipose-derived stem cells, which are harvested from lipoaspirate (which would normally be discarded after liposuction surgery) [15]. Like bone marrow derived MSCs, adipose-derived stem cells may undergo osteogenic, adipogenic, myogenic or chondrogenic differentiation in response to appropriate culture conditions. Adipose-derived stem cells show huge potential within the field of tissue engineering, and have been shown to form greater numbers of colonies and have higher proliferative capacities than bone marrow-derived MSCs [14-16].

2.2. Scaffolds in tissue engineering

Key among the challenges of tissue engineering are the problems of finding an appropriate cell scaffold, and also of vascularisation – how to engineer an artificial blood supply within a tissue construct to supply cells with nutrients and oxygen. *In vivo* the maximum distance between capillaries is 200 µm (correlating to the diffusion limit of oxygen), and so engineered tissues must contain a network equivalent to this in order to maintain cell viability and prevent necrosis [17].

In order to create a viable tissue construct in the first place, cells must be provided with a suitable scaffold to mimic the *in vivo* three-dimensional extracellular matrix (ECM). The ECM provides physical support for cell attachment as well as influencing cell migration, proliferation, differentiation, and cell-cell communication [18]. Composed of collagens, proteoglycans and glycoproteins, the ECM also acts as a reservoir for growth factors and cytokines [19]. As the cells can receive signals and biological cues from the ECM, they can also rearrange and remodel the ECM around themselves. In bone, osteoblasts create the ECM which is composed largely of dense type 1 collagen mineralised with hydroxyapatite as well as proteins such as osteopontin, a calcium-binding protein, and osteonectin, which anchors hydroxyapatite to collagen fibres [20].

For the development of an artificial scaffold, Agrawal et al. identified ten key properties it should possess [21]:

> "*1. The scaffold should be biocompatible.*
>
> *2. It should be biodegradable or capable of being remodelled.*
>
> *3. It should biodegrade in tune with the repair or regeneration process.*
>
> *4. It should be very porous.*
>
> *5. It should be highly permeable to allow for proper diffusion.*
>
> *6. It should have the correct pore size for the candidate cells.*
>
> *7. It should possess adequate mechanical properties to provide the correct microstress environment for cells.*
>
> *8. It should provide a surface conducive for cell attachment.*
>
> *9. It should encourage the formation of ECM by promoting cellular functions.*
>
> *10. It should possess the ability to carry biomolecular signals such as growth factors*."

While biocompatibility is a property intrinsic to a material, many of the other properties listed here will depend on the processing steps and final form of the scaffold itself. Thus in choosing a potential scaffold material, biocompatibility should be assessed primarily, and design of the scaffold optimised to fit as many of these ideal criteria as possible.

2.2.1. Promoting cell adhesion & encapsulation

While an advantage of using naturally-derived materials over synthetic polymers is that they are often cell adhesive, this is not always the case. For example, although alginate is biocompatible, it does not support cell attachment and must be modified in order to facilitate this [22]. As stated previously, an ideal cell scaffold would be capable of promoting cell adhesion, possibly with the ability to recruit specific cell types.

If the material is not naturally cell adhesive, cell attachment can be improved through surface modification of the scaffold, for example with the amino acid sequence arginine - glycine - aspartic acid (RGD) [23]. Integrins are cell surface proteins that mediate cell adherence to the ECM, and the RGD sequence is a key component of the integrin-binding protein. This sequence accounts for the high level of cell adhesion to materials such as collagen and gelatin [24].

There are cell-specific peptide motifs that can be used to target a particular cell type, such as the arginine-glutamic acid-aspartic acid-valine (REDV) sequence, which endothelial cells selectively adhere to [25]. Alternatively the use of bound antibodies targeting specific cell surface markers can be used to selectively bind a certain cell type to the scaffold [26]. Directing specific cell adhesion in this way could allow for the development of highly organised cell/scaffold constructs. However, it would be preferable to work with a material requiring minimal improvements, especially to avoid expensive antibody modifications.

A simple alternative to chemically modifying a non-adhesive material is to blend it with a material that does promote cell adhesion. To use the same examples, alginate can be blended with collagen to produce a scaffold that combines the properties of both [27-29]. While alginate allows for the rapid formation of a stable hydrogel in a non-temperature dependent manner, collagen supports cell adhesion and growth.

An alternative approach to create a more homogenous cell distribution is to encapsulate cells within the scaffold itself. Initially investigated as an immunoprotective barrier for transplanted cells producing therapeutic proteins, cell encapsulation has since been recognised as a useful method for tissue regeneration applications [22]. Cells encapsulated

in gels are considered to be in a more realistic 3D environment and show improved functional behaviour [30, 31]. This is in comparison to cells grown on sponge-like scaffolds, where the cells are in three dimensions with respect to each other but are only attached to the scaffold in a two-dimensional manner [22]. Hydrogels (e.g. collagen, gelatin, alginate) are particularly well suited for cell encapsulation as they provide a highly hydrated tissue-like environment, are easily handled, and can form in mild, biologically-compatible conditions [32].

2.2.2. Scaffold strength & biodegradability

The mechanical properties of the scaffold are important and the elasticity, toughness and strength of a scaffold should match that of the target tissue. A scaffold designed to replace or repair injured bone must obviously be strong enough to bear the same loads as the native tissue, whereas a soft tissue scaffold does not have the same mechanical requirements. The strength of a scaffold can be affected by its structure and processing – a highly cross-linked structure will be stronger than a less cross-linked version. Scaffold elasticity is also relevant at a cellular level – this property can strongly influence cell behaviour. Engler et al. showed that MSCs grown on substrates with different elastic constants differentiated to distinct lineages. MSCs cultured on gels with a stiffness of 25-40 kPa, designed to mimic the stiffness of osteoids, were shown to develop an osteoblastic phenotype, while MSCs grown on substrates with a softer elasticity of 10 kPa favoured a myogenic pathway. The ability of cells to sense the stiffness of their microenvironment is thought to be mediated by non-muscle myosin II isoforms, which apply tension to cortical actin structures linked to focal adhesions [33].

The biodegradability of a scaffold is also an important consideration. Within tissue engineering, most scaffolds are created with the intention of allowing cells to lay down and remodel native matrix to replace the artificial scaffold over time. The implanted scaffold should support initial cell growth and provide structural support, but degrade at a rate equivalent to the production of new ECM. The products of biodegradation should be carefully considered, since the release of any toxic or harmful moieties will obviously prove detrimental to the healing and recovery process. While naturally-derived materials are generally subject to enzymatic biodegradation *in vivo* (collagen is susceptible to the action of matrix metalloproteinases [34]), many synthetic materials will not degrade under physiological conditions, or if they do, may release acidic breakdown products which negatively affect biocompatibility [35, 36].

In bone, degradation of a substitute matrix occurs by both physicochemical degradation and osteoclast-mediated resorption Osteoclasts play a role in natural bone remodelling, through acidification and proteolysis of the bone ECM. Their effects on biomaterial degradation is strongly influenced by the biomaterial composition, and to a lesser extent, properties such as crystallinity, density and surface topography [37, 38].

2.2.3. Growth factor release and delivery

As well as supporting long term cell growth, the potential of a scaffold to deliver relevant proteins, growth factors or even drug compounds would prove useful [39]. Growth factors can be incorporated into scaffolds to direct cell differentiation or growth [23, 40]. The scaffold can act as a reservoir for the compound in question, to provide steady release over a period of time throughout the entire structure [41]. Combining a scaffold with drug delivery functionality could prove a highly efficient approach to improve scaffold integration *in vivo* by directing cells to angiogenesis or by attracting resident cell populations to the site of the implant.

2.2.4. Scaffold structure design

Scaffolds used for adherent cell culture traditionally consist of a relatively large porous structure, designed in a particular shape or configuration. However, it can be difficult to ensure cells are distributed evenly throughout the scaffold and to maintain viability in order to produce a cell-dense, mature tissue [42]. Without perfusion of media, scaffolds of this type can frequently develop necrotic central regions as cells seeded within the inner areas are starved of oxygen and nutrients while waste products accumulate.

In recent years, modular or ‘bottom up’ approaches have emerged as a viable alternative to these ‘top down’ preformed scaffolds. Starting with small units of scaffold, cells can either be evenly seeded on the surface of the material or encapsulated within it. Most tissues consist of small, repeating functional units organised in three dimensions. Microparticle cell carriers, previously used for scaling up the production of anchorage-dependent cells are an example of an alternative scaffold structure that can mimic this arrangement. Once seeded, cell-laden microparticles can be physically moulded into a larger, complex structure with cells evenly spread throughout the entire volume. Using small building blocks theoretically

allows for precise control of combinations of different cell types or even scaffold types, in order to replicate native tissue architectures.

Constructs created in this manner still suffer from the lack of defined vasculature, meaning that over time central areas will become necrotic. An ideal system would be a construct created with an integrated pseudo-vasculature to allow the perfusion of media through the structure, maintaining cell viability during cell proliferation and construct maturation. Once implanted *in vivo* this pseudo-vasculature could undergo anastomosis with the host vasculature to integrate with the native tissue.

2.2.5. Microparticle cell carriers as scaffolds

As discussed, microparticle cell carriers provide an alternative to the more traditional top down scaffold-based approach to tissue fabrication. Cells can be encapsulated within carriers, seeded on them after formation, or indeed both. A bottom up approach can be used to assemble the particles into larger, more complex structures, with cells distributed evenly throughout.

Both biopolymers and synthetic polymers have been used to create bead-like microparticles [30, 43]. Growing cells on microparticles, either as a monolayer on the surface or as multilayers within a porous structure, allows high yields of up to 2 million cells per millilitre [44]. A microparticle system may therefore allow both the expansion of cells to a therapeutically relevant quantity, and the creation of a tissue construct. Minimising the number of steps in the overall process could prove highly beneficial, especially if it removes the need to detach and re-attach cells to different matrices.

The term ‘microparticle’ is typically used to describe particles of 100-500 μm (commercial microparticles are in the range of approximately 100-300 μm). The smaller the microparticles, the larger the surface area for a given volume, therefore increasing the area available for cell adhesion. Microparticles are typically used in stirred suspension cultures, while for fluidised and fixed bed bioreactors, larger particles (0.6-5 mm) are more commonly used due to their higher sedimentation rate. Particularly in fixed bed reactors, larger particles are preferred as they give larger channels for media delivery between individual particles that are less likely to become blocked by cell growth [45].

A narrow size distribution of carriers is desirable to maximise homogeneity of culture conditions. This ensures cells are experiencing the same environment, which could otherwise vary dramatically between different sized carriers as a result of surface curvature.

The size of polylactide-co-glycolide (PLGA) microparticles has been shown to affect the proliferation and differentiation of rabbit MSCs [46]. However, commercially available carriers often show significant variation in particle size: Cultispher-S carriers (Percell) are described as ranging from 130 – 380 μm [47].

Cell expansion on microparticles

Cells are seeded onto microparticles in suspension cultures, often in spinner flasks [48]. Alternative systems include rotating wall vessel bioreactors and perfusion cultures. Rotating wall systems have been shown to provide a low fluid shear environment which allows cell aggregates to form based on natural cell affinities, producing differentiated tissues [49], though more specific equipment is required for this system. Other systems for the culture of cell-laden microparticles include packed beds, though these may suffer from poor oxygen transfer, and fluidized beds, with improved oxygen transfer, but both of these approaches are more suitable for the manufacture of a secreted product than for cell expansion.

Macroporous beads allow the cells to attach within the bead itself. These cells are shielded from the shear stresses that externally seeded cells are exposed to in suspension cultures. Macroporous beads can deliver higher cell densities than solid beads. The average cell has a diameter of 10 μm and pores larger than this allow for cell invasion into the particle interior. Microparticles may also be meso- or microporous (pores less than 50 nm), meaning that molecules and media can diffuse through the particles themselves.

For scaling up cell numbers, it is easiest to grow the cells on the surface of the beads so they are easier to harvest. However, for tissue engineering applications it might be desirable to encapsulate cells within the beads as well as on the surface to produce a more homogenous cell distribution.

Production of microparticles

Different methods of producing microparticles exist and the most appropriate will depend on the material used as well as the desired properties (e.g. size, porosity) [50]. The advantages and disadvantages of several possible methods are described below.

One method of microparticle production is the emulsion of two immiscible solutions. Commonly a hydrogel precursor would be in an aqueous solution, and stirring or homogenisation causes this to emulsify within a hydrophobic oil phase, producing a suspension of hydrogel microparticles. Depending on the material, the microparticles may

stabilise into solid structures as a result of temperature change or chemical cross-linking. Size control of the particles is achieved by altering the viscosity of the solutions and the stirring rate (i.e. shear rate), though control is limited. This approach can be easily scaled up but the particles produced in this way have a wide size distribution [50].

Unlike emulsification, photolithography provides a high degree of control over the size and shape of the final microparticles. In this system, a hydrogel precursor is mixed with a photo-initiator. Upon exposure to ultraviolet light, the photo-initiator catalyses cross-linking of the hydrogel to produce a solid structure. To create microparticles in this way, Dendukuri et al. generated a system in which their polymer/photo-initiator solution flowed through a microfluidic channel fitted with a photo-mask with cut-outs in the shape of the desired particles. Ultraviolet light was shone through the mask to produce hydrogels in a variety of shapes and sizes in a continuous flow process [51]. Though this is a highly controllable method, photo-initiators are often cytotoxic, limiting the use of this technique for cell encapsulation, and are more typically run as batch processes.

While techniques such as spray-drying and emulsification are effective methods for particle production, the size distribution of the resultant particles is often large [52]. Microfluidic approaches, however, have been shown to generate particles with a much narrower distribution [53]. Systems of this sort consist of two immiscible co-flowing streams, and utilise the predictable break-up of these streams to produce homogenous, discrete droplets. Using a polymer solution as the disperse phase allows the production of microparticles. Alternatively, an air flow can be used to disrupt the disperse phase instead of a secondary liquid.

In a typical flow-focussing system, the continuous flow consists of an oil, while the disperse flow is an aqueous (bio-) polymer solution. The polymer solution is directed into the faster flowing oil phase, causing the shear forces of the oil flow to pull out droplets of the polymer from its source. The flow rates are adjusted to a level and ratio at which the inner fluid forms droplets, rather than a jet of fluid. Drop formation is a balance between the viscous drag of the outer fluid pulling on the nascent droplet and surface tension [54]. Cross-linking the droplets produces solid microparticle spheres. The size of the particles can be altered with the flow rate ratio of the two phases allowing easy control over particle diameter in a continuous process [50, 55].

Microparticles as building blocks for tissue engineering

The use of microparticles to expand cell populations produces ready-made building blocks for a bottom up approach to tissue construct fabrication, and removes the need to harvest cells from the microparticles before further processing. Cell-laden microparticles may form aggregates in suspension cultures through cell-cell, cell-ECM or cell-scaffold interactions, but to create larger macroscopic constructs moulds are frequently employed. This process is summarised in Figure 2.02. This approach has been used by Matsunaga et al. to create a macroscopic tissue construct from atelocollagen microparticles in a custom mould. Though the resultant construct was only several millimetres in size, this demonstrated the flexibility of the approach and the ability to incorporate different cell types as co-cultures within the structure [30]. Taking the process another step further, Twal et al. moulded cell-laden Cultispher-G microparticles into small ring structures which were then stacked to produce a tube. Cellular bridges fused the component rings together [56].

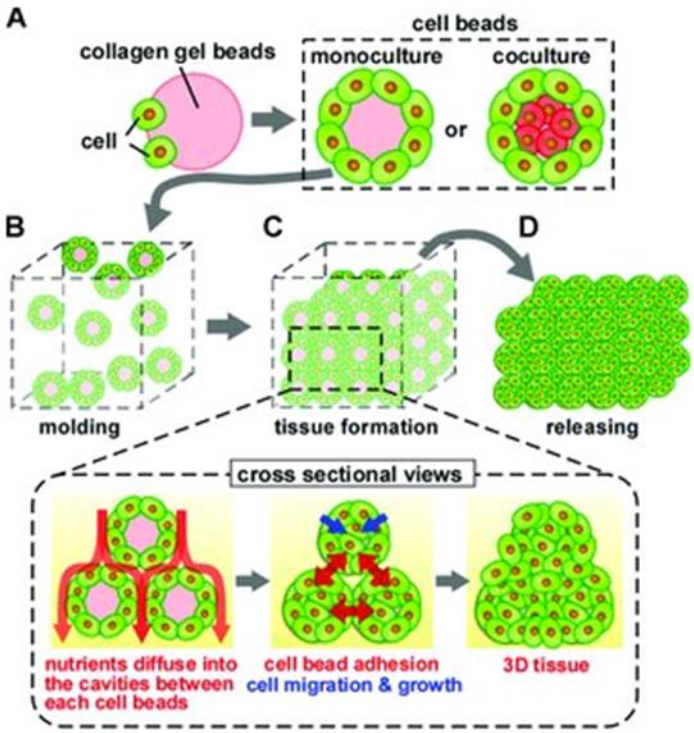

Figure 2.02: Assembling cell-laden microparticles into a 3D tissue. (A) Cells are seeded onto, or encapsulated within, hydrogel beads. (B) The cell carriers are assembled within a small mould, and (C) cells on adjacent beads form cell-cell attachments, creating a homogenous tissue construct. (D) The three-dimensional construct can be released from the mould whilst retaining its shape. Figure reproduced from Matsunaga et al. [30], © 2011 WILEY-VCH Verlag GmbH & Co. KGaA, Weinheim. Reprinted by permission of John Wiley and Sons, Inc.

While the constructs above were simply incubated in static conditions following formation, Chen et al. packed gelatin Cultispher-S particles, seeded with human amniotic MSCs, into a perfusion culture system [57]. This produced a centimetre-sized bone construct, but the osteogenic differentiation of the cells within the construct was affected by the relative stresses experienced in different regions of the perfused chamber. In long term cultures however, the same group observed cell death in the inner regions of the construct. This is likely due to a dense cell layer on the outer surface of the structure preventing efficient oxygen perfusion. To overcome this, the perfusion chamber, acting as a mould, was fitted with glass rods (1 mm diameter) which were removed after the construct formation to leave microchannels through the structure. This allowed for better nutrient/oxygen delivery to central regions of the construct. However, this was a proof of concept for cell viability using Cytopore-2 carriers and fibroblasts, so the ability of this scaffold format to support differentiation or the culture of a clinically relevant cell type was not investigated [58]. In addition, the use of commercially available microparticles, though convenient, raises questions about the production and cross-linking protocol used, proprietary information which would be valuable in establishing the suitability of these scaffolds for *in vivo* use. Commonly used gelatin cross-linking agents like glutaraldehyde are toxic, and can leach out from scaffolds during degradation [59].

2.3. Material choices

Naturally-derived biopolymers have found widespread use as scaffolds for cell culture. Commonly used biopolymers include collagen and hyaluronic acid, which are natural components of the ECM, as well as agarose, alginate, fibrin and gelatin. Silk fibroin is another naturally-derived polymer that is suitable for use in cell scaffolds [60, 61]. Generally, natural materials of this type have high biocompatibility and bioactivity. Their mechanical properties and biodegradation rates can be tuned through varying concentrations and levels of cross-linking. These materials are generally processed using environmentally-friendly aqueous-based protocols, and their degradation products are not cytotoxic [62].

Though synthetic polymers, such as polylactic acid (PLA) and polyglycolic acid (PGA), are also biocompatible, these materials are not generally as cell adhesive as naturally-derived materials and require modification to correct this. Though they can be fabricated into different architectures, synthetic materials generally form stiff structures which may be useful for load-bearing applications but less so for soft tissue engineering [63]. In addition, the synthesis of these materials can require extensive processing using organic solvents,

which can negatively impact biocompatibility if not fully removed. For these reasons, this section will concentrate on a small selection of naturally-derived materials.

2.3.1. Mulberry silk fibroin

Silk fibres have a long history of use in biomedical applications: for hundreds of years silk was used as suture thread. As a material, it is lightweight, elastic and thermally stable, as well as biocompatible [61]. Silk is produced on a large scale by the textile industry, so there are many sources available at a reasonable cost, and as it is insect-derived, it avoids the bioburdens potentially associated with mammalian-derived materials.

Mulberry silk, collected from the cocoon of *Bombyx mori*, the domesticated silkworm, accounts for 90% of international silk production [64]. Tussah silk, eri silk, and muga silk are also widely produced, and are collected from different species of silkworm, summarised in Table 2.01.

Table 2.01: Summary of silkworm species and silk types produced [64].

Silkworm species	Silk produced	Country of origin
Bombyx mori	Mulberry	China
Nangnoi srisaket	Mulberry	Thailand
Antheraea yamamai	Tussah	Japan
Antheraea pernyi	Tussah	China
Philisamia ricini	Eri	China, Korea
Antheraea assamensis	Muga	India

These different silks have different amino acid sequences: *Bombyx mori* SF has a higher proportion of glycine, while *Antheraea pernyi* SF has more acidic and basic amino acid residues. These differences can result in varied levels of biocompatibility, biodegradability and solubility [65, 66]. Most investigations of silk as a biomaterial have used *Bombyx mori*-derived silk, and unless otherwise specified, references to silk or SF within this thesis denote

Bombyx mori products. However, it is estimated there are more than 3,000 different strains of *Bombyx mori* alone [67]. It is possible that silks collected from different strains could have variations in their properties as a result of amino acid sequence deviations.

Native silkworm silk consists of two fibroin brins encased in a coat of glue-like sericin proteins, as shown in Figure 2.03. A number of studies have identified sericin as being responsible for adverse hypersensitivity reactions to silk, and so it must be removed from the fibroin before use as a biomaterial [68]. To remove immunogenic sericin, native silk is 'de-gummed' by boiling in sodium carbonate, then washed. The regenerated SF may be further processed into hydrogels, non-woven micro-fibrous nets, mats or membranes, sponges, tubes, microspheres, and fibres. This wide range of potential formats means silk can be used for a variety of applications [69]. SF is characterised as a natural block copolymer, consisting of ordered hydrophobic blocks which tend to form β-sheets or crystals, combined with less ordered hydrophilic blocks [61]. In *Bombyx mori* SF, the β-sheet regions are composed of glycine-alanine repeats, while in *Antheraea pernyi* they are primarily alanine repeats [65]. The high glycine content allows for tight β-sheet packing, which in turn provides a rigid structure to the material [70].

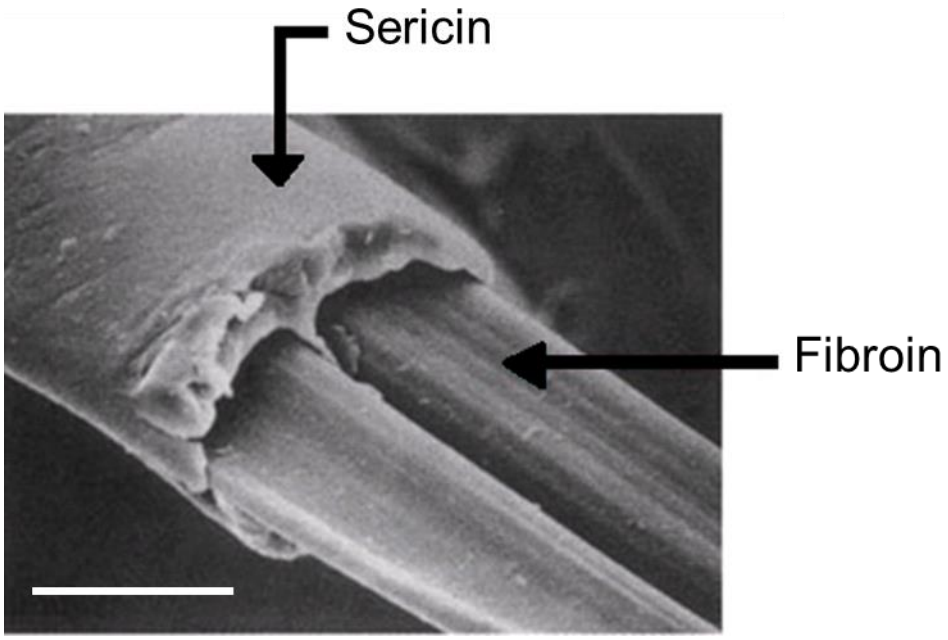

Figure 2.03: SEM image of an untreated silk fibre. The fibroin forms two filaments, held together by the gummy sericin. A *Bombyx mori* silk fibre is typically triangular in shape. The mean of the base and height of the triangle is reported to be 12.9 μm [71]. Image reproduced from [72]. Scale bar represents 10 μm.

The biocompatibility of silk films is comparable to that of collagen films and smaller inflammatory responses have been observed for implanted silk films than collagen or PLA

in vivo [68, 73]. Coating polymer scaffolds with SF, and incorporating SF within a scaffold, have been shown to improve cell-scaffold interactions [61, 74]. The carboxy-terminal region of *Bombyx mori* SF is basic and arginine-rich, and hence positively charged. This results in favourable electrostatic interactions with cells (negatively charged due to sialic acid residues on the cell surface) [75]. The variety of processing techniques can result in SF scaffolds with a range of mechanical properties, appropriate to different applications. SF scaffolds have been used for both ligament engineering, as silk fibre cords, and for soft tissue engineering, as freeze-gelled scaffolds [76, 77]. Meinel et al. demonstrated that human MSCs (hMSCs) on salt-leeched porous 3D silk scaffolds showed higher levels of attachment, proliferation and metabolic activity than those on equivalent collagen scaffolds. The extent of chondrogenesis (measured by the deposition of sulphated glycosaminoglycans) in this model was greater on the silk scaffolds over the 4 week investigation, possibly due to the slower degradation rate of the silk relative to the collagen [78].

SF degrades slowly, and although silk sutures are defined as non-degradable by the US Pharmacopeia, they are actually proteolytically degraded over months and years due to a foreign body response. They are susceptible to macrophage-produced chymotrypsin and protease cocktails. SF is degraded to its component peptides and amino acids which can be metabolised *in vivo*, such that the products of degradation cause no toxicity [79]. The rate of absorption of sutures depends on a range of variables, including the health of the patient and alterations to the silk protein structure as a result of processing [68]. The β-sheet content of the processed silk affects the rate of degradation so that the higher the content, the slower the degradation. It has been shown that the rate of silk scaffold degradation affected the metabolism of hMSCs and the rate of osteogenesis *in vitro*, such that more rapid degradation supported increased osteogenesis [80].

The properties of SF can also be modified by combination with other materials, such as starch, chitosan and synthetic polymers [74, 81-83]. This can improve the stability, biocompatibility and cell adhesion to the resultant material, producing a final material with better characteristics than each component part [65]. Mixing SF with collagen or gelatin has been shown to produce final scaffolds with higher compressive moduli than the pure protein controls: in the case of freeze-dried sponges this has been attributed to thicker pore walls and a more homogenous pore distribution [84, 85]. Collagen and gelatin are also strongly cell adhesive and therefore their inclusion can improve this property of SF blended materials [84, 86, 87]. For example, Moisenovich et al. proposed a SF/hydroxyapatite/gelatin blend as a bone tissue engineering scaffold, having observed higher fibroblast proliferation on these scaffolds compared to SF alone. Similarly, the polysaccharide chitosan has been

blended with SF to provide scaffolds more cell adhesive than SF alone, and with improved osteoinductive properties as shown by the enhanced osteodifferentiation of bone marrow MSCs [88, 89].

By the criteria listed in Section 2.2, SF shows a great deal of potential as a scaffold material it is biocompatible, biodegradable, cell-adhesive, and its mechanical properties can be varied by its final format, of which a variety are possible.

2.3.2. Alginate

Alginate is a polysaccharide isolated from brown algae, and is composed of a mixture of β-D-mannuronic acid and α-L-guluronic acid residues, though the ratio between the two can vary. Alginate forms a hydrocolloid in an aqueous medium, and gelation is induced by the presence of divalent cations (e.g. Ca^{2+}, Ba^{2+}). The cations form an electrostatic interaction between the guluronic carboxylic acid residues. Alginate is not cell adhesive but modification with RGD residues, or blending with cell-adhesive materials, can improve this [22]. Alginate has been widely used for cell encapsulation, and stem cell encapsulation in strontium cross-linked alginate has been investigated as a short term alternative to cryopreservation [90].

Traditionally divalent calcium ions have been used to cross-link alginate into a hydrogel for biological purposes but the resultant gels are susceptible to attack by chelating agents, including phosphate. On top of this, non-gelling ions like sodium will exchange with the calcium ions in physiological solutions, causing calcium alginate gels to swell, destabilise and rupture. To overcome this, gels can be formed using barium ions instead. Barium ions have a higher affinity towards alginate so should therefore give stronger, more stable gels, though in reality this is dependent on the ratio of mannuronic acid to guluronic acid in the alginate. A further consideration is that barium can inhibit membrane potassium channels at concentrations of 5-10 mM and so its concentration should be kept as low as possible [91].

The loss of divalent cations from alginate hydrogel *in vivo* results in slow and uncontrolled degradation, producing high and low molecular weight alginate units, as well as free calcium ions which are reported to inhibit cell growth at high concentrations [92]. Periodate oxidation of alginate produces a dialdehyde derivative, which is much more susceptible to biodegradation via hydrolysis. This results in more rapid biodegradation which may be useful for tissue engineering applications such as cell delivery [93, 94]. Oxidation has also

been show to produce more porous gels, as a result of changes in gel mass, with positive effects on cell viability. The oxidised alginate gels are also less stiff than their unmodified counterparts [95].

2.3.3. Collagen & gelatin

Collagen is a fibrous ECM protein with key structural roles in tissues. It is the most abundant protein in the human body, and has 29 recognised forms. Type I collagen, the most common, has a triple helix structure, and self-assembles to a fibrillar structure under physiological conditions. It is, unsurprisingly, cell adhesive. However, collagen hydrogels are weak, and as a result contract greatly when encapsulating cells, due to cells exerting forces on fibres within the collagen [22]. Cross-linking collagen with a chemical agent such as glutaraldehyde improves gel strength and stability though milder cross-linking agents are necessary for biological applications to prevent accidental fixation of the cells themselves [96]. Collagen has been used to produce a variety of scaffold types, including microparticles [97]. However, collagen gel formation is temperature, pH and ionic strength dependent, and these particular conditions can limit the ease of handling, which is why it has also been used in combination with materials such as alginate and fibrin [27-29, 98, 99].

The hydrolysis of collagen is achieved by acid or alkali treatment, yielding Type A or Type B gelatin respectively. These differ in their isoelectric points and their net charges at physiological pH. Gelation is achieved by dissolving gelatin in aqueous solutions at approximately 60°C before allowing the solution to cool to room temperature [100]. It is biodegradable, and is used for culinary, pharmaceutical and medical applications [22]. It is more cheaply available, and its gel formation is less sensitive to environmental factors than collagen. Gelatin retains the crucial RGD motif from collagen, facilitating high levels of cell adhesion [101, 102]. However, when reheated to physiological temperatures or higher, gelatin hydrogels will melt and therefore must be cross-linked to improve their stability under these conditions. A number of cross-linking substances have been used for this purpose, including glutaraldehyde, genipin, and EDC [59, 100, 103]. EDC is a zero length cross-linking agent, and does not become incorporated into the final structure, unlike aldehyde or isocyanate cross-linkers, but is instead lost as a water soluble urea derivative. The degree of cross-linking, which influences the final stiffness of the gel, can be controlled by altering the cross-linker concentration or the length of exposure to it.

2.3.4. Decellularised tissue materials

Whole decellularised organs have been used as tissue engineering scaffolds, and a number of decellularised tissue products are commercially available [104]. Decellularisation leaves behind the ECM components of the tissue (such as collagen, glycoproteins, and fibronectin) that are ideal scaffolds for cell reseeding, and materials of this sort have been shown to exert angiogenic and chemoattractant effects [105]. ECM components can be harvested from a variety of tissues including the small intestine, skin, and liver [18, 106]. One example is small intestine submucosa (SIS), a resorpable collagen-based matrix that is used clinically to reinforce and strengthen soft tissue remodelling [107, 108]. Once decellularised, the organ scaffold can be reseeded with the patient's own cells and implanted once mature [109]. Although this approach removes much of the risk of immune rejection of the 'new' organ, it still requires a donor in the first place. Although the availability of donor organs would increase for a given patient once immunocompatibility is no longer an issue, there is still a dependence on consenting donors and thus this approach is unlikely to ever be suitable as an 'off-the-shelf' solution. The applications of these scaffolds can also be limited by their shape or geometry.

To overcome this, it is possible to process the decellularised matrix into an injectable form, which would increase the possible applications for a scaffold of this type [110]. An injectable scaffold can be implanted in a minimally-invasive process, which reduces patient discomfort, infection risk, and cost compared to open surgical procedures. Additionally, injectable scaffolds have advantages over pre-formed implantable scaffolds when the defect to be repaired is of an irregular or unknown size [111, 112]. Injectable powders, produced using waste material from liposuction procedures, have been shown to support the development of highly vascularised grafts *in vivo* [113].

Several groups have also used ECM products as microparticle scaffolds, by encapsulating the decellularised product within alginate beads [114, 115]. In the case of Mazzitelli et al., the alginate acts as an immunoprotective barrier for the encapsulated cells during transplant [55]. Alternatively, injectable hydrogels can be created directly from decellularised ECM materials, solubilising ECM products by digestion. The resultant products contain a high proportion of collagen, allowing the formation of hydrogels under physiological conditions [110, 116, 117]. However these resultant hydrogels are generally quite soft and require gentle handing.

Methods of decellularisation

The removal of cellular antigens is an essential step for the production of decellularised ECM materials, as otherwise the presence of antigens may induce an inflammatory and immune response [118, 119]. The removal of cellular components can be achieved through three main approaches: chemical, enzyme-based, or physical.

Physical methods include mechanical agitation, freeze/thaw cycles and sonication, while enzymatic treatments can include the use of trypsin, and endo- and exonucleases. Chemical methods are more varied, and can involve the use of acid or alkali solutions, hypo- and hypertonic solutions, and ionic, non-ionic and zwitterionic detergents such as Triton X-100, SDS and CHAPS respectively [120]. A combination of these approaches is likely to be most effective. A variety of factors such as tissue type, tissue density and the desired end product affect the choice of methodology.

Crapo et al. define the following criteria as requirements for successful decellularisation [46]:

1. The material should contain less than 50 ng dsDNA per milligram of dry ECM.
2. DNA fragments should be less than 200 base pairs in length.
3. No nuclear material is visible in tissue sections stained with H&E or DAPI.

Although the focus here is on DNA content, this is logical given that DNA levels are proportional to adverse host reactions, and DNA can act as an indicator for other cell residues remaining within the ECM [104]. Fulfilling these criteria imparts confidence in the safety of the material for *in vivo* use, having removed immunogenic stimuli.

Skeletal muscle-derived substrates

As the ECM varies with tissue type, it has been assumed that the best matrix for a particular cell type will be the one that most closely resembles its natural *in vivo* environment. For example, for myoblast expansion, rat skeletal muscle was processed by decellularisation, lyophilisation and milling into a powdered form. The extract was re-dissolved for use as a coating material for tissue culture plastic, which resulted in enhanced proliferation and differentiation of myogenic cells relative to uncoated/collagen-coated surfaces [121]. Cell-type specific coatings can be created in this way, useful for *in vitro* culture or possibly for

coating medical devices *in vivo* [122, 123]. For three-dimensional culture, a gel or similar structure would be required.

Adipose-derived substrates

Adipose-derived scaffolds have been investigated due to the wide availability of human adipose tissue, a waste product from liposuction surgeries [124]. Human ECM powders can be generated from adipose tissue by homogenising the blood- and oil-free tissue, followed by freeze-drying and milling. Such powders support human adipose-derived stem cell (ASC) adhesion and proliferation *in vitro*. Seeded powders injected into nude mice supported adipogenesis and new blood vessel formation, as opposed to untreated adipose tissue or unseeded ECM powders [111]. Though powders alone do not confer much in the way of structure, hydrogels have been created in a similar way. Decellularised, lipase-treated adipose samples were solubilised with pepsin and upon exposure to physiological temperature and pH, self-assembled to form a hydrogel with a nanofibrous structure. This matrix supported normal human ASC growth and proliferation and could prove useful for soft tissue regeneration applications [105].

2.4. Bioreactors for tissue-engineered constructs

The culture and scale-up of three-dimensional tissue constructs requires the development of bioreactor systems which can support cell growth and tissue maturation. This may be simply through the provision of oxygen and nutrients, or in more complex designs, the generation of mechanical stimuli designed to aid cell differentiation. Statically cultured tissue constructs as small as 1 cm^3 can develop central necrotic regions, as internally seeded cells exist in an oxygen and nutrient depleted environment, while those on the periphery maintain their viability [125]. In order to overcome this, and so that tissue constructs can be made sufficiently large to be clinically relevant, dynamic bioreactor cultures can be used to improve mass transfer. In short, bioreactors are systems in which certain parameters are controlled to maintain stable environments throughout a culture. Commonly controlled conditions for cell culture applications include temperature, pH, oxygen and nutrient supply, in addition to the removal of waste products such as lactic acid [126].

There are a variety of bioreactor types and the choice of bioreactor will depend on the size, shape and design of each tissue construct. Some bioreactor designs, such as stirred tanks, can be used both for initial cell seeding of a scaffold as well as for its long term culture,

while other systems would require a separate cell seeding or encapsulation method. Some of the most commonly used bioreactors are discussed in more detail below, though for a given application each bioreactor design can be modified and optimised.

2.4.1. Spinner flasks

Spinner flasks are the simplest form of bioreactor, and can be used to culture either cell-laden microparticles, freely suspended, or larger scaffolds suspended by wire into the vessel. These systems are easy to assemble and use, and rMSCs cultured on PLGA scaffolds for 21 days in a spinner flask showed improved proliferation, alkaline phosphatase activity, osteocalcin expression and calcium deposition over statically cultured controls [127]. However, the size of constructs that can be grown in spinner flasks is limited. Increasingly large constructs require increased rotation rates to deliver nutrients to core regions, producing higher shear stresses on the outer regions of the structure which leads to cell death [125].

2.4.2. Perfusion systems

Perfusion bioreactors can overcome the size limitations of spinner flasks by continuously pumping media through a porous scaffold (or packed microparticles, in the case of Chen et al.) [57]. Care must be taken to ensure the media flows through the scaffold, rather than around it, but when correctly assembled, nutrient transport is improved to central scaffold regions [128]. Perfusion systems can also be used to seed cells onto porous scaffolds, which for top down scaffolds encourages a more homogenous cell distribution than passive seeding, by transporting cells directly into internal pores [129].

Improved osteogenic outcomes have been observed for structures cultured in perfusion bioreactors, compared to static and spinner flask systems, possibly due to the action of flow-mediated stresses, which are known to upregulate osteogenic differentiation and mineralisation [130, 131]. However, the same shear stresses provided by continuous perfusion can be responsible for ‘washing out’ newly formed ECM, delaying or inhibiting tissue maturation [42].

2.4.3. Hollow fibre bioreactors

Hollow fibre membrane bioreactors separate mass transfer from shear stresses. Cells are typically cultured on the exterior of hollow fibres, packed within a cartridge. Media is fed through the fibres, and while nutrients and oxygen diffuse through the membrane towards the cells, waste products travel the opposite way, in accordance with concentration gradients. Hollow fibre bioreactors provide high surface areas for cell attachment and cells are protected from shear stresses. Alternative arrangements are possible – for example cells could be grown inside the fibres or encapsulated in scaffolds around them [132]. However, hollow fibre bioreactors have primarily been investigated as a method of cell expansion rather than for the development of tissue constructs [133, 134].

2.4.4. Stimuli-providing bioreactors

Mechanical conditioning of tissue engineered constructs has been shown to improve the final properties of the product over a range of applications. For example, mechanical stretching has been shown to enhance the proliferation of cardiomyocytes on gelatin scaffolds, as well as the deposition and organisation of ECM by the cells [135]. Similarly, the application of pulsatile radial stress to tubular smooth muscle cell-seeded scaffolds improved the rupture strength of the resultant construct [136]. In a sense, most bioreactors provide some mechanical stimuli if only through the application of shear stress. However, for bone tissue engineering, bioreactors have been developed in order to replicate some of the mechanical stimuli bone and cartilage experience *in vivo*, such as compression, bending and tension. An example of this is the perfusion compression bioreactor. Osteosarcoma MG63 cells cultured in this system showed significantly higher levels of osteogenic markers compared to cells cultured under perfusion conditions only [125].

The use of mechanical cues is crucial in conditioning tissue engineered constructs but the processes by which this can be achieved are varied. Problems include how best to deliver force into a bioreactor, as well as choosing a scaffold material that can withstand the force provided without rapid degradation.

2.5. Conclusions

While the steps necessary to create a functional tissue construct are relatively well-defined, there is a lack of consensus about the most appropriate scaffold design approach, and indeed the scaffold material itself.

For bone tissue engineering, the most suitable cell type for autologous or allogenic transplants is the mesenchymal stem cell, which is capable of osteodifferentiation as well as adipogenic and chondrogenic differentiation. The conditions required to induce each of these pathways are generally well-understood. As adult MSCs can be harvested from a number of tissues including bone marrow, adipose tissue, or peripheral blood, for research purposes the most appropriate source is likely to be determined by the resources or donors available. For preliminary experiments however it may be more convenient and rapid to use immortalised cell lines.

It can be difficult to evenly seed cells throughout a traditional top down scaffold and specific arrangements of different cell types is also hard to achieve. In comparison, taking a bottom up approach to scaffold building allows for the even distribution of cells and a degree of control over cell type placement: seeding different cells types on different scaffold units can provide the ability to physically build in layers of complexity and hierarchy as the structure is assembled. Microparticles are ideally suited for use as the scaffold units of building blocks in this approach: cell culture on and in microparticles is well-established as a method of adherent cell expansion in stirred tank bioreactors, and these small spheres can be produced rapidly and easily.

However, the choice of scaffold material will affect the specific processing techniques required for microparticle productions. Naturally-derived materials, such as SF, gelatin, collagen and alginate, are biocompatible and their degradation products are non-toxic. The mechanical properties can be finely tuned through different processing steps, and the environment they provide can closely mimic the natural ECM. By blending these different materials together, their beneficial attributes can be combined, and the resultant products can be developed to give a range of scaffolds. In particular, blends of SF and gelatin show promise as cell adhesive, osteogenic materials.

However, the limiting factor in the development of engineering tissues and organ is the need for cells to be within 200 μm of an oxygen supply. Without a local oxygen supply, central construct regions will necrose rapidly. This can be overcome through the use of bioreactors to provide perfused media flow through a scaffold, or through the design of a pseudo-vasculature within the construct itself. There is potential for these approaches to be

combined in the development of a hollow fibre bioreactor, in which the fibres themselves are integrated within the construct.

2.6. Aims & Objectives

The aim of the work is to use blends of naturally-derived biomaterial microparticles, for use as cell-bearing scaffolds in bone tissue engineering applications. The materials in question are SF, alginate and ECM proteins. Microparticle scaffolds are proposed due to their suitability as cell carriers and the ability to mould individual scaffolds together into a macroscopic tissue-like construct. The eventual aim of producing such a construct would be for its use in replacing damaged tissues *in vivo*, or for use in *in vitro* studies to minimise animal use for research. As the viability of tissue constructs is dependent on the proximity of cells to a source of nutrients and oxygen, a final target of this work is to create a pseudo-vasculature within the structure by moulding particles around hollow fibres. The objectives of this work are therefore as follows:

- Investigate the biocompatibility, and characterise the physical properties, of blends of SF, alginate, and ECM protein materials in two and three dimensional systems.
- Determine the best method for the production of gel-forming decellularised ECM materials.
- Establish methods for the production of monodisperse microparticles for various material blends.
- Isolate and culture rMSCs and investigate their osteodifferentiation on the materials in question.
- Establish protocols for seeding or encapsulating cells within the microparticles to maintain cell viability.
- Mould cell-laden microparticles into a macroscopic tissue construct, and characterise cell viability, distribution and construct strength.
- Design a hollow fibre bioreactor system for moulding cell-laden microparticles into a tissue construct with integrated pseudo-vasculature, and use for the creation of a centimetre-scale bone tissue construct.

Chapter 3

Materials & Methods

This chapter includes the experimental procedures, material sources and analysis methods used throughout this thesis. Unless otherwise specified, materials were obtained from Sigma-Aldrich.

3.1. Experimental methods

3.1.1. Cell culture

All cell culture work was carried out under sterile conditions in a class II biological safety cabinet. Cells were maintained at 37 °C, at saturation humidity and 5% CO_2. Cells were passaged regularly, at approximately 80% confluence, by trypsinisation. Trypsin was used at 0.25%, supplemented with 0.02% ethylenediaminetetraacetic acid (EDTA), in phosphate-buffered saline (PBS; Oxoid).

Where it was necessary to culture cells outside of the atmosphere-controlled incubator, CO_2-independent medium (Gibco) was used to ensure the pH remained constant. The basal medium was supplemented with 10% v/v foetal bovine serum (FBS; Gibco), 4 mM L-glutamine (Gibco), 100 U/mL penicillin and 100 µg/mL streptomycin. Cell lines were adapted to this medium by initially introducing 25% v/v of CO_2-independent medium into the normal cell line media, and increasing the proportion to 50%, 75% and finally 100% v/v over a week of culture.

Culture of 3T3 fibroblasts

NIH 3T3 fibroblast cells (93061524; Health Protection Agency) were cultured in complete Dulbecco's Modified Eagle's Medium (DMEM; D5796) with 10% v/v FBS (Gibco), 100 U/mL penicillin and 100 µg/mL streptomycin. 3T3 fibroblasts were used as they were routinely cultured in the laboratory.

Isolation & culture of rat mesenchymal stem cells (rMSCs)

rMSCs were extracted from the bone marrow of juvenile Wistar rats as described by Zhang and Chan [137]. Cells were selected by adherence to tissue culture plastic (TCP), followed

by fluorescence-activated cell sorting (FACS) analysis, using the antibodies listed in Table 3.01. Cells were trypsinised and counted, then divided into microcentrifuge tubes containing between 10^5 and 10^6 cells per sample (one for each isotype control and antibody, as well as a tri-labelled sample for sorting). Samples were pelleted by centrifugation (300 x *g*, 5 minutes) and washed in cold FACS buffer consisting of PBS with 1% v/v FBS before 30 minutes incubation on ice. Samples were again pelleted then re-suspended in 50 µL of FACS buffer. The antibodies and isotype controls were added to each sample as appropriate, in the dilutions listed in Table 3.01. The samples were incubated for 1 hour on ice, protected from light. Finally, the samples were washed twice by pelleting and re-suspending in FACS buffer, then re-suspended in 500 µL of PBS, at which point FACS was carried out using a Becton Dickinson FACS Aria III.

Table 3.01: List of antibodies and isotype controls used for the identification of rMSCs by FACS.

Antibody	**Conjugate**	**Dilution used**	**Product code; Supplier**
Mouse anti-rat CD90.1	Vioblue	1:11	130-102-637; MACS Miltenyi Biotech
Mouse anti-rat CD54	FITC	1:3.5	FAB5831F; R&D Systems
Mouse anti-rat CD45	PE-Cy7	1:50	561588; BD Pharmingen
Isotype control mouse IgG2a	Vioblue	1:11	130-098-898; MACS Miltenyi Biotech
Isotype control mouse IgG2b	FITC	1:3.5	130-099-119; MACS Miltenyi Biotech
Isotype control mouse IgG1κ	PE-Cy7	1:11	560906; BD Pharmingen

The population positively labelled for CD90.1 and CD54 and negative for CD45 was reserved. These cells were cultured in Minimum Essential Medium Eagle's, alpha modification (αMEM, M8042) with 10% v/v FBS (Gibco), 2 mM L-glutamine (Gibco), 100 U/mL penicillin and 100 µg/mL streptomycin. This is referred to hereafter as basal medium.

Cells were discarded after passage 8, as older cells lose activity, proliferative capacity and ability to differentiate [138].

Tri-lineage differentiation assays

Adipogenic induction medium consisted of basal medium, supplemented with 1 µM dexamethasone, 0.5 mM 3-isobutyl-1-methylxanthine (IBMX), 100 µM indomethacin and 10 µg/mL of insulin. Adipogenic maintenance medium consisted of basal medium supplemented with 10 µg/mL of insulin only. rMSCs were seeded at 1.1 – 1.5 x 10^4 cells/cm^2 in basal medium and grown to 100% confluence before switching to differentiation media [139]. Confluent cell monolayers underwent media changes according to the following protocol:

Days 1, 3, 5, = adipogenic induction medium

Day 7 = adipogenic maintenance medium

Days 9, 11, 13 = adipogenic induction medium

Day 15 = adipogenic maintenance medium

Days 17, 19, 21 = adipogenic induction medium

Chondrogenic differentiation medium consisted of DMEM High Glucose (4.5 g/L) supplemented with 10% v/v ITS+1 Premix Tissue Culture Supplement (insulin-transferrin-sodium selenite, linoleic-bovine serum albumin), 0.1 µM dexamethasone, 1 µM ascorbate-2-phosphate, 1 mM sodium pyruvate (Invitrogen), and 10 ng/ml transforming growth factor-beta 1 (TGF-β1, Invitrogen). Chondrogenesis was induced by means of pellet culture. 8 x 10^5 cells were centrifuged in a 15 mL polypropylene tube at 450 x *g* for 10 minutes. The resulting pellet was then cultured in chondrogenic medium for 21 days, with medium changes 3 times per week [140].

For osteogenic differentiation assays, rMSCs were seeded at 1.1 – 1.5 x 10^4 cells/cm^2 in basal medium and grown to 100% confluence before switching to differentiation media. Osteogenic differentiation medium (ODM) consisted of basal medium supplemented with 0.1 µM dexamethasone, 0.2 mM ascorbic acid 2-phosphate and 10 mM glycerol-2-phosphate [141]. Cells were cultured in ODM for up to 28 days with medium changes 3 times per week.

Analysis of rMSC differentiation can be found in Section 3.2.3.

Seeding microparticles with cells

To prevent cells preferentially adhering to TCP over microparticles, multiwell plates were coated with 1% w/v agarose in DMEM. The solution was heated until the agarose dissolved, then sufficient volume to cover the base of the wells was added to each. The agarose was allowed to cool and set before the plates were used.

In a total volume of 500 µL, 3.75 x 10^5 cells/mL were seeded onto microparticles (4 x 10^3 /mL) in an agarose-coated 24 well plate. The plate was incubated under normal cell culture conditions on a plate rocker. After 24 hours, the suspension was filtered through a 70 µm cell strainer to separate unattached cells, which were manually counted to calculate seeding efficiency:

Where x is the concentration of unattached cells in the filtrate:

$$\text{Seeding efficiency} = 100 \times (3.75 \times 10^5 - x)/3.75 \times 10^5 \quad \textbf{(Equation 3.01)}$$

Where required, gelatin Cultispher-S microparticles (Percell Biolytica) were reconstituted as per the manufacturer's directions, by autoclaving and washing in PBS (Oxoid), followed by washing in culture media.

Cell encapsulation in alginate/collagen microparticles

Cells (either 3T3 fibroblasts or rMSCs) were trypsinised, pelleted, and re-suspended in 3 mg/mL rat tail collagen I solution (Invitrogen) at a concentration of 2 x 10^6 cells/mL. The collagen cell suspension was then mixed in a 1:1 ratio with 2.5%-oxidised medium viscosity (MV) alginate solution at a concentration of 10% w/v (with a final cell concentration of 1 x 10^6 cells/mL). Alginate oxidation is described in Section 3.1.5. 1 M sodium hydroxide was added at 2.5% of the volume of collagen used, in order to neutralise the collagen and allow gel formation. The mixed cell suspension was aspirated into a sterile syringe which was then attached to the air flow focussing system (see Section 3.1.9). The resulting cell-laden microparticles were incubated under normal cell culture conditions in a multiwell plate, on a plate rocker.

3.1.2. Moulding cell-laden microparticles into larger constructs

Cell-laden microparticles were moulded using a re-purposed cloning cylinder and non-adhesive agarose-coated plates. Cylinders were secured in wells by pushing them firmly into the agarose gel layer. Cell-laden microparticles were gently pipetted into the mould created by the cylinder, with media filling the entire well over the height of the cylinder to ensure the sample did not dry out, as shown in Figure 3.01. After 7 days, the mould was removed with a pair of forceps. If successful, the microparticles held the shape of the mould independently, and the structure was stable to manual manipulation.

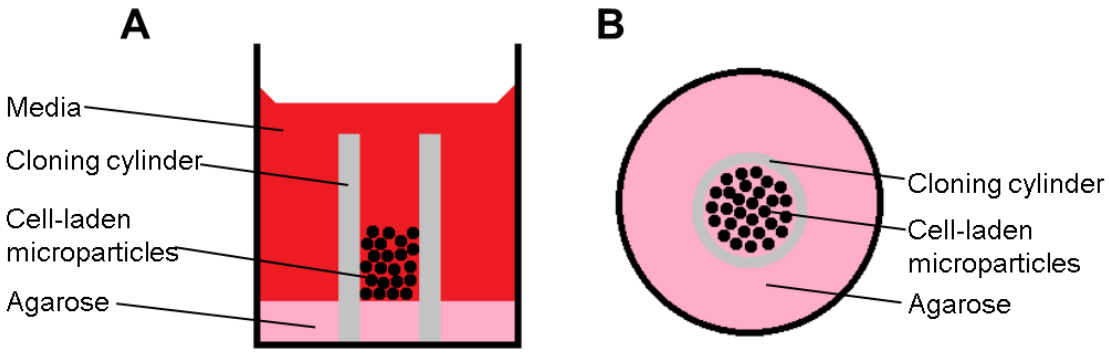

Figure 3.01: Schematic of system for moulding microparticles together. (A) Cross-section; & (B) top view of a media filled 24-well plate well coated with an agarose layer, fitted with a cloning cylinder filled with microparticles. Not drawn to scale.

3.1.3. Bioreactor design and assembly

A custom bioreactor was created from commercially available parts and fittings. A diagram is shown in Figure 7.01. The body of the chamber was made from a Thermo Scientific Pierce Spin Column (Part no. 69705), with a length of polyvinylidene fluoride (PVDF) hollow fibre (KrosFlo® Implant Membrane, Spectrum Laboratories) fixed through the centre. A filter disc from the spin column set was pierced to produce a ring-shaped polyethylene frit that was pushed down around the hollow fibre to provide a flat surface at the bottom of the chamber. At this stage the hollow fibre was primed by 30 minutes soaking in 100% ethanol. The system was then sterilised by a further 30 minute soak in 70% ethanol, followed by washing in autoclaved distilled water. Peristaltic pump tubing (PharMed® BPT tubing 14; Cole-Parmer) was connected in line with silicone tubing to create a closed system around the hollow fibre chamber.

Protein diffusion into the chamber

For investigating protein diffusion through the hollow fibre into the spin column chamber, the top of the chamber was sealed with the 'screw top to Luer' cap provided, which was in turn connected to a Y-shaped 3 barb connector. The hollow fibre was threaded through, and sealed where it exited the connector, to prevent backflow. Tubing was fitted over the barb/hollow fibre. The third outlet was sealed with a removable cap, to allow for sampling of the chamber fluid at defined time points.

A solution of 0.4 mg/mL bovine serum albumin (BSA) in PBS was pumped through the system at 10 mL/minute. The chamber was initially filled with PBS alone. At various time points over 2 days, 50 µL of the solution from inside the chamber was sampled. Protein concentration was determined using the Pierce™ BCA protein assay (Life Technologies).

Cell culture in the bioreactor

The chamber was seeded with 2 x 10^3 cell-laden microparticles before the Luer fitting on the screw cap was attached directly to a Luer-to-barb connector, which in turn connected directly with the tubing. The space between the hollow fibre and barb fitting was sealed to prevent medium falling back into the chamber from the end of the hollow fibre and ensure medium travelled in one direction only. The medium reservoir was kept at 37°C in a water bath, as was the bioreactor chamber. Cells cultured in the bioreactor were adapted to CO_2-independent medium to allow growth outside the normal incubator environment (see Section 3.1.1). The flow rate was set to 10 mL/minute. Where medium samples were collected for analysis, these were drawn from within the chamber itself.

Control samples were cultured in a static, non-perfused environment (a sealed Eppendorf tube) for the same length of time, in the same volume of media as the bioreactor chamber held (2 x 10^3 cell-laden microparticles/0.5 mL).

3.1.4. Processing silk fibroin (SF) and gelatin (G)

In order to purify SF from raw silk, *Bombyx mori* cocoons (Homecrafts Direct) were first boiled in 0.2 M sodium carbonate in distilled water for 1 hour to remove sericin proteins. The silk was then washed 5 times in distilled water and air-dried. Once dry, the SF was dissolved in 9 M lithium bromide at 15% w/v, at 60°C for 4 to 5 hours before the solution was dialysed against regularly changed distilled water for approximately 2 days, or until the

conductivity of the water stopped increasing. The concentration of the aqueous SF solution was determined by drying a known volume of the solution. It was stored at 4 °C, and used at a concentration of 5% w/v unless stated otherwise. Solid SF was obtained by lyophilising the solution (using a Thermo Savant MicroModulyo bench top freeze-dryer).

Type A porcine gelatin was dissolved in distilled water at approximately 60 °C, at a concentration of 5% w/v, immediately before use.

Coating plates with SF and SF/G blends

SF and gelatin were adsorbed onto TCP to investigate their effects on cell adhesion. Silk fibroin, gelatin and silk fibroin/gelatin blends (SF/G 75:25, 50:50, 25:75) were each diluted to 50 µg/mL in 0.02 M acetic acid, and added to a 96 well plate at 5 µg/cm^2. The plate was incubated at room temperature for at least 1 hour, before the solutions were aspirated from the wells. The wells were washed 3 times with PBS to remove any remaining acid. Plates were either seeded immediately with 3T3 fibroblasts at 1.25 x 10^4 cells/cm^2, or air-dried and stored at 4 °C.

To create thin films of SF, gelatin and SF/G blends, SF and gelatin were dissolved in hexafluoroisopropanol (HFIP, Alfa Aesar) at 2% w/v. SF and gelatin were blended in ratios of 75:25, 50:50 and 25:75, and films were cast by allowing the solution to evaporate to dryness (20 µL/well in a 96 well plate, 200 µL/well in a 24 well plate). Once dry, films were cross-linked by exposure to 50 mM 1-ethyl-3-(3-dimethylaminopropyl) carbodiimide (EDC, Alfa Aesar) in methanol for 24 hours at 4°C before washing three times with distilled water. Dry plates were sterilised by exposure to UV light for 30 minutes (253.7 nm, 0.115 kW, Bioquell), and then stored at 4°C until use.

Samples for determination of Young's Modulus

To produce films for use in tensile testing, 2% w/v solutions of SF, SF/G blends and gelatin in HFIP were cast into silicone moulds. Films were cross-linked using 50 mM EDC in methanol for 24 hours, washed three times with distilled water and air dried. The films were peeled off the silicone mould and trimmed to size (10 x 20 mm).

To produce solid discs for compression testing of SF/G materials, 1.5 mL of 5% w/v solutions were added to wells of a 12 well plate. Plates were cooled to 4°C to set the discs, which were then treated with 50 mM EDC in methanol for 24 hours, and finally washed three

times in PBS. Once removed from the plates, discs were punched out of the solid materials using a cork borer. This produced uniform discs of 13.5 mm diameter, and 3-4 mm height.

Mineralisation of SF/G films

SF, SF/G blends and gelatin films were cast onto glass coverslips, and cross-linked with EDC as previously described. Once dry, the film-coated coverslips were weighed and individual masses were recorded. The coverslips were then incubated in a modified simulated body fluid (MSBF) as described by Murphy and Mooney, consisting of 141 mM NaCl, 4 mM KCl, 0.5 mM $MgSO_4$, 1 mM $MgCl_2$, 4.2 mM $NaHCO_3$, 5 mM $CaCl_2$ and 1 mM KH_2PO_4 [142]. The films were incubated in the solution (at pH 6.8) for 7 days at 37 °C, then washed, dried, and weighed again. Control samples were treated identically but incubated in distilled water rather than MSBF.

3.1.5. Production of oxidised alginate

Oxidised alginate was produced by treatment with sodium periodate [93]. 100 mL of 1% w/v sodium alginate solution was reacted with 0.25 M sodium periodate for 24 hours, protected from light. The volume of sodium periodate was adjusted to provide a certain number of molar equivalents to the sodium alginate to produce the desired level of oxidation. For example, to produce 5% oxidation, 0.05 molar equivalents of sodium periodate were added. The reaction was stopped by the addition of 1 mL ethylene glycol, and 2.5 g sodium chloride was added. 200 mL of ethanol was added to the solution in order to precipitate the product, which was collected by centrifugation (910 x *g*, 10 minutes). The precipitated product was re-dissolved in 100 mL of distilled water, and re-precipitated with 200 mL ethanol. The precipitate was collected and lyophilised (using a Thermo Savant MicroModulyo bench top freeze-dryer).

To investigate the level of oxidation, the remaining sodium periodate in the solution was quantified as described elsewhere [95, 143]. Before the reaction was quenched, 120 µL aliquots of the reaction mixture were collected, and mixed with 80 µL of an indicator solution consisting of 0.75% w/w starch and 15% w/v potassium iodide. The absorbance of the solution at 486 nm (due to the presence of tri-iodide starch complexes) was measured using a BMG Labtech FLUOstar Omega plate reader. The periodate concentration was calculated using a standard curve. The difference between the initial periodate and final amount in the

sample corresponds to the number of glycol groups oxidised to aldehyde groups, and therefore the level of oxidation [143].

3.1.6. Production of fine calcium carbonate particles

Calcium carbonate particles were produced from calcium chloride and sodium carbonate. 2.5 mL of 1 M sodium carbonate was added to 650 µL of 5 M calcium chloride and stirred vigorously for 10 minutes. After this time, 5 mL of distilled water was added and any large calcium carbonate particles (that precipitated without centrifugation) were discarded. The calcium carbonate was collected by centrifugation (581 x *g*, 5 minutes), and the supernatant was discarded. The product was lyophilised using a Thermo Savant MicroModulyo bench top freeze-dryer [144].

3.1.7. Decellularising porcine skeletal muscle

SDS decellularisation

Adipose tissue was removed from a 5-10 g sample of porcine skeletal muscle (PSM; F. Griffiths & Sons, Ashcott), which was then finely sliced. The samples were washed in distilled water for 30 minutes, and then stirred in 1% w/v sodium dodecyl sulphate (SDS) in PBS for 48-50 hours, until all colour had faded and the samples became 'feathery' in appearance. The samples were then rinsed in distilled water for approximately 6 hours, with the water changed several times. Decellularisation was assessed at this stage (see Section 3.2.7). Finally the decellularised PSM was lyophilised (Thermo Savant MicroModulyo bench top freeze-dryer) and ground into a powder.

The ground powder was digested with 1 mg/mL of pepsin in 0.1 M hydrochloric acid, at a concentration of 10 mg of decellularised PSM per 1 mL of hydrochloric acid. After approximately 60 hours, or when no particles were visible in the solution, the mixture was neutralised to pH7.4 with sodium hydroxide and PBS. The solution of solubilised ECM was stored at 4 °C.

Triton X-100/EDTA decellularisation

Tissue samples were decellularised as described by Stern et al. [121]. Briefly, samples were sliced thinly, and washed in distilled water for 2 days, before treatment with 0.05% trypsin with0.02% EDTA for 1 hour. All solutions were used at a ratio of 1 L per 40 g of starting material. To neutralise the trypsin the samples were placed in DMEM with 10% v/v FBS overnight. The samples were then exposed to 1% v/v Triton X-100 for 5 days, and finally washed for 2 days in distilled water and 1 day in PBS. Decellularisation was assessed at this stage (Section 3.2.7).

Homogenisation and solubilisation

PSM was decellularised using a method described by Abberton et al. [145]. Samples of PSM were weighed, then washed, finely sliced, and homogenised three times in ice-cold 3.4 M sodium chloride buffer, containing 0.5 mM phenylmethylsulfonyl fluoride, 2 mM EDTA, 0.1 M 6-aminocaproic acid, and 2 mM *N*-ethylmaleimide. After each homogenisation, the samples were centrifuged at 1780 x *g* for 5 minutes, and the supernatant was discarded. The samples were then homogenised again with fresh buffer. The total volume of buffer used was equal to three times the initial mass of the sample.

The samples were then treated with 2 M urea in 0.05 M Tris/0.15 M sodium chloride (TBS) buffer, overnight at 4 °C, in a volume equal to the initial sample mass. Following this, the samples were centrifuged (10,000 x *g*, 30 minutes) and the supernatant reserved. The pellets were re-homogenised in 2 M urea/TBS and left overnight again at 4 °C. The supernatant was collected. The combined supernatants were dialysed against 0.5% v/v chloroform in TBS for 1 day, then against several changes of TBS, and finally against DMEM. The product was stored at 4 °C. Protein concentration was determined by the Pierce™ BCA protein assay (Life Technologies).

3.1.8. SF and SF/G microparticle production

Emulsions

Initially SF particles were formed using an emulsification method. Approximately 80 mL of corn oil was mixed using an IKA DI 18 homogeniser. 500 µL of aqueous SF solution was added to the beaker and homogenised until the SF droplets appeared evenly distributed

throughout the oil phase. 0.8 mL Tween 20 was then added to the emulsion to give a concentration of approximately 1% v/v, followed by approximately 8 mL of methanol (1/10th of the initial volume of corn oil). The solution was centrifuged (327 x *g*, 4 minutes) and the aqueous top layer, containing the particles, was collected. The particles were incubated in fresh methanol overnight, then washed 3 times in PBS.

Axisymmetric microfluidic flow focussing

A schematic of the axisymmetric focussing device constructed in this work is shown in Figure 3.02. The main casing consisted of a T-junction piece (Tee LP PEEK 1/4-28 1/16" 0.040" Thru Hole, Kinesis), fitted with a glass capillary (Hollow Round Glass Capillaries ID 0.50mm OD 0.70mm, CM Scientific) running centrally through the junction. The outer diameter of the capillary measured 0.7 mm while the diameter of the lumen is slightly larger (1 mm), allowing the continuous phase to flow evenly between the capillary and the lumen wall. The inner and outer phases were fed into the T-junction through PEEK tubing (Tubing PEEK 1/16" OD x 0.03" (0.75mm), Kinesis) and the output travelled through the same tubing with a smaller inner diameter (Tubing PEEK 1/16" OD x 0.02" (0.50mm), Kinesis). The input tubing pieces were connected to Luer lock syringes via tubing-to-cone and cone-to-Luer fittings (Fingertight fitting two-piece PEEK 10-32 Long, Adaptor female Luer to 10-32 female PEEK, both Kinesis). The parts described are shown in Figure 3.03.

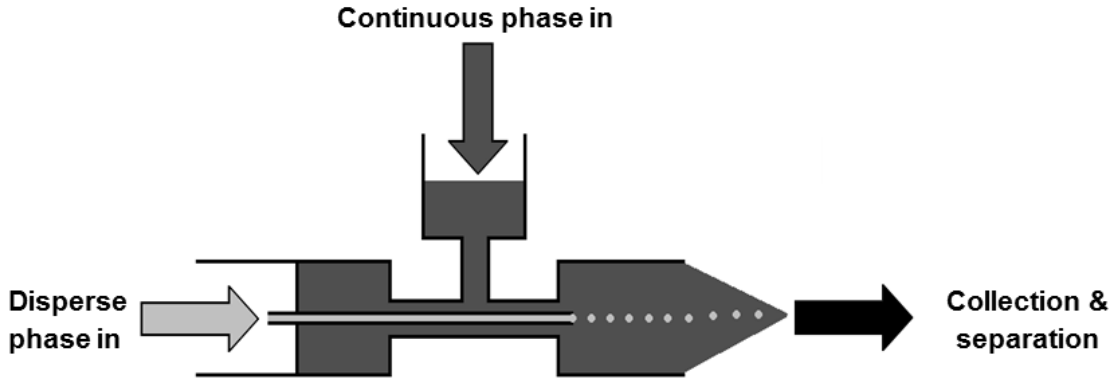

Figure 3.02: Schematic of the axisymmetric focussing device used to produce microparticles. The outer phase is shown in dark grey, while the inner phase is shown in light grey. The inner phase flows through the central capillary to break into droplets on exit. Schematic not to scale.

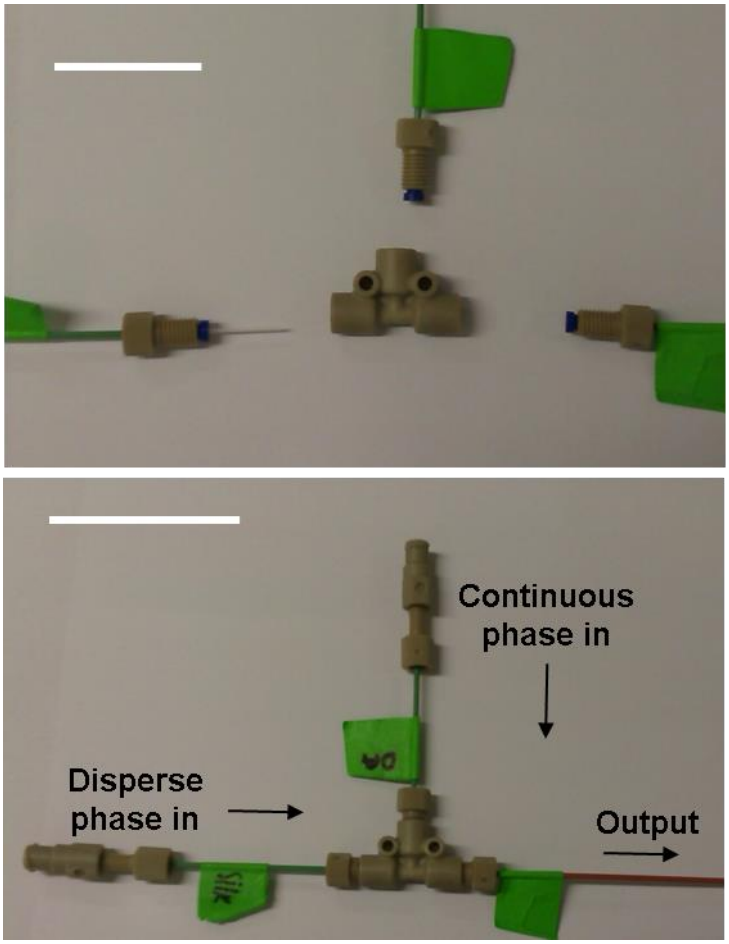

Figure 3.03: Component parts of the axisymmetric flow focussing device. The glass capillary in shown in the left hand image. In the right hand image, the capillary has been threaded through the central lumen of the T-junction. Scale bars represent 5 cm.

The outer continuous phase flowed in an L-shape through a port at a right angle to the capillary. The third port acted as the output. The two phases were controlled by separate syringe drivers (Harvard Pump 11 plus/Cole Parmer single syringe infusion pump). The inner phase consisted of the aqueous protein solution while the outer phase was oil-based. The outer phase consisted of oleic acid (Alfa Aesar), methanol and Span 80, in the volume ratio of 73:25:2 [55]. The inner flow rate was set to 0.36 mL/hour while the outer flow rate was set to 7.2 mL/hour. The output was collected into a 1:1 mixture of excess outer solution and methanol. Microparticles were then soaked in methanol, and gelatin-containing particles were cross-linked using 50 mM EDC for 24 hours. After this, the microparticles were washed once in a 1% v/v Tween 20 solution then three times in PBS. Microparticles for use in cell culture were autoclaved in PBS.

Porous particle production

To create SF microparticles with large interconnected pores, the use of porogens was investigated. SF solution was blended with 1% or 10% w/v sodium chloride, 10% w/v polyethylene glycol (PEG), or 5%, 10% or 20% w/v calcium carbonate, and microparticles were created as described above. To leach out sodium chloride and PEG, the microparticles were soaked in distilled water overnight. To dissolve calcium carbonate, the microparticles were incubated in acidified methanol (1.5 mM hydrochloric acid in methanol) overnight before washing with distilled water.

3.1.9. Alginate and alginate/ECM microparticle production

Axisymmetric microfluidic focussing

Alginate particles were produced in the flow focussing device described earlier in Section 3.1.8. For this application, the inner phase consisted of a slurry of 2% w/v insoluble calcium carbonate particles in alginate solution. The outer phase consisted of corn oil with 1% v/v Tween 20, acidified with 5% v/v acetic acid. The inner flow rate was set to 0.36 mL/hour while the outer flow rate was set to 7.2 mL/hour. The alginate microparticles were collected into an excess of the outer solution and allowed to settle before the majority of the oil was aspirated away. Hexane was added to dissolve the remaining oil and as much as possible was aspirated. Particles were washed in a calcium chloride washing buffer (80 mM $CaCl_2$ with 0.1% v/v Tween 20) before microscopy analysis.

Air flow focussing

An air flow focussing device was set up to rapidly produce alginate or oxidised alginate particles (from 1-10% w/v, MV or LV). A schematic of the system is shown in Figure 3.04. The flow of alginate solution from the end of a fine stainless steel capillary was evenly broken up by a coaxial flow of nitrogen gas, controlled by a regulator. Parts used included the Tee LP PEEK 1/4-28 1/16" 0.040" Thru Hole, flangeless fittings for 1/16” OD tubing, PEEK bulkhead union 1/4-28 flat-bottom, and stainless steel capillary tubing 1/32” OD 0.010” ID (all Kinesis). The droplets were collected in a bath of 135 mM (1.5% w/v) calcium chloride or 10 mM (0.208% w/v) barium chloride which cause rapid gelation of the alginate producing microparticles. The solution flow was controlled by a syringe pump (Cole Parmer single syringe infusion pump).

10% w/v 2.5%-oxidised MV alginate solution was blended with the decellularised homogenised/solubilised PSM extract (7-11.4 mg/mL), or 3 mg/mL collagen (Invitrogen) to create alginate-protein particles. The air flow rate was set at 0.5 bar and the alginate solution flow rate was set to 1 mL/minute.

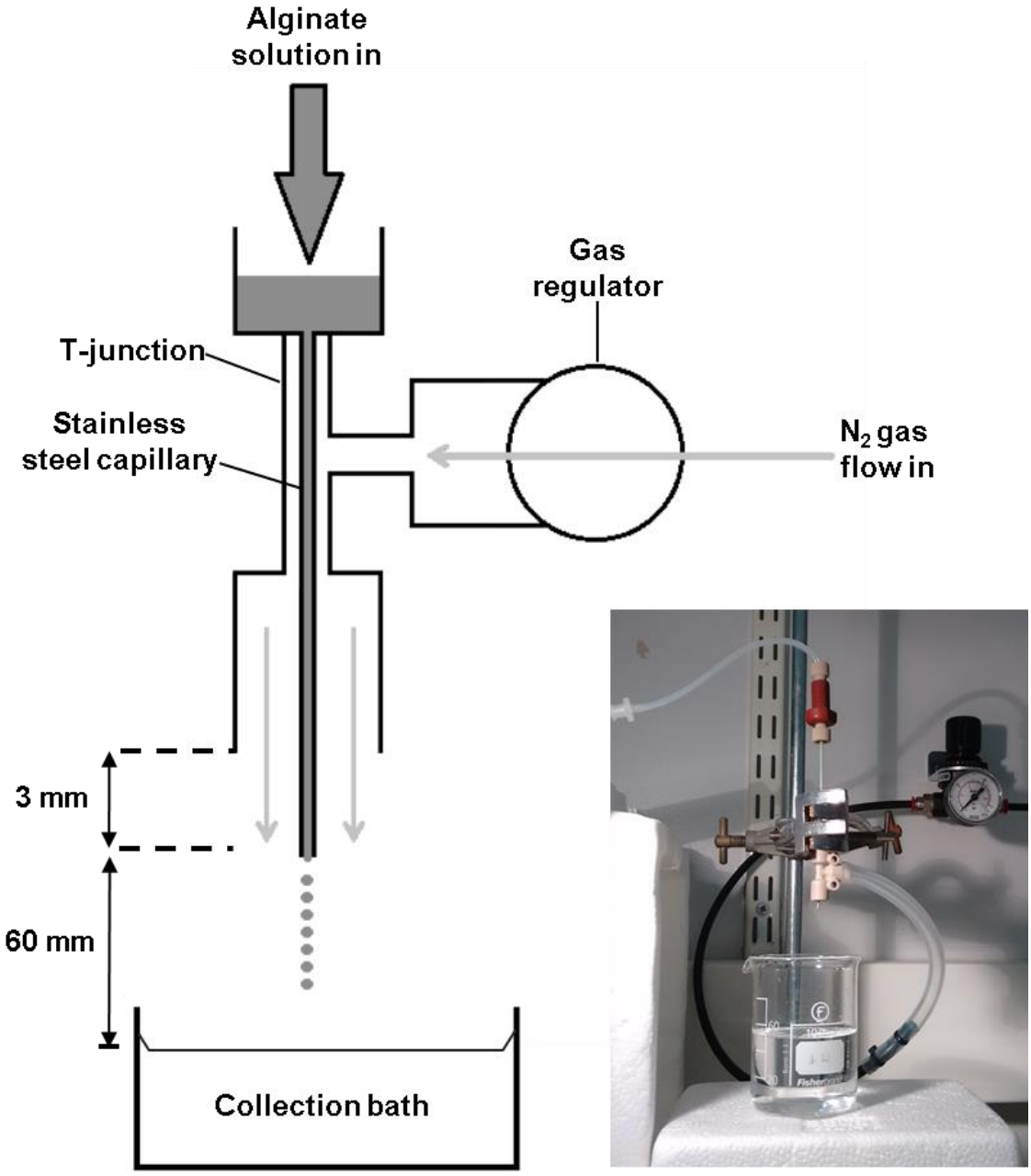

Figure 3.04: Schematic and photo of air flow focussing set up. The nitrogen air flow pulls drops off the end of the capillary tube and propels them into the collection bath. The alginate solution input was controlled by a syringe driver. The nitrogen flow was controlled by an inline regulator. Schematic not drawn to scale.

3.2. Analytical methods

3.2.1. Measuring cell number, metabolism & proliferation

Cell metabolism was assessed using the CellTiter 96® AQ_{ueous} One Solution Cell Proliferation Assay (MTS, Promega) according to manufacturer's instructions. Unless otherwise specified, three days after seeding cells, 20 µL of MTS reagent per 100 µL media was added to each well. After 2 hours incubation the absorbance of the plate was read at 490 nm using a BMG Labtech FLUOstar Omega plate reader.

Cell proliferation was alternatively measured using the reduction of resazurin solution. A 0.15 mg/mL solution of resazurin in PBS, pH 7.4, was added to cells (in freshly replaced media) at 20% v/v and incubated at 37 °C. After 2 hours, the fluorescence of the media was measured at Ex/Em 560/590 nm, again using a BMG Labtech FLUOstar Omega plate reader.

Cell numbers in microparticle cultures were analysed using fluorescent measurements of Hoechst-stained cell lysate [146]. Briefly, media was removed from the samples, which were frozen at -80 °C, then thawed at 37 °C. Distilled H_2O was added to each sample before sonicating for 15 minutes (VWR Ultrasonic Cleaner USC300TH) and then re-freezing. Samples were again thawed at 37 °C, and sample supernatants were added to an equal volume of 20 µg/mL Hoechst 33342 in TNE buffer (10 mM Tris-HCl, 1 mM EDTA, 2 M NaCl; pH 7.4). A standard curve was constructed using samples with known cell numbers. Fluorescence was read at 350/460 nm (BMG Labtech FLUOstar).

3.2.2. Analysis of cell viability by fluorescent staining

Samples were stained with LIVE/DEAD ®, consisting of calcein AM (2 µM) and ethidium homodimer 1 (2 µM) in PBS. Cells were washed with PBS, then incubated in the LIVE/DEAD solution in the dark for 30-40 minutes at room temperature, or for 20 minutes at 37 °C. Samples were then viewed under fluorescent light (Ex/Em calcein = 494/517 nm; Ex/Em DNA-bound ethidium homodimer 1 = 528/617 nm) (Leica DMI4000B).

Z-stacks of cell-laden microparticles were obtained using a Zeiss LSM510 confocal microscope.

3.2.3. Analysis of rMSC differentiation

Adipogenesis

To confirm adipogenic differentiation, cultured cells were stained with Oil Red O. Cells were fixed with 4% w/v paraformaldehyde for 30 minutes, and then washed 3 times with PBS for 5 minutes each. Two rinses with distilled water followed this, before the cells were treated with Oil Red O solution. The solution was prepared by diluting a 0.5% w/v stock solution of Oil Red O in 2-propanol with distilled water in a ratio of 3:2. The diluted solution was filtered and used immediately. Samples were incubated for 50 minutes at room temperature in this solution, after which time it was aspirated, and the samples were washed 3 times with distilled water. A positive result was indicated by the presence of red-stained lipid droplets within the cells.

Chondrogenesis

Chondrogenic cell pellets were fixed in 4% w/v paraformaldehyde, dehydrated and embedded in paraffin wax. 5 µm slices were sectioned using a microtome (Leica RM2125), and de-waxed using HistoChoice® Clearing Agent (2 x 2 minute washes). Samples were re-hydrated in a series of ethanol solutions (100%, 95%, 90%, 70%, 50%; 1 minute in each), then in distilled water for 1 minute. This was followed by staining with Toluidine Blue (1% w/v in distilled water) for 1 minute. Samples were then washed 3 times in distilled water, dehydrated and mounted using DPX Mountant. A purple stain indicated the presence of cartilaginous extracellular matrix, while blue staining showed undifferentiated tissue.

Osteogenesis – alkaline phosphatase activity

To confirm osteogenic differentiation, alkaline phosphatase (ALP) activity was assayed. Media was aspirated from the cell cultures, which were then carefully washed in PBS. The cells were exposed to 4% w/v paraformaldehyde for 60 seconds, then washed in washing buffer (PBS + 0.05% Tween 20). The cells were then covered in BCIP®/NBT Liquid Substrate System (5-bromo-4-chloro-3'-indolyphosphate p-toluidine salt/nitro-blue tetrazolium chloride) and incubated at room temperature for 10 minutes. The samples were then rinsed again in washing buffer before PBS was added. A positive result was indicated by dark blue/purple deposits, while a lack of ALP activity resulted in a colourless sample.

Osteogenesis – mineral staining

Von Kossa stain was used to investigate the presence of calcium deposits. Samples were washed three times in distilled water, then incubated in 1% w/v silver nitrate under an ultraviolet light for 20-30 minutes before washing again in distilled water. To remove unreacted silver, samples were treated with 5% w/v sodium thiosulphate for 5 minutes, then washed again. Samples were counterstained with 0.1% nuclear fast red solution for 5 minutes and washed in distilled water. Calcium salts are stained black or very dark brown by the Von Kossa stain, and nuclei are stained red by nuclear fast red.

Alizarin Red was also used to stain calcium deposits. Cell culture samples were washed in PBS (Ca^{2+} and Mg^{2+} free) and fixed with 4% w/v paraformaldehyde for 30 minutes. Following fixation, samples were incubated in Alizarin Red solution (2% w/v, pH 4.1-4.3, filtered) for 45 minutes at room temperature, protected from light, and then washed with distilled water four times. Mineralised deposits are stained bright red by Alizarin Red.

Osteogenesis – protein expression

Expression of osteocalcin was determined using the LI-COR Biosciences In Cell Western Assay. Cells grown in 96 well plates were washed in PBS, then fixed for 10 minutes in 4% w/v paraformaldehyde, before again washing in PBS. Cells were permeabilised by washing 5 times in PBS + 0.1% Triton X-100, and then blocked by 30-90 minutes exposure to Odyssey Blocking Buffer (LI-COR Biosciences). Cells were then labelled with a 1:50 dilution of primary antibody, rabbit anti-mouse osteocalcin (sc-30045, Santa Cruz Biotechnology Inc.) overnight at 4 °C, before washing 5 times in PBS + 0.1% Tween 20. The antibody was reported to have rat reactivity. The secondary antibody (goat anti-rabbit IRDye 800CW; 925-32211, LI-COR Biosciences) was added to the plates for 1 hour at a 1:800 dilution, protected from light at room temperature. The plates were finally washed 5 times with PBS + 0.1% Tween 20 before reading on the LI-COR Odyssey CLx infrared imaging system. The data was normalised by cell number, ascertained by counts of Hoechst-stained nuclei. Samples were stained by incubation with 5 µg/mL Hoechst 33342 in PBS, and images of stained nuclei were recorded and quantified using ImageJ software (NIH, Bethesda, MD, USA; http://imagej.nih.gov/ij).

Osteopontin levels were quantified from cell culture media supernatants using a commercially available enzyme-linked immunosorbent assay (Mouse/Rat Osteopontin

Quantikine ELISA Kit, R&D systems). This data was normalised by cell number, determined by Hoechst staining of lysed cells.

3.2.4. Determination of Young's modulus values

Uniaxial, unconfined compression measurements were performed on SF, SF/G blends and gelatin discs using an Instron 5965 testing machine at room temperature. All samples were measured under a loading rate of 0.2 mm/minute. Samples were measured for 6 minutes.

Unidirectional tensile tests were carried out on SF, SF/G blend and gelatin films. The thicknesses of the dry films, trimmed to 10 mm x 20 mm, were measured using a micrometer screw gauge. Films were fixed into cardboard holders, which were in turn clamped into the Instron 5965 with an initial distance of 10 mm between vices, and tension was applied at a rate of 0.5 mm/minute until material failure.

Young's modulus values were calculated from linear regions of the stress-strain curve using the following equation:

Young's modulus = (load/initial cross-sectional surface area) / (extension/initial length)

(**Equation 3.02**)

3.2.5. Scanning electron microscopy and energy-dispersive X-ray spectroscopy

Samples were examined by scanning electron microscopy (JEOL JSM6480LV).

Cell-free samples were lyophilised (Thermo Savant MicroModulyo bench top freeze-dryer) before sputter coating with gold (Edwards Sputter Coater 5150B). Cell-laden samples were prepared by fixation in 2.5% glutaraldehyde in DMEM with 1% w/v potassium ferrocyanide, for 2 hours at 37 °C. After washing with DMEM, the samples were post-fixed in 1% aqueous osmium tetroxide with 1% w/v potassium ferrocyanide for 1 hour at room temperature. Samples were then washed twice with distilled water over 10 minutes, and stained with 2% aqueous uranyl acetate for 1 hour, in the dark, at room temperature. Finally samples were dehydrated in a graded series of aqueous acetone solutions (50, 70, 90, 100% acetone) followed by 1:1 acetone:hexamethyldisilazane (HMDS) and 100% HMDS. Once the majority of the HMDS had been aspirated, samples were left for 1-2 hours for the remaining solvent

to evaporate. Once dry, samples were sputter coated with gold before SEM images were recorded.

For energy-dispersive X-ray spectroscopy (EDX), samples were sputter coated with chromium. EDX was carried out in combination with SEM, using an Oxford ISIS X-ray analyser.

3.2.6. Microparticle size analysis

Bright field images of microparticles were captured using a Leica digital microscope (Leica DMI4000B). Image J software was used to calculate the Feret's diameter (the maximum measured diameter) of the microparticles within each image.

3.2.7. Confirming and quantifying decellularisation

Decellularisation was confirmed with Haematoxylin & Eosin (H&E) staining, Hoechst 33342 staining and DNA content quantification, measured by the Quant-iT™ PicoGreen ® dsDNA assay (Life Technologies).

For H&E staining, samples were fixed in 4% w/v paraformaldehyde, embedded in wax and sectioned. Sections were de-waxed in HistoChoice® Clearing Agent (2 x 2 minute washes), then re-hydrated in a series of ethanol solutions (100%, 95%, 90%, 70%, 50%; 1 minute in each), then in distilled water for 1 minute. Sections were stained with filtered Harris Haematoxylin (0.7% w/v) for 3 minutes, washed gently with running tap water for a further 3 minutes then placed in concentrated hydrochloric acid in 70% ethanol for 30 seconds. The sections were then placed in 1% ammonia in 70% ethanol for 1 minute and washed in 70% ethanol for 30 seconds. Eosin staining was then achieved by placing the sections in filtered Eosin Y (0.25% w/v) for 1 minute, then very briefly washing in 70% ethanol (3 seconds maximum), 95% ethanol (5 seconds) and 100% ethanol (5 seconds). The sections were finally washed again twice in HistoChoice® Clearing Agent and mounted under coverslips using DPX Mountant.

For nucleic acid staining with Hoechst 33342, samples were fixed in 4% w/v paraformaldehyde, embedded in wax and sectioned. Sections were de-waxed in HistoChoice® Clearing Agent (2 x 2 minute washes), then re-hydrated in a series of ethanol solutions (100%, 95%, 90%, 70%, 50%; 1 minute in each), then in distilled water for 1

minute. Protected from light, sections were incubated in Hoechst solution (2 µg/mL) for 10 minutes at room temperature, before rinsing briefly with PBS and mounting. Samples were kept protected from light and fluorescent images were recorded immediately (Leica DMI4000B).

For quantification, DNA was extracted from lyophilised, ground samples. Weighed samples (10-30 mg) were suspended in 0.5 mL of extraction buffer (0.1 M NaCl, 10 mM Tris, 1 mM EDTA pH 8.0, 1% SDS) with 5 µL of 10 mg/mL Proteinase K, and incubated at 50°C for 24 hours. To extract nucleic acids from proteins, the samples were shaken with 0.75 mL phenol/chloroform/isoamyl alcohol (25:24:1 v/v) and centrifuged (12,000 x *g*, 15 minutes). The upper aqueous phase, containing the nucleic acids, was retained. The extraction was repeated. To precipitate DNA from the solution, 2 volumes of 100% ethanol and 0.1 volume of 3 M sodium acetate (pH 5) were added to each sample. The samples were incubated at -20 °C for 3 hours, and then centrifuged (12,000 x *g*, 15 minutes) to collect each DNA pellet, which was washed in 70% ethanol and air-dried. The pellets were re-suspended in 1 mL TE buffer (10 mM Tris, 1 mM EDTA pH 8.0) and stored at 4 °C before use in the PicoGreen assay.

3.2.8. Gel electrophoresis of homogenised/solubilised muscle extract

Samples were analysed by sodium dodecyl sulphate-polyacrylamide gel electrophoresis as described by Abberton et al. [145]. Briefly, samples were mixed in a 1:1 ratio with 2x concentrated Laemmli solution (4% w/v SDS, 20% v/v glycerol, 10% v/v 2-mercaptoethanol, 0.004% w/v bromophenol blue and 0.125 M Tris HCl, pH 6.8) to give a final sample concentration of 1 mg/mL, and heated at 90 °C for 5 minutes. 20 µL of each sample, and 5 µL of a molecular ladder solution were loaded onto the stacking gel, and separated in 10% polyacrylamide resolving gels for 45 minutes at 200 V. After this, the gel was removed from its frame, rinsed with distilled water and stained with SimplyBlue SafeStain™ (Invitrogen) for 1 hour at room temperature to identify separated protein bands.

3.2.9. Histology of three-dimensional samples

Samples were fixed in 4% paraformaldehyde for 24 hours and embedded in wax before microtome slicing. Sections were de-waxed in HistoChoice® Clearing Agent (2 x 2 minute washes), then re-hydrated in a series of ethanol solutions (100%, 95%, 90%, 70%, 50%; 1

minute in each), then in distilled water for 1 minute. Samples were stained with H&E to identify cell cytoplasm and nuclei within the construct, as described in Section 3.2.7.

3.2.10. Measuring viscosity

Viscosity measurements were obtained using a Bohlin C-VOR rheometer under dynamic conditions at 25 °C. Samples were placed between a flat plate and PU40 cone (40 mm diameter cone with 4° angle) and measurements were obtained using a stepped shear stress test (10 steps between 2 and 13 Pa). Each sample type was measured three times (using fresh solution each time) and the viscosity was calculated from the mean average of all measurements.

3.2.11. Statistical analysis

Statistical analysis was performed with one-way analysis of variance (ANOVA) with Tukey's honest significant difference post-hoc test using R software (R Foundation for Statistical Computing, Vienna, Austria; http://www.R-project.org). A value of $p<0.05$ was considered statistically significant.

Chapter 4

Silk fibroin & gelatin blends as biomaterials

4.1. Introduction

Silk as a biomaterial

As discussed in Section 2.3.1, silk fibroin (SF) has been highlighted as a promising biomaterial due to its mechanical and biological properties. Native silk fibres are produced with a core of fibroin coated in glue-like sericin. Though sericin can promote cell proliferation when added as a supplement to culture media, it has also been found responsible for adverse immunogenic reactions *in vivo* [68, 147]. Sericin must therefore be removed from silk before use in tissue engineering or other biological applications. Fortunately this is an easy process, as boiling native silk in sodium carbonate removes sericin proteins from the fibroin core [148]. Regenerated SF has been shown to have both good biocompatibility at levels equivalent to other commonly used biomaterials, including collagen, Teflon and poly-glycolic acid [68, 73, 149]. Indeed, the extensive use of silk sutures means that the reaction of the body to the introduction of SF is well-characterised. Although traditionally defined as non-degradable, there is evidence that SF breaks down over time as a result of proteolytic degradation [150-152]. SF is a thermally stable material, and can be sterilised by autoclaving without compromising structural integrity [80].

SF has been investigated as a scaffold for osteogenic and chondrogenic tissue engineering in a variety of formats, including films. A number of cell lines, including fibroblasts and colon adenocarcinoma cells, were shown to have equivalent growth rates on SF films compared to collagen films [153, 154]. Human MSCs have been successfully differentiated down osteogenic, chondrogenic and ligament lineage routes on SF scaffolds [76, 155, 156]. Saos-2 osteoblast-like cells were shown to have undergone bone formation on RGD (arginine - glycine - aspartic acid)-modified SF films, as RGD residues provide attachment sites for cell integrin receptors, facilitating cell adhesion [102].

Silk fibroin/gelatin scaffolds

While there are many reports of successful cell adhesion and proliferation on SF materials, there are a number of instances where SF has been blended with other biopolymers such as collagen, gelatin and cellulose to improve its properties [84, 157].

Gelatin is a product of collagen hydrolysis, and the two materials share many characteristics. Gelatin forms a temperature-dependent hydrogel in aqueous solutions, and is strongly cell-adhesive as a result of RGD residues within its structure [101, 102]. Where SF has been reported have low cell adhesion, this has been significantly improved by the inclusion of even small proportions of gelatin. Yang et al. found that including 1.2% gelatin in SF films improved the attachment of 3T3 fibroblasts, and that blended films containing 10-20% gelatin supported higher proliferation than either SF or gelatin alone. A summary of papers reporting improved biological and physical properties from blended SF/gelatin (SF/G) materials is shown in Table 4.01.

Table 4.01: Summary of published results comparing SF scaffolds alone to SF/G blended materials.

Scaffold type	Ratio SF:gelatin	Benefit compared to SF alone	Cell type	Reference
2D films	50:50	Increased elastic modulus; increased tensile strength; higher observable cell densities.	Mouse C2C12 cardiomyocytes	Taddei et al. [158]
2D films	80:20 90:10 95:5 97.5:2.5 98.75:1.25 99.375:0.625	Increased cell attachment and proliferation with increased proportion of gelatin.	Mouse 3T3 fibroblasts	Yang et al. [159]
2D films 3D discs	67:33 57:43 50:50	Increased cell adhesion and decreased rate of apoptosis with increased gelatin incorporation.	Human hepatic QZG cells	Yang et al. [87]
Porous freeze-dried discs	60:40	Increased cell adhesion and proliferation.	Mouse embryonic fibroblasts	Orlova et al. [160]
Porous freeze-dried discs	70:30	Higher compressive strength; Increased cell survival and proliferation; increased ECM deposition.	Rat chondrocytes	Chomchalao et al.; Tiyaboonchai et al. [84, 86]
Salt-leeched porous discs	90:10	Increased cell viability and proliferation.	Mouse embryonic fibroblasts	Moisenovich et al. [161]

4.2. Aims & Objectives

As described, SF is an attractive scaffold material for tissue engineering. The decision was therefore taken to investigate SF as a scaffold for osteogenic cell culture, initially in two-dimensional formats. Given reports of variable levels of cell adhesion to SF materials, investigation into the effects of blending SF with gelatin was proposed as a method to improve cell attachment.

The aim of the work in this chapter is to investigate SF based scaffolds for use as osteogenic biomaterials:

- Investigate the properties of SF and SF/G materials.
- Confirm the biocompatibility of SF and SF/G blends, and investigate their ability to support cell growth.
- Isolate and characterise rat mesenchymal stem cells (rMSCs), and explore whether SF and SF/G materials support osteodifferentiation.

4.3. Results & Discussion

4.3.1. Topography of SF & SF/G films

When examined by scanning electron microscopy (SEM), films of SF and SF/G blended materials appeared flat and even, with no pores or holes revealing the surface underneath. This confirms that when cells are seeded onto these films, they are interacting with the film rather than the material underneath. Examples of these films are shown in Figure 4.01. The film of SF/G 50:50 was typical of all blends of SF/G. While all films completely covered the surface with no visible gaps, the SF and SF-containing films appeared smoother than those composed entirely of gelatin. This is similar to effects observed for films composed of blends of SF and cellulose, where increasing the SF proportion produced increasingly smooth films [157].

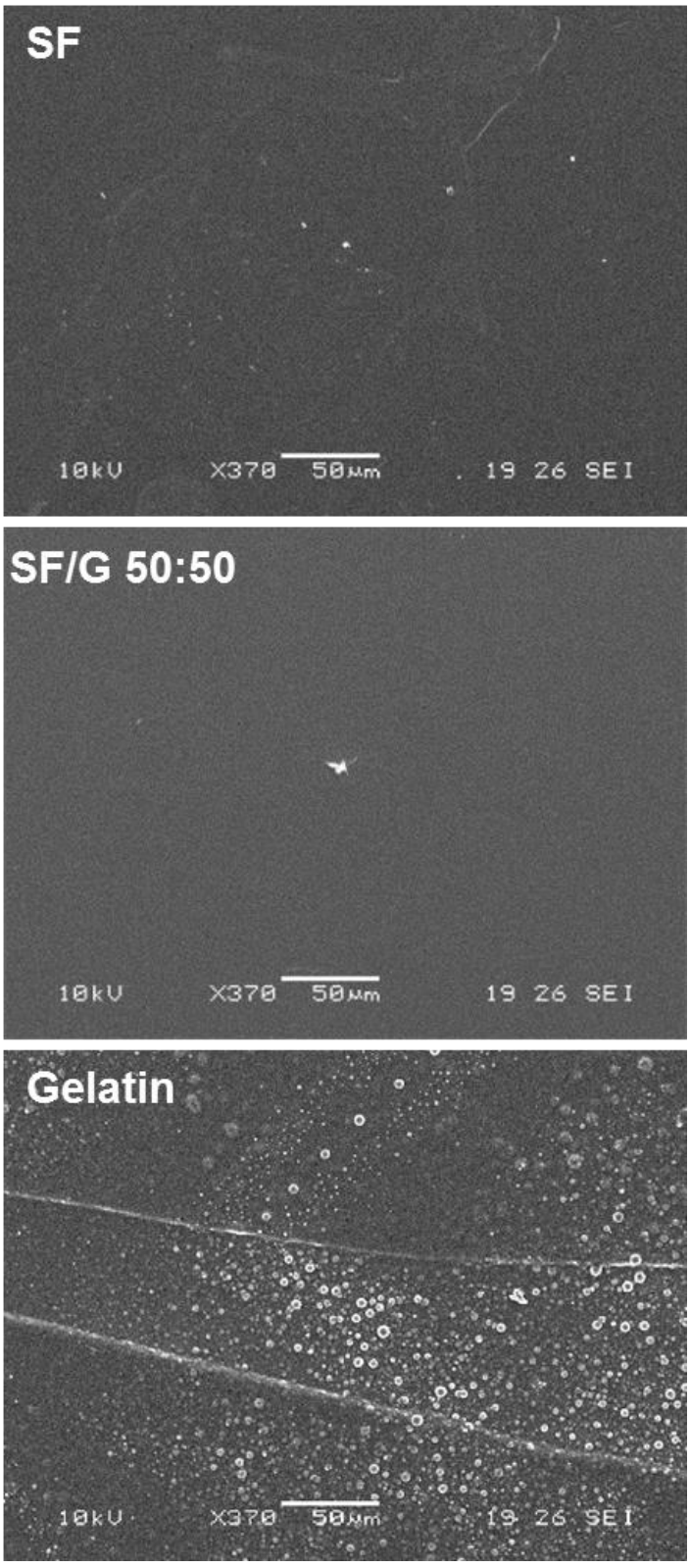

Figure 4.01: SEM images of SF, SF/G 50:50 and gelatin films cast on glass coverslips.

4.3.2. Mineralisation of SF & SF/G films

To investigate whether the SF/G materials would be suitable as scaffolds for bone tissue engineering applications, their ability to support mineralisation was investigated. The predominant mineral component of human bone is carbonated hydroxyapatite. If a material has the appropriate surface properties, it can become mineralised which is highly desirable, as coating polymeric materials with hydroxyapatite improves their integration with native bone, increases cell adhesion and supports the osteodifferentiation of stem cells [162, 163]. *In vivo* mineralisation of extracellular matrix proteins requires a high degree of control over the physical processes related to mineral growth. This is initially mediated by the organisation of collagen fibrils into parallel sheets around anionic spaces, rich in phospho- and glycoproteins, which attract calcium-rich mineral nuclei leading to mineral growth [142, 164].

Films of SF, SF/G 50:50 and gelatin were incubated in a modified simulated body fluid (MSBF) described by Murphy and Moody [142]. Simulated body fluid (SBF) is designed to contain ion concentrations very close to those of human plasma, and the presence of calcium and phosphate ions allows for the spontaneous growth of apatite on bioactive materials incubated in the solution. The development of apatite layers on materials in SBF is an accurate predictor of *in vivo* bone bioactivity [165]. Typical SBF experiments can be time-consuming but by increasing the concentration of calcium and phosphate to produce the MSBF, the apatite coating process is accelerated.

As can be observed in Figure 4.02, the films incubated in MSBF increased in mass while those incubated in dH_2O showed smaller increases or slight decreases. The mass increase indicates a deposition of mineral crystals, also evidenced by the crystals observed on the films in Figure 4.03. The loss of mass in dH_2O-treated samples is likely due to slight damage to the films, especially at the edges, during washing steps.

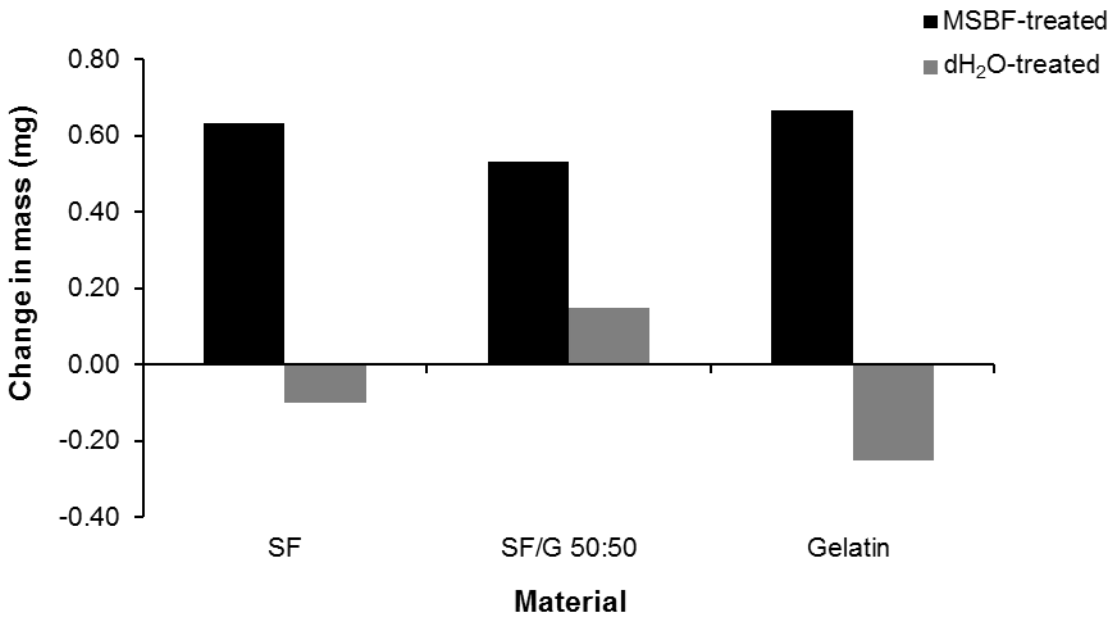

Figure 4.02: Change in dry mass of films incubated in MSBF or dH_2O for 7 days. The average initial mass of the films + coverslips is 41.1 mg. Three films were weighed for each sample type (n=3).

The films were examined by energy dispersive X-ray spectroscopy, and deposits on the MSBF-treated film surfaces gave elemental signals typical of calcium hydroxyapatite, for example calcium, phosphorous and oxygen (Figures 4.03, 4.04 and 4.05). Films incubated in water did not show signals typical of calcium phosphates. The silicon signals in Figure 4.03 spectrum 2, Figure 4.04 spectrum 2 and Figure 4.05 spectrum 1 are likely due to the penetration of x-rays into the glass coverslip underneath the film, while the iron signal in Figure 4.04 spectrum 1 can be attributed to the contaminant particle visible on the film surface, most likely accidentally incorporated during processing for SEM. The SF, SF/G 50:50 and gelatin films all behaved equivalently in this context.

It was reported by Choi et al. that SF particles (of a 1-10 μm diameter) supported the generation of calcium-deficient hydroxyapatite crystals, mediated by negative charges caused by the deprotonation of functional groups on the particle surfaces [166]. It is likely a similar interaction occurs in the SF and SF/G materials described in this thesis. This group also described the effect of pH on mineral deposition, with high pH solutions producing smaller, finer plate-like crystals and lower pH solutions producing larger crystals that were sparsely distributed. The experiment described in this work was carried out using MSBF at pH 6.8, as described by Murphy and Mooney, to prevent the homogenous precipitation of calcium phosphide phases, so the process could be optimised by altering the pH of the solution or even the constituents of it to produce different crystal formations [142].

This experiment shows that SF and SF/G materials are suitable substrates for mineralisation. *In vitro* apatite formation on a material corresponds directly to apatite formation on the same material *in vivo*, and thus accurately predicts the ability of the material to bind to and become integrated with living bone. Materials that do not mineralise may instead become encapsulated in fibrous tissue, isolated from bone [165]. These results therefore strongly suggest that all the materials examined, SF, SF/G 50:50 and gelatin, are suitable for bone tissue engineering applications. The ability of these materials to develop an apatite coating could also be utilised by creating a highly osteo-inductive surface before seeding with osteo-progenitor cells to encourage differentiation.

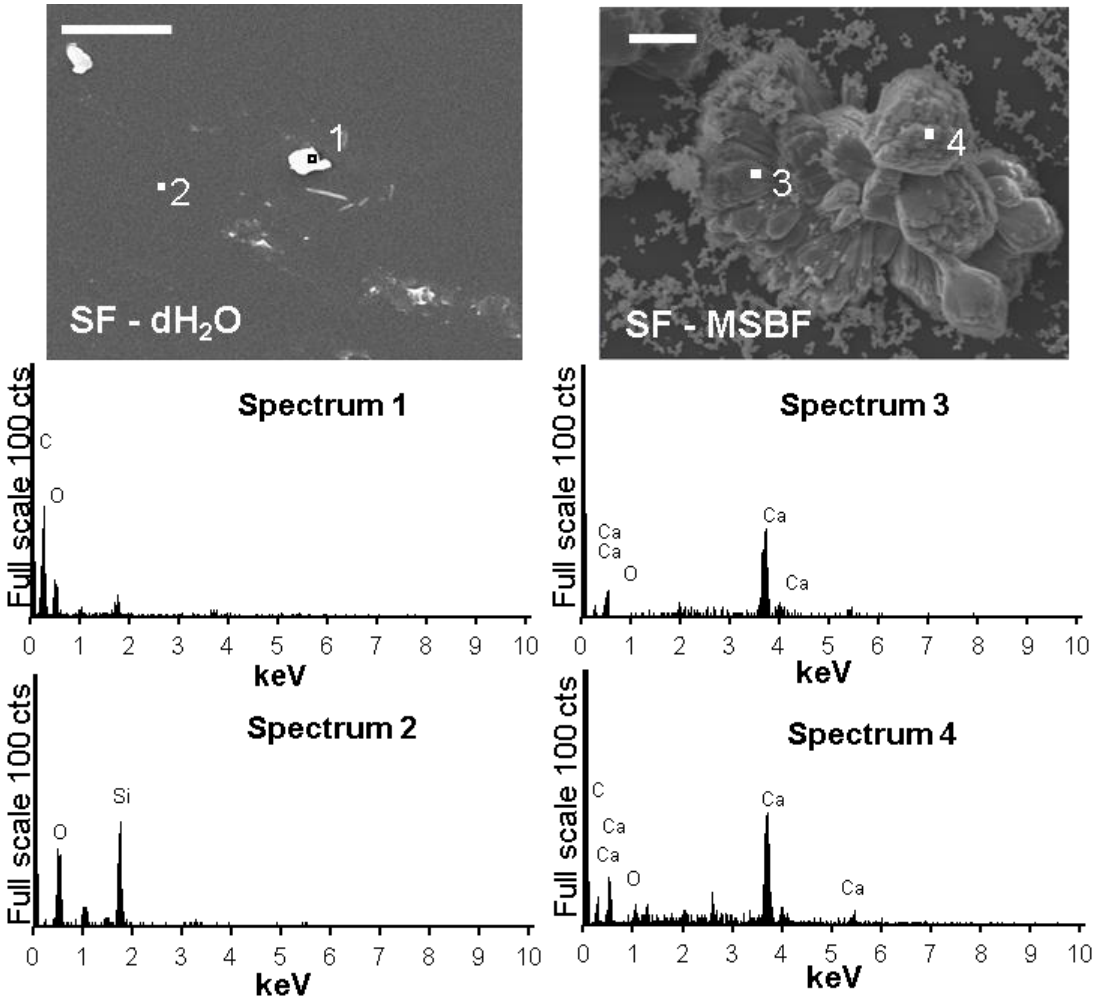

Figure 4.03: Representative SEM images coupled with energy dispersive X-ray spectra of mineral deposits on MSBF- and dH_2O-treated SF films. Scale bars represent 10 μm.

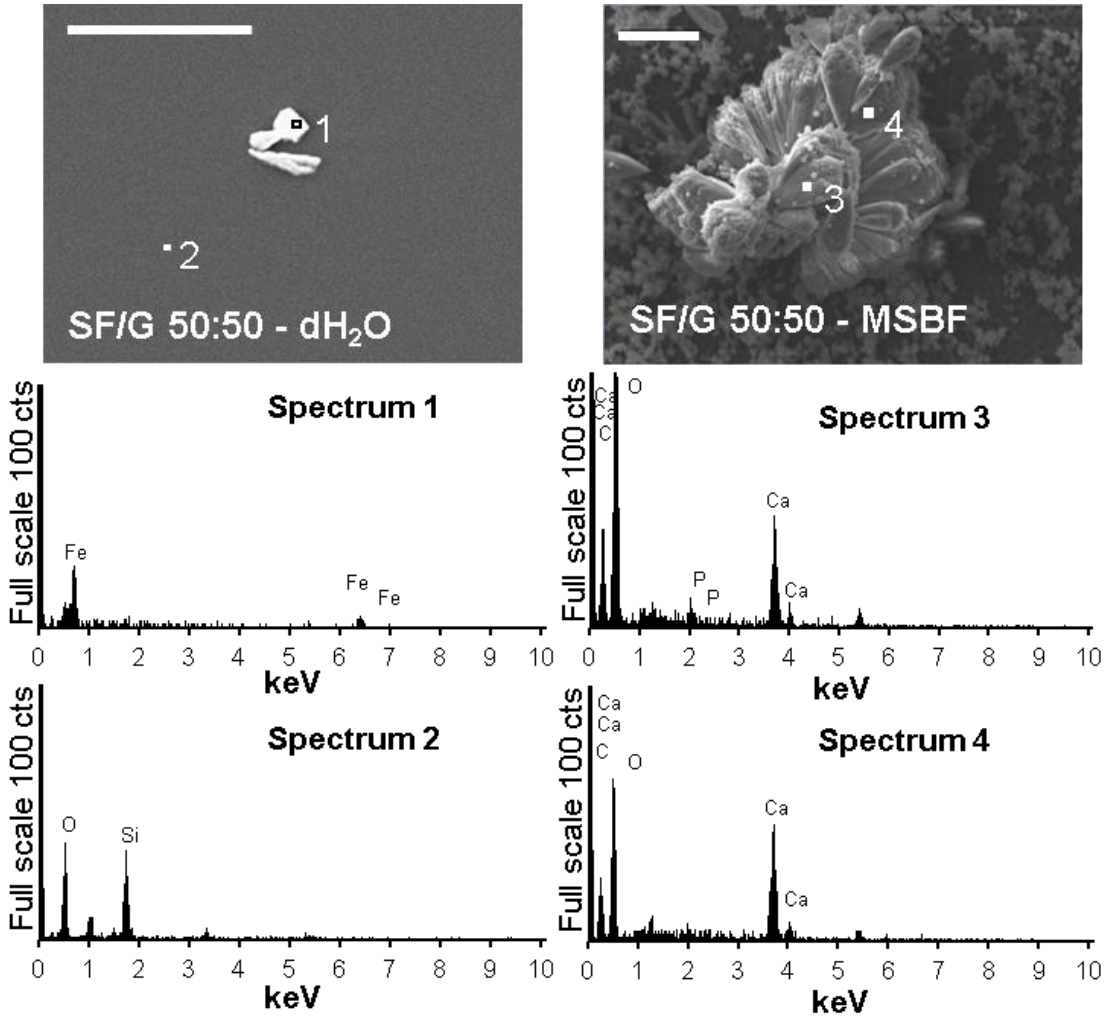

Figure 4.04: Representative SEM images coupled with energy dispersive X-ray spectra of mineral deposits on MSBF- and dH_2O-treated SF/G 50:50 films. Scale bars represent 10 µm.

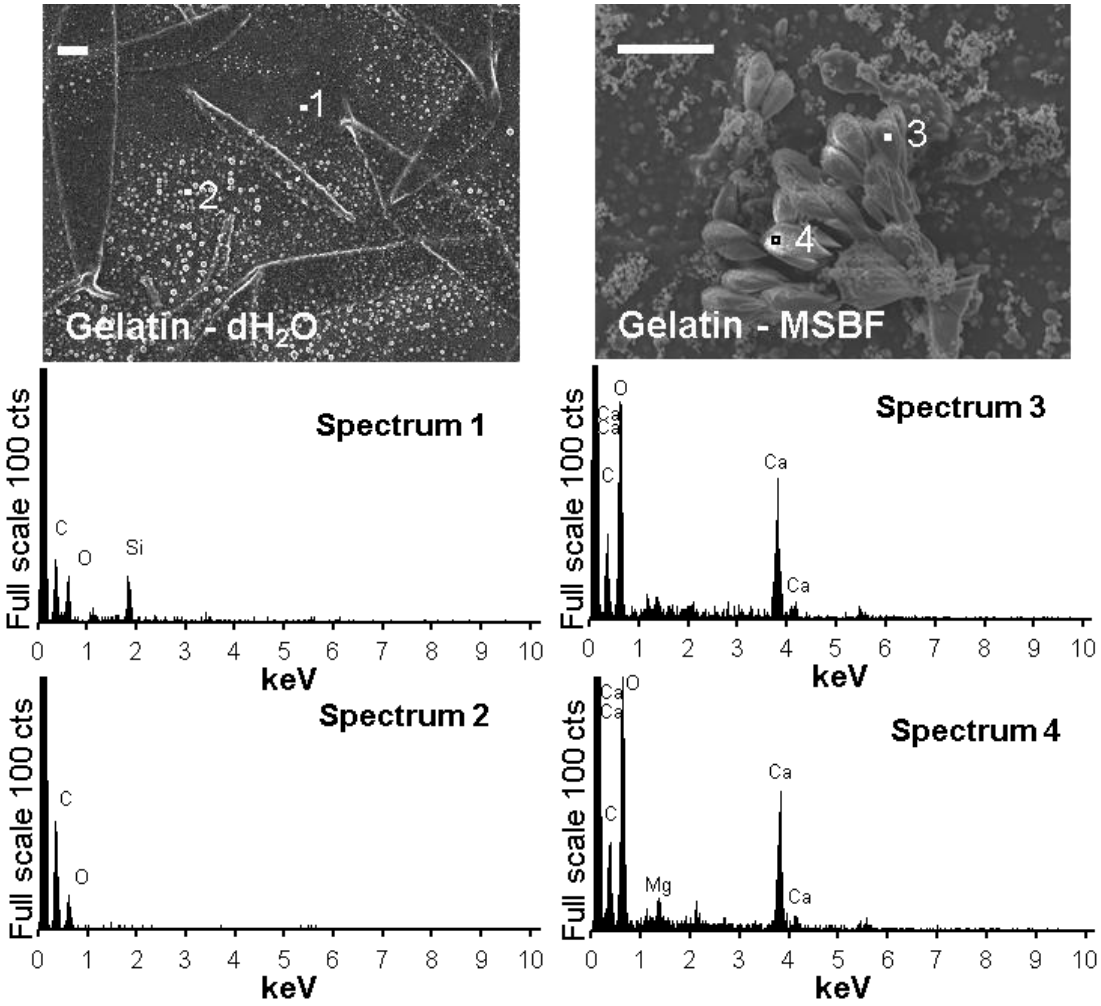

Figure 4.05: Representative SEM images coupled with energy dispersive X-ray spectra of mineral deposits on MSBF- and dH_2O-treated gelatin films. Scale bars represent 20 µm.

4.3.3. Young's modulus of SF, SF/G & gelatin films

The Young's modulus of a material can have a profound effect on the behaviour of the cells grown on it [33, 167, 168]. By matching the Young's modulus of a proposed scaffold to that of the target tissue, the cell response can be optimised by encouraging appropriate differentiation. It has been observed that stiffer cell culture substrates favour osteogenic differentiation of MSCs as the culture environment more closely mimics the bone niche *in vivo.* A Young's modulus of in the region of 30 kPa has been shown to sufficiently rigid as to induce osteogenic differentiation, with increasing rigidities resulting in more advanced differentiation [33, 169].

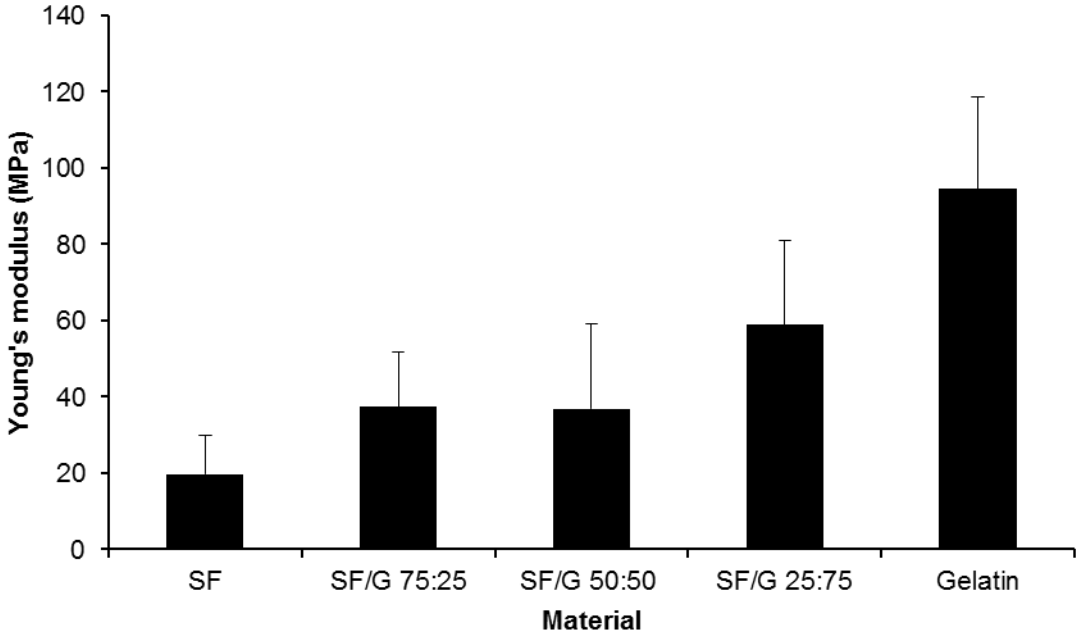

Figure 4.06: Young's modulus of SF, SF/G and gelatin films (10 x 20 mm) determined by tensile testing. Data shown represents mean + standard error (n=3).

SF/G materials were analysed by tensile testing, wherein films cast from SF, SF/G blends and gelatin were clamped between two vices and uniaxial force was applied to stretch the films until failure. The results are shown in Figure 4.06. Unexpectedly, SF films gave the lowest values of Young's modulus at 19.8 MPa, suggesting these are the least rigid of the materials tested. The value observed for SF is consistent with previously reported values: SF films cast from 5% w/v solutions (in formic acid) were found to have Young's modulus values of ~35 MPa [170]. Although no statistical significance was observed, a trend of increasing rigidity with increasing proportion of gelatin is apparent.

The value obtained for gelatin is difficult to compare to literature values, since different cross-linking protocols result in different stiffnesses. Cross-linked gelatin films have variously been reported as having Young's moduli of 2.7-4.9 GPa [158], 10-30 MPa [171], 4 MPa [101] and 20 kPa – 1MPa [172]. The value of 94 MPa measured here is within this wide range of values. It is also potentially useful to be able to control the stiffness of gelatin across such a wide range by altering the cross-linking protocol.

The stiffness of human cortical bone is reported as ranging between 10 MPa and 40 GPa [167, 173]. The results obtained here put all of the SF/G materials within this range, confirming the potential of SF/G blends as scaffolds for osteogenic tissue engineering. However, these data relate to SF/G films and not any other form of scaffold, which should

be tested independently. It is also important to note that due to practical limitations, the films were dry when tested, but for biological applications are likely to be wet. Literature evidence suggests that for SF and similar materials, such as spider dragline silk and keratin, mechanical properties, such as Young's modulus, are reduced when wet [174, 175]. It has been observed than SF scaffolds have lower compressive moduli when wet compared to their dry state, and wet regenerated SF fibres tested by Plaza et al. also showed a significance decrease in stiffness and tensile strength from the values measured for their dry counterparts [176, 177]. It is therefore likely that the values obtained in Figure 4.06 would decrease for the same materials in wet conditions.

4.3.4. Seeding fibroblasts on SF- & SF/G-coated tissue culture plastic

To confirm the biocompatibility of SF materials, 3T3 fibroblasts were seeded onto SF and gelatin coated surfaces. 3T3 fibroblasts proliferate more rapidly than harvested rMSCs, and can be used to a higher passage number [178, 179]. They are therefore a useful tool for preliminary experiments of this sort. In this experiment, the protein solutions of SF, SF/G and gelatin were adsorbed onto tissue culture plastic (TCP). Cells were seeded and after three days, cell metabolic activity was measured using the MTS assay as a measure of relative cell number. The results were confirmed visually.

The data shown in Figure 4.07 suggests that SF itself does not strongly support the adhesion or proliferation of 3T3 fibroblasts, contrary to many reports in the literature. Many groups have reported good cell attachment to a variety of reconstituted *Bombyx mori* SF scaffolds, with cells ranging from fibroblasts to bone marrow-derived MSCs [77, 153, 156]. This quality has been attributed to the presence of positively charged amino acid residues in the SF sequence which interact favourably with the negatively charged surface of mammalian cells [75]. One reason for this discrepancy could be the variety in sources of silk cocoons, as there are reportedly over 3,000 different strains of *Bombyx mori* and the exact strain used is not frequently known [67]. Indeed, there is evidence to suggest that different *Bombyx mori* strains produce silks with different compositions, affecting both cell adhesion and differentiation [66].

However, it was found that by mixing SF solution with gelatin, cell adhesion was significantly increased. This is most likely due to the presence of the RGD tripeptide in gelatin which is recognised by cell integrin receptors and implicated in cell attachment [101, 102]. SF and gelatin were blended in three different ratios (SF:G 75:25, 50:50, and 25:75) and these were

shown to be equivalent to gelatin alone in terms of cell attachment. The blends outperformed TCP, suggesting that these materials were a suitable candidate for tissue engineering scaffold materials, at least in terms of their biocompatibility and cell adhesion properties.

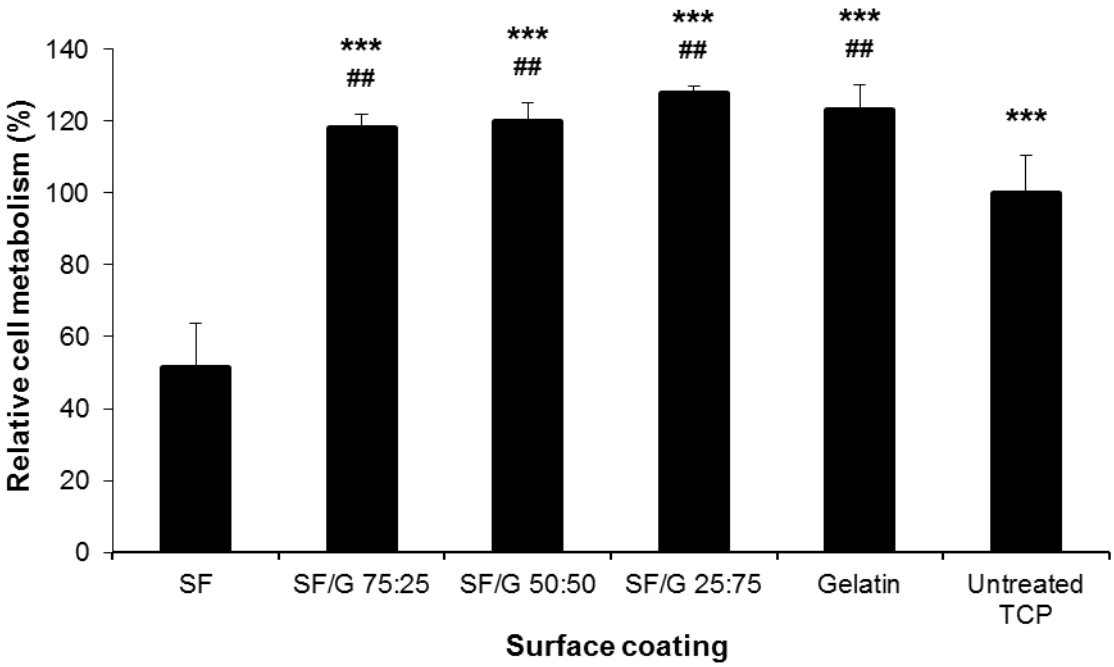

Figure 4.07: 3T3 fibroblast metabolism assessed 3 days after seeding. Values are expressed as a percentage of the signal obtained for the control (untreated TCP). Higher values suggest higher cell viability on the substrate in question. Data shown represents mean + standard error (n=4). *** p<0.001 w.r.t SF alone. ## p<0.01 w.r.t untreated TCP.

4.3.5. MSC harvest and identification

MSCs were harvested from rat bone marrow by their selective adhesion to tissue culture plastic [180]. After one passage, cells underwent fluorescence-activated cell sorting (FACS) analysis to collect a population positive for the MSC markers CD90 and CD54, and negative for the leukocyte marker CD45 [137]. Extracting MSCs from bone marrow means there is a high risk of haematopoietic cells contaminating the culture, but by excluding CD45-positive cells this can be avoided. By selecting cells positive for MSC markers, the identity of the cell type is confirmed. In this case, cells were labelled for the intercellular adhesion molecule CD54 (or ICAM-1) and the extracellular CD90 (or Thy-1) protein. The population identified as dual positive for CD90 and CD54, population ‘Q2’ as shown in Figure 4.08, was collected and cultured. In the example shown, the ‘Q2’ dual positive population made up 94.3% of the total cell number, showing that simply selecting MSCs by their adhesion to TCP provides

an efficient method for collecting these cells. The average dual positive proportion of the population was 88.5 ± 7.3% (mean ± SD, n=5).

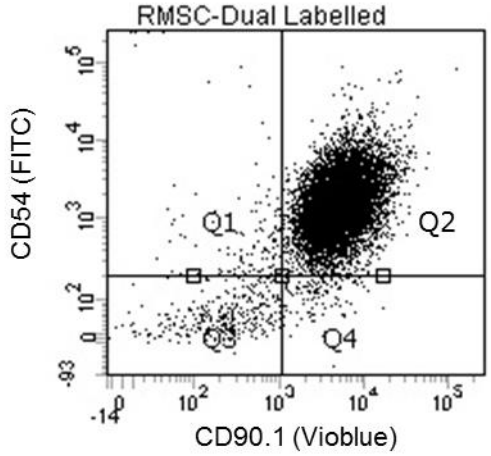

POPULATION	# EVENTS	% PARENT	CD54 (FITC)	CD90.1 (VIOBLUE)	CD45 (PE-CY7)
All events	10,000	n/a	2,281	5,563	811
Q2	9,426	94.3	2,254	5,835	711

Figure 4.08: rMSCs sorted by the presence of the MSC markers CD54 and CD90.1. Anti-CD54 was conjugated to FITC; anti-CD90.1 was conjugated to Vioblue. The table shows the number and proportion of cells sorted into population Q2 and the relative signals obtained for each fluorescently labelled antibody.

The multipotent properties of the collected cells were confirmed through standard tri-lineage differentiation assays. Cells were cultured in adipogenic, chondrogenic or osteogenic conditions and analysed by staining with Oil Red O for intracellular lipid droplets, Toluidine Blue for cartilage and Alizarin Red for mineralisation respectively. The results are shown in Figure 4.09 and demonstrate that the putative rMSCs were capable of differentiation down adipogenic, chondrogenic and osteogenic pathways. The cells grown under adipogenic conditions show the presence of intracellular lipid droplets typical of adipocytes, while cells grown under osteogenic conditions have organised themselves into discreet, mineralised nodules typical of osteoblasts. The small purple region in the Toluidine Blue-stained image indicates the presence of proteoglycans, a major component of cartilage. Although this a small proportion of the visible section, this could be a result of the culture conditions: while the adipogenic and osteogenic cultures were grown in monolayers, the chondrogenic

differentiation assay requires cells are grown in a pellet. The pellet must then be fixed, embedded in wax and sliced before staining. It is therefore possible the proteoglycan positive region extended in a direction perpendicular to the slice. It is also possible that the pellet had not been cultured long enough to fully differentiate or for the cells to deposit chondrogenic extracellular matrix. It could be a result of bone marrow-derived MSCs having poorer chondrogenic potential compared to MSCs from other sources, such as synovium [181]. The results observed are nonetheless sufficient to confirm the identity of the harvested cells as MSCs.

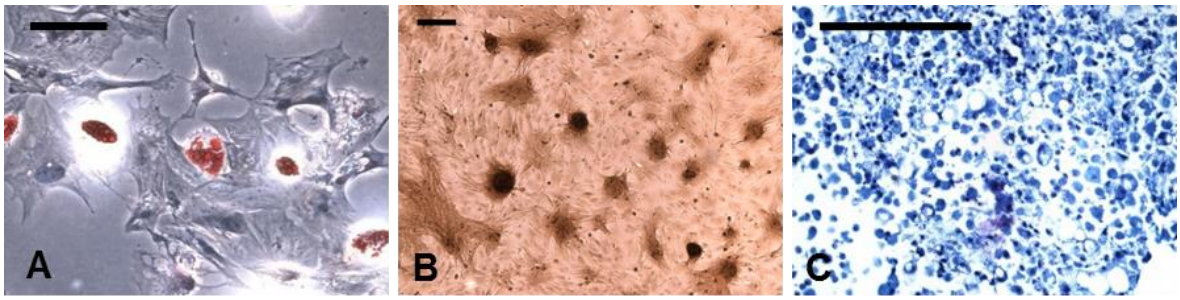

Figure 4.09: rMSCs differentiated down three distinct pathways. (A) rMSCs that underwent the adipogenic differentiation protocol stained with Oil Red O. (B) rMSCs treated with osteogenic media stained with Alizarin Red. (C) rMSCs treated according to the chondrogenic differentiation protocol stained with Toluidine Blue. Scale bar in (A) represents 100 µm; scale bars in (B) and (C) represent 200 µm.

4.3.6. Adhesion of rMSCs to films of SF & SF/G materials

After the preliminary results using fibroblasts were obtained, the adhesion experiment was repeated using rMSCs seeded onto SF/G films cast from 2% HFIP solutions (examples of which are shown in Figure 4.01). Whereas the initial experiment using adsorbed protein was sufficient to test biocompatibility of the materials in question, the films were used to examine the behaviour of cells on SF/G materials fully in contact with these materials. The results are shown in Figure 4.10, and confirm that rMSCs remain viable when seeded onto SF/G material blends. As observed with 3T3 fibroblasts (Figure 4.07), the cells show very low metabolism on SF films. This could be due to their initial poor adhesion to the surface, resulting in lower numbers of cells in the SF samples. Unexpectedly, the rMSCs also showed relatively low metabolism in the wells coated with gelatin. Gelatin is sometimes adsorbed onto plasticware to increase cell adhesion and so it would be expected that cells would adhere well and show higher metabolism on gelatin films. The low level observed

here could be a result of the thin films of gelatin absorbing a large volume of media and thus becoming very soft.

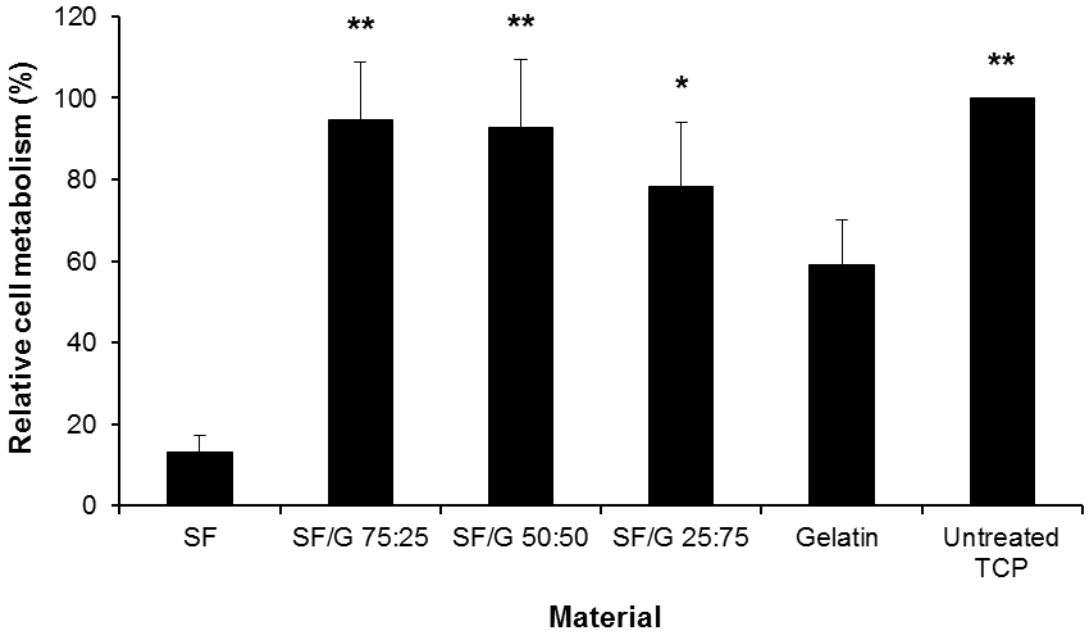

Figure 4.10: rMSC metabolism assessed 3 days after seeding. Values are expressed as a percentage of the signal obtained for the control (untreated TCP). Higher values suggest higher cell adhesion to the substrate in question. Data shown represents mean + standard error (n=4). * $p<0.05$ w.r.t SF alone. ** $p<0.01$ w.r.t SF alone.

Swelling of gelatin in physiological conditions is well documented and the level of hydration affects its physical properties [182]. The more liquid it absorbs, the softer the structure. Cross-linking can decrease swelling by reducing the number of hydrophilic groups in the structure (EDC cross-linking consumes amino groups), but cross-linked gelatin is still prone to swelling [183, 184]. SF has a more hydrophobic character and thus is less likely to absorb liquid from aqueous solutions [185]. This behaviour does not reflect the results obtained from tensile testing (Fig. 4.06), wherein gelatin appeared to be the most rigid of the materials in question. However, as described previously, that data was collected using non-hydrated films. To measure the hydrated stiffness of these materials a different method would be required, such as indentation atomic force microscopy.

In Figure 4.10, the blends of SF/G all show improved cell viability at the day 3 time point over SF and gelatin alone. For the SF/G blends, there does appear to be a slight trend of improved cell viability with increasing proportion of SF, despite the very low metabolism observed for SF alone. This could be the effect of a balance between the availability of RGD

residues provided by gelatin and the beneficial effects of SF on the mechanical properties of the films themselves. In the absence of RGD, the rMSCs may struggle to adhere to the material surface, resulting in the very low values seen for SF. However, blends with high proportions of gelatin could suffer from reduced mechanical properties, hindering cell proliferation.

Nonetheless, the results shown here continue to support the use of SF/G blends as scaffold materials, as they allow for greater cell adhesion and viability than either SF or gelatin alone in this case. Cells grown on SF/G films show a similar level of cell metabolism to those on TCP. These results are consistent with literature reports of SF and gelatin blended scaffolds, in which the blended materials show improved biological properties over SF alone (Table 4.01).

4.3.7. Proliferation of rMSCs on SF, SF/G & gelatin films

Having established that rMSCs would adhere to and remain viable on SF/G materials, cell proliferation was investigated over a 7 day period. Again, rMSCs were seeded onto films of SF, SF/G and gelatin, but on this occasion were cultured for 7 days and assayed using resazurin at days 1, 4 and 7. The results are shown in Figure 4.11.

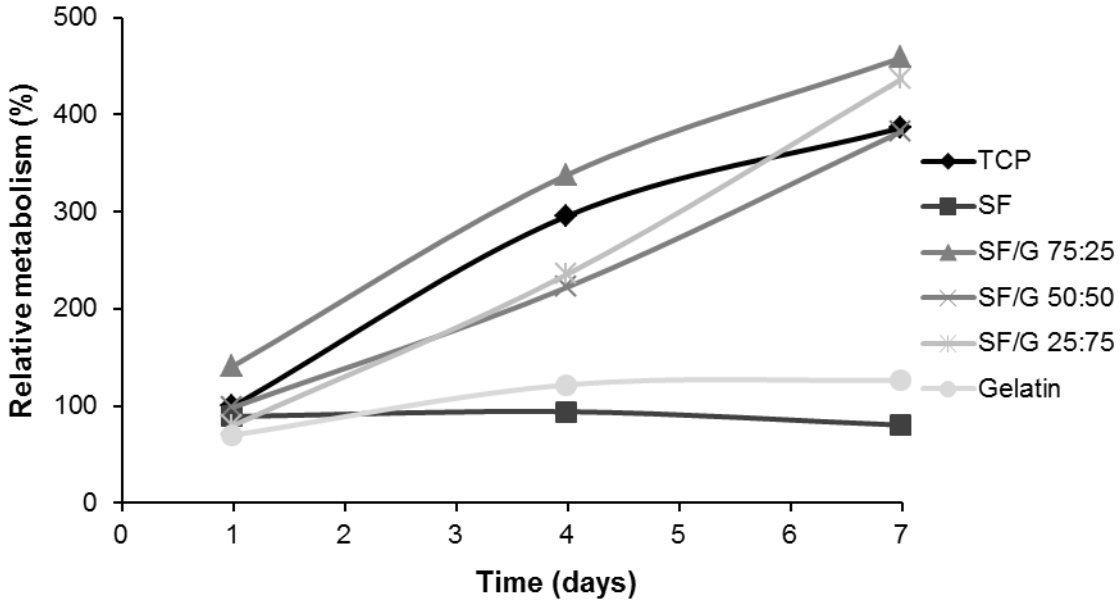

Figure 4.11: Proliferation of rMSCs on films of SF/G blends, measured by reduction of resazurin. Data is presented as the percentage of signal compared to that of TCP at day 1. Data shown represents the mean value (n=3).

Mirroring the previous results, the rMSCs showed consistent proliferation over 7 days when grown on films composed of SF/G blends at a level almost equivalent to those grown on TCP. Predictably, rMSCs grown on SF films did not show an increase in cell number, confirming yet again that SF alone is not a good candidate for a scaffold material. However, rMSCs on gelatin films also showed a low level of proliferation. Gelatin is known to support cell growth and proliferation, and so these results are unexpected, but consistent with the results observed in Figure 4.10. Again, a possible explanation is that the gelatin films absorb more liquid than SF/G films, and thus become very soft, inhibiting cell proliferation. However, it is encouraging that the blended SF/G films all show better properties than SF or gelatin alone. There was not a significant difference in performance between the three blends of SF/G; they all supported cell proliferation at a level equivalent to the TCP control, and greater than SF or gelatin alone. Again, this is likely due to the benefit of combining the materials: while gelatin provides cell adhesion sequences, SF prevents excessive hydration and softening of the film.

4.3.8. Osteodifferentiation of rMSCs on SF, SF/G & gelatin films

The ability of the SF/G materials to support osteodifferentiation was investigated by culturing rMSCs, seeded on SF/G films, in osteogenic differentiation media (ODM).

Normally osteogenesis is assessed by staining for mineralisation of cell cultures, for example with Alizarin Red or Von Kossa. However, this was not appropriate in these experiments due to the high level of background staining that the SF/G films developed in the absence of cells. It was therefore necessary to use other methods to analyse osteodifferentiation.

Alkaline phosphatase (ALP) is an enzyme that is present in most cells of the body but is particularly elevated in certain cell types, particularly osteoblasts [186]. ALP activity is commonly used to show evidence of osteodifferentiation in MSC cultures and it has been reported for mouse MSCs that ALP-2 protein is expressed continuously over 28 days of osteodifferentiation [187]. In the NBT/BCIP (nitro-blue tetrazolium chloride/5-bromo-4-chloro-3'-indolyphosphate p-toluidine salt) assay, the action of ALP results in the production of an insoluble blue precipitate from the initial pale yellow solution.

rMSCs seeded onto SF/G films in 96 well plates were cultured for 14, 21 and 28 days in either ODM or unsupplemented basal media, and after each of these time points cultures were assayed for ALP activity. A set of typical results from one of these assays in shown in

Figure 4.12. Although there is evidence of ALP activity in cells grown on SF/G materials, those cultured in basal media appear to have produced more of the blue formazan product than those cultured in ODM. However, this is not a quantitative assay so reading too much into the relative levels of 'blueness' is to be avoided. One possible explanation for the results observed is that the cells cultured in basal media undergo spontaneous low-level differentiation causing the cells to produce ALP. Meanwhile, the cells in ODM are prompted to full differentiation by the presence of the osteogenic supplements in the media, and differentiate fully, rearranging themselves into dense bone nodules, where ALP activity in the well is focussed. This causes small dark blue regions, as observable for SF/G materials in ODM, day 28, in Figure 4.12, rather than the widespread blue colouring observed for the less fully differentiated rMSCs in basal media.

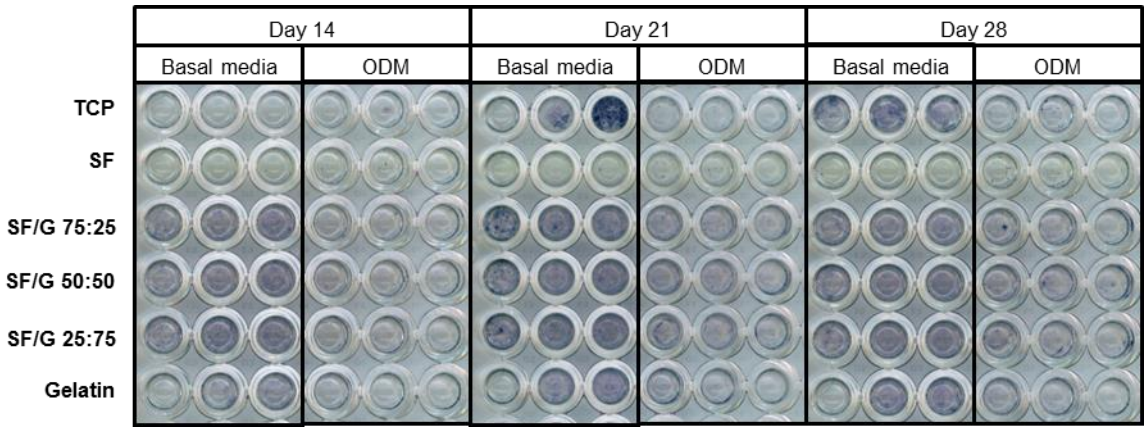

Figure 4.12: rMSCs cultured on SF/G materials for 14, 21 and 28 days stained for alkaline phosphatase activity. ALP activity is indicated by the presence of insoluble blue deposits.

An alternative, and preferably quantitative, method of analysis for osteogenesis was sought. The In Cell Western Assay was chosen as it would allow for the quantification of osteocalcin, with the ability to normalise data by relative cell number. Osteocalcin (sometimes called bone gamma-carboxyglutamic acid-containing protein) is a well-defined marker of osteogenic maturation, as it is produced solely by osteoblasts [188]. rMSCs were again cultured on SF/G films for 14, 21, and 28 days in either basal media or ODM before fixation, permeabilisation, and labelling with anti-osteocalcin antibody. The results of these experiments are shown in Figures 4.13 and 4.14. The results for cells grown on SF or gelatin coatings are not included in the data below, since their poor capacity to support cell proliferation hindered any potential differentiation.

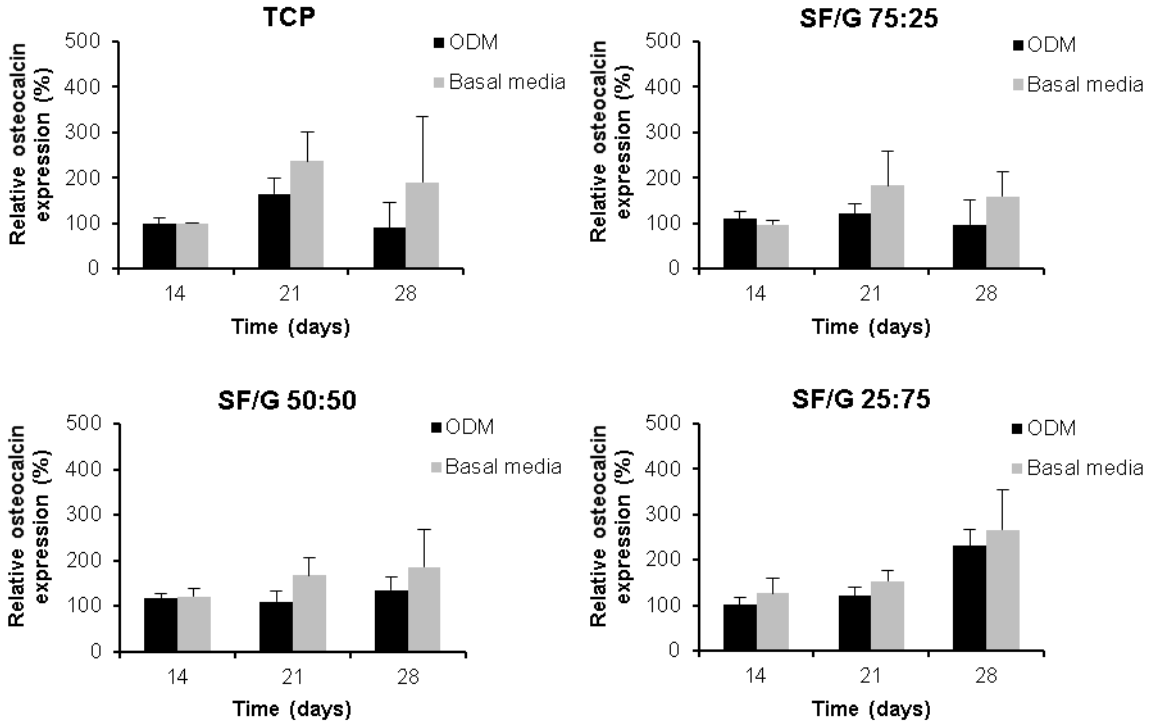

Figure 4.13: Relative expression of osteocalcin in rMSCs grown on SF/G materials over 28 days, cultured either in basal media or ODM. The data shown is normalised by relative cell number and expressed as a percentage of the signal observed for rMSCs on TCP at day 14 in basal media. Data represents mean + standard error (n=3).

The levels of osteocalcin expression would be expected to be highest in cultures grown in ODM, and to increase with time, since the cells would have had longer to deposit osteocalcin alongside other extracellular matrix proteins.

The results in Figures 4.12 and 4.13 are consistent to a certain degree. It appears in both cases that there is a higher level of differentiation in the rMSCs cultured in basal media, rather than ODM, indicated by the 'bluer' colour caused by higher ALP activity in Figure 4.12 and the higher osteocalcin expression in Figure 4.13. This counters the earlier suggestion that the increased deposition of the ALP reaction product from rMSCs in basal media could be due to widespread, low level differentiation, compared to controlled, specific differentiation of rMSCs grown in ODM. If it were the case that the cells in ODM had undergone more advanced osteogenic differentiation, it would be expected that the levels of osteocalcin, a late differentiation marker, would be much higher in these cultures than those in basal media. However, this is not the case. It is worth noting that the differences in osteocalcin expression between cells grown in basal media and ODM are not statistically significant.

The osteogenic differentiation of MSCs can typically be divided into three stages. The first stage, typically between days 0 and 4, consists primarily of cell expansion and cell numbers peak during this time. The second stage, days 5 to 14, involves early cell differentiation and is typified by high ALP expression which reaches a peak during this phase, and then begins to decline. The final stage, from day 15 onwards, consists of terminal differentiation and matrix maturation. The main markers of this stage are osteocalcin, osteopontin and mineral deposition [187, 189].

For rMSCs grown on SF/G 50:50 and 25:75, osteocalcin expression does seem to increase slowly over time, but for the cells cultured on TCP and SF/G 75:25, osteocalcin expression unexpectedly peaks at day 21. This is mirrored in the observed ALP activity, at least for the cells grown in basal media. However, to gain a better understanding of ALP activity within these cultures, the experiments should be repeated using a quantitative method of detection, such as colorimetric hydrolysis of *p*-nitrophenyl phosphate to *p*-nitrophenol or reverse transcription PCR.

Expression of osteocalcin appears fairly low across all materials. Nonetheless, it is encouraging that the SF/G 25:75 cultured cells show higher osteocalcin expression than TCP particularly at day 28, in both ODM and basal media. This is shown in Figure 4.14, which shows only the data from the cells grown in ODM.

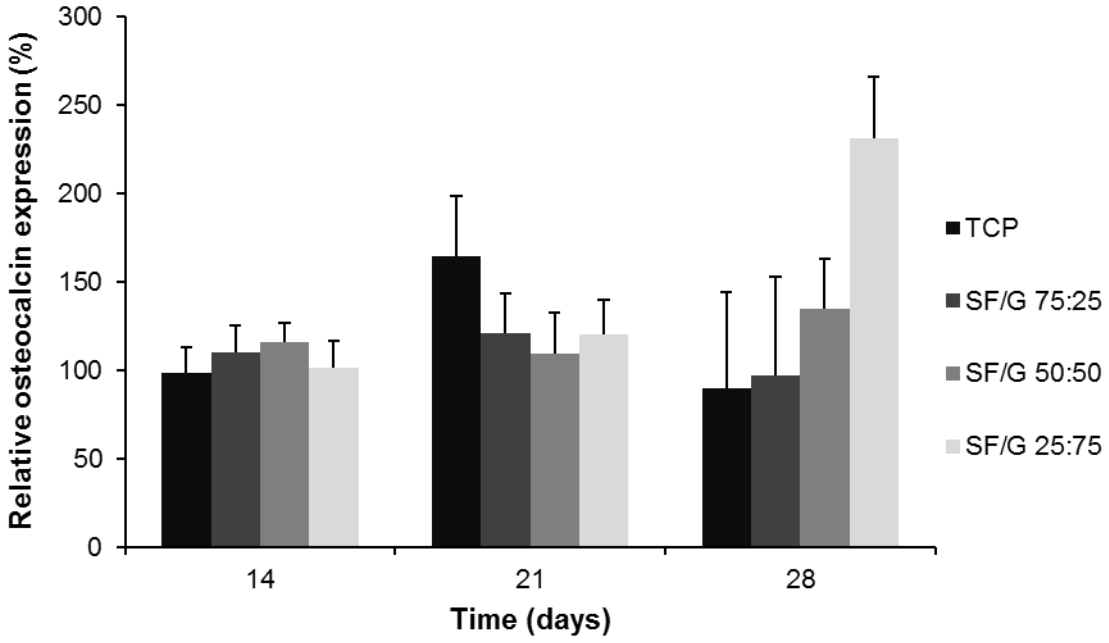

Figure 4.14: Relative expression of osteocalcin in rMSCs grown on SF/G blended films in ODM for 14, 21 and 28 days. The data is expressed as a percentage of the expression in rMSCs grown on TCP in basal media at day 14. Data shown represents mean + standard error (n=3).

Since this data appeared to contradict the well-established understanding that ODM should increase osteogenic differentiation relative to unsupplemented basal media, a third method of analysis was pursued to confirm the osteogenic differentiation of rMSCs on SF/G materials.

A third marker of osteogenesis is osteopontin (or bone sialoprotein I), an osteoblast-secreted protein with roles in biomineralisation and bone remodelling. Levels of osteopontin in culture media were measured using an ELISA and normalised by cell number. Due to time and cost constraints, these cultures were analysed at day 14 only. The results are shown in Figure 4.15. As discussed, this is a relatively early time point for a mature marker of osteodifferentiation and it is possible that higher levels of osteopontin expression would have been observed at later time points.

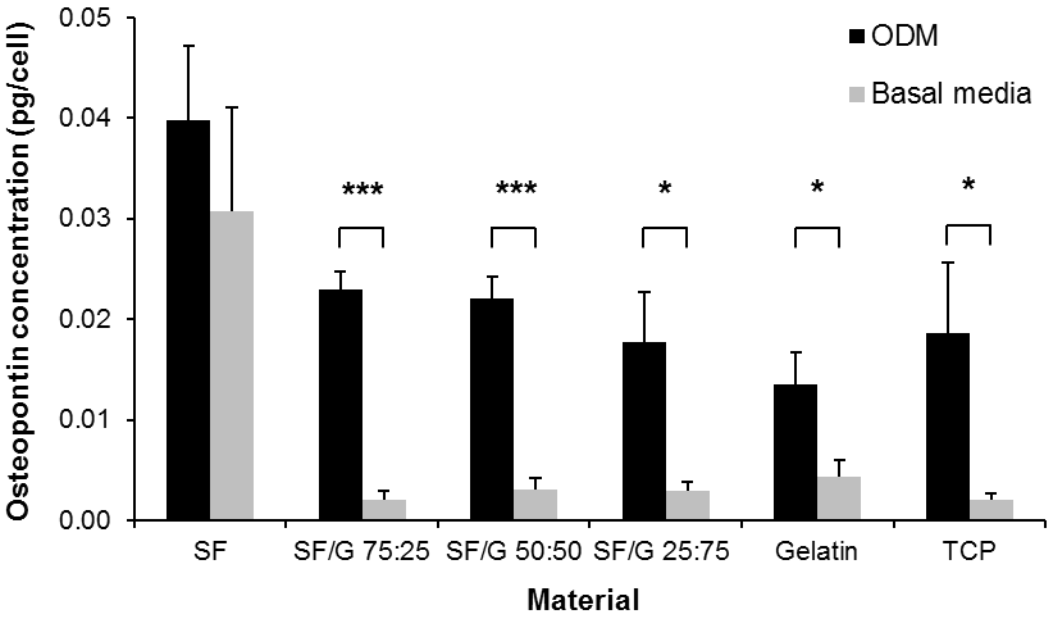

Figure 4.15: Expression of osteopontin from rMSCs grown on SF/G films for 14 days. The data shown represents mean + standard error (n=3). ** represents p<0.001, * represents p<0.05.

Unlike the data obtained for expression of osteocalcin and ALP, the expression of osteopontin is significantly higher in cells grown in ODM than in unsupplemented basal media. A notable result from the expression of osteopontin is the relatively high expression from cells grown on SF surfaces. While SF supports cell attachment very poorly, for those cells that do adhere, the surface appears to be strongly osteogenic. This is not the case for gelatin, which shows the lowest level of osteopontin expression of all the materials tested. This is consistent with previous results in this work, showing poor rMSC adhesion and proliferation on gelatin and SF films (Figures 4.10 and 4.11).

For the cells grown in ODM, levels of osteopontin expression are equivalent between the various SF/G blends and TCP. This is consistent with the expression of osteocalcin detected at day 14, in Figure 4.14. There is a slight trend between increased SF proportion and increased osteopontin expression in Figure 4.15 but more replicates would be required to establish significance in this case. Taken together, the results for rMSCs differentiated on SF/G materials suggest that SF/G blends support osteogenesis at a level equivalent to TCP, but the effect of media supplements is unclear.

There is a small selection of papers reporting the successful osteogenic differentiation of both human and rat bone marrow derived MSCs on SF and SF-blended scaffolds which strongly suggest SF materials are capable of supporting this process. Examples include SF/chitosan nanofibres produced by Lai et al., and gelatin-coated SF porous scaffolds from Wongputtaraksa et al. (though in this case it is unclear if the cells themselves interact with the SF) [89, 190]. In another example, Vorrapakdee et al. used coatings of Thai silk and gelatin to modify decellularised bone samples, resulting in higher levels of calcium deposition and ALP activity from differentiating rMSCs. This technique could be useful in the optimisation of allografts, but was not compared to the effects of Thai SF or gelatin alone [191]. Human nasal inferior turbinate tissue derived MSCs encapsulated in SF/G bio-ink were also shown to be capable of osteogenic differentiation, as evidenced by increased expression of RUNX2, ALP and osteopontin [192]. A number of reports also claim SF alone is capable of supporting osteogenesis, though in the case of Meinel et al. the hMSCs themselves were entrapped in Matrigel within a silk sponge, so again the contribution of the SF itself is questionable [193]. This report, and others, employed BMP-2 to direct osteogenesis, an expensive supplement not used in this work [80, 156, 194, 195].

The SF-blended examples cited here are generally in 3D structures, rather than 2D films, and this could be a crucial factor in the ability of cells to differentiate on these materials. While cells grown in 2D environments are frequently used for quantitative assays, it is generally accepted that cells in 3D cultures behave much more like their native counterparts in physiological tissues [196, 197]. Cell behaviour is dependent on a number of factors, such as mechanical and biochemical cues, tissue-specific architecture, and cell-cell interactions. These signals are oversimplified in 2D cultures, and this can affect protein expression, cell migration and apoptosis [198, 199]. It therefore seems reasonable to suggest that the differentiation of MSCs might also be affected.

The evidence obtained in this chapter suggests that SF/G materials are capable of supporting osteogenic differentiation, in particular the blend of SF/G 25:75, and there is sufficient evidence to warrant further investigate these materials in a 3D format.

4.4. Conclusions

In this chapter, the properties of SF and SF/G films have been investigated in a 2D format. It has been shown they are capable of becoming mineralised, and in the form of thin films, have Young's moduli equivalent to human bone. While SF alone has poor cell adhesion, this is greatly improved in SF/G blends (SF:G 75:25, 50:50 and 25:75), which also support cell proliferation over 7 days.

Blends of rMSCs were successfully isolated from the bone marrow of juvenile Wistar rats and shown to be capable of multi-lineage differentiation. Osteogenic differentiation was shown to take place on SF/G materials, despite the uncertainty surrounding the efficacy of basal media compared to ODM.

The osteogenic differentiation of bone marrow derived rMSCs on blended *Bombyx mori* SF and gelatin scaffolds has not been previously reported. The results obtained using 2D films of the SF/G blends show that the combination of SF and gelatin produces scaffolds with improved Young's moduli and improved abilities to support cell adhesion and proliferation, over SF or gelatin alone. The next chapter will therefore investigate the translation of these blended materials into 3D formats.

Chapter 5

SF/G microparticles as osteogenic building blocks for tissue engineering

5.1. Introduction

SF/G scaffolds for tissue engineering

Blends of SF and gelatin have been shown to have both mechanical and biological properties greater than each material alone, as described in Chapter 4. This is reinforced by a number of literature reports of the benefits of combining the two (see Table 4.01). In short, it has been shown that incorporating even small percentages of gelatin into a SF structure significantly improves cell attachment and proliferation [159, 160]. At the same time, the recorded tensile strength of SF/G films, and compressive strength of SF/G discs, are increased over SF alone [84, 158]. These results are summarised in Table 4.01. SF/G blended scaffolds have been shown to support the osteodifferentiation of mesenchymal stem cells, though in the case of reports from Vorrapakdee et al. and Wongputtaraksa et al., SF was derived from Thai silk, from the *Nangnoi srisaket* silkworm rather than the more common *Bombyx mori* [190, 191]. While osteogenic differentiation was observed in human mesenchymal progenitor cells encapsulated in sonication-cross-linked SF/G scaffolds, these scaffolds were not stable in cell culture media [192]. There is no evidence that bone marrow derived MSCs have been cultured on three-dimensional SF/G microparticle scaffolds for the purpose of osteodifferentiation, though the two-dimensional results from Chapter 4 suggest that these blended materials do support osteogenic differentiation.

Microparticles & three-dimensional tissue constructs

While most SF-based scaffolds have taken the form of freeze-dried, porous discs, this approach is limited. This top down approach to scaffold design can be problematic in terms of ensuring even cell distribution through the structure, as cells will naturally settle and adhere on the outer edges. Initially this is due to the increased accessibility of the outer regions, but even where cells do migrate into internal regions, viability can be compromised by lack of oxygen and nutrient supply, and build-up of waste products.

Instead of starting with a relatively large scaffold, an alternative approach is to seed cells onto much smaller units of scaffold material. In this way, cells are provided with a large surface area for attachment, increasingly the likelihood of even cell distribution. These cell-

laden scaffold units can then be built up into larger shapes, utilising cell-cell and cell-scaffold interactions to bind the structure together. This promise of this bottom up approach has been demonstrated by several groups, frequently starting with microparticles as the initial scaffold unit and moulding them together to form macroscopic tissue constructs [30, 57]. Their small size means that they can also act as injectable cell delivery systems, for example into irregularly sized bone defects. Cells alone may rapidly migrate away from the injection site, whereas injected cell-laden microparticles entrap cells and provide structural support to the tissue.

Microparticles have been used extensively for the scale-up of adherent cell lines in stirred tank bioreactors, including for the culture of embryonic cell stems [200], and are discussed more fully in Section 2.2.5. A number of microparticles are commercially available, such as Cultispher and Cytodex beads, but information about the exact constituents and cross-linking protocols are unknown. Though microparticles of a suitable size have been produced from SF alone, the only SF/G microparticles in the literature were investigated for controlled release applications and were therefore smaller than would be desired for cell culture applications [55, 201]. Microparticles for cell culture are typically 100-300 μm in diameter. It is therefore desirable to investigate the potential of creating a homogenous population of SF/G microparticles approximately 200 μm in diameter, for use in tissue engineering and cell delivery applications.

5.2. Aims & Objectives

Having shown how SF/G materials can support cell growth and differentiation in two-dimensional culture, the next stage is to move to a three-dimensional system. The objectives of this chapter are therefore:

- To reproducibly create homogenous populations of microparticles from SF/G materials.
- To seed cells onto SF/G microparticles and culture cells in a three-dimensional environment.
- To mould cell-laden microparticles into a macroscopic tissue construct and characterise cell viability, cell distribution and construct strength.
- To confirm rMSCs are capable of osteodifferentiation in the SF/G microparticle cultures.

5.3. Results & Discussion

5.3.1. Development of an axisymmetric flow focussing device for particle production

Different techniques were investigated for the production of microparticles. The first was the use of a homogeniser to create an emulsion of an aqueous protein solution in an immiscible solvent such corn oil. However, it became apparent that although homogenisation of the two solutions rapidly produced a large number of droplets of protein solution that could be processed into solid microparticles, control over the system was limited. The faster the homogeniser rate, the smaller the microparticles produced, but the homogeniser itself could not be finely tuned to a specific rate, and even when set at a fixed speed (e.g. the lowest possible), the size distribution of the droplets produced was very large. While Baimark et al. reported some success in preparing SF microparticles from water-in-oil emulsions, the size distribution of these particles remained large, and the method required hazardous organic solvents such as dichloromethane for the production of spherical microparticles [202].

Ideally, the microparticles produced for cell culture would have a narrow size distribution since the diameter of the microparticles affects the curvature of the particle surface. Therefore cells cultured on differently sized microparticles are subject to markedly different environments. A technique that would allow for a more homogenous output was therefore desirable. Microfluidic approaches have been shown to generate microparticles with a much narrower size distribution [203]. Systems of this sort consist of two immiscible co-flowing streams, and utilise the predictable break-up of these streams to produce homogenous, discrete droplets. Using a polymer or protein solution as the disperse phase allows the production of microparticles.

The system used to produce SF microparticles was based on a design by Terray et al., though the design was altered to be composed entirely from unmodified off-the-shelf fittings allowing easy, rapid and reproducible assembly [204]. This is a clear advantage over systems using custom modified pieces such as those described by a number of groups [30, 55]. The ability to take the device apart for cleaning and to remove any blockages is also a benefit of using component parts over single-piece three-dimensional-printed devices such as that described by Morimoto et al. [203]. The final design of the flow focussing device, and the parts used in assembling it, are described in Section 3.1.8.

The solvent system used was based on that reported by Breslauer et al., and consisted of 73% oleic acid, 2% Span 80 and 25% methanol [55]. The Span 80 surfactant acts to stabilise the droplets and prevent them coalescing before they solidify. The inclusion of

methanol causes the aqueous SF to undergo a conformational change into its insoluble β-sheet structure [148]. In this way the droplets produced in the axisymmetric flow focussing system are collected as microparticles. While higher proportions of methanol cause more rapid solidification of SF, this can lead to blockages within the narrow channels of the flow focussing device, whereas lower proportions cause the droplets to solidify too slowly, resulting in the coalescence of individual droplets. The inclusion of 25% methanol strikes a balance between these competing outcomes. This was not affected by the inclusion of gelatin in the disperse protein phase, which utilised the temperature-dependent hydrogel formation of gelatin in combination with the phase change of SF to produce solid microparticles. The SF/G solutions were maintained at above 35 °C, the approximate melting point of gelatin, while in the input syringe, and the output was collected into the oleic acid/Span 80/methanol solution on ice, causing the gelatin component of the droplets to solidify.

By altering the flow rates (Q_{outer} (flow rate of the continuous phase) and Q_{inner} (flow rate of the disperse phase)) in the axisymmetric flow focussing device, the size of the microparticles can be controlled [50, 205]. The higher the ratio between the two flow rates, the smaller the microparticles. This is illustrated in Figure 5.01. The degree of control shown here is much greater than that which could be achieved using the emulsion method.

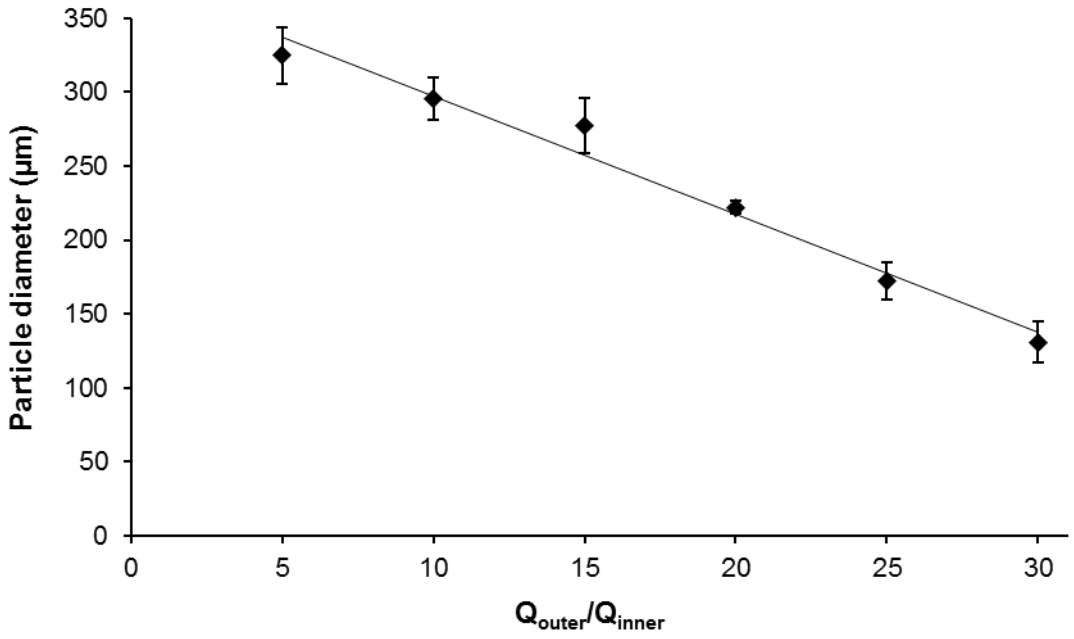

Figure 5.01: Mean diameters of SF/G 75:25 microparticles produced under selected flow rate ratios. Q_{inner} was fixed at 0.05 mL/min (n=1). Data shown represents mean ± standard deviation (n=1). R^2=0.9771.

5.3.2. Topography & size of SF/G microparticles

The size distribution data and mean microparticle diameters are summarised in Table 5.01. Images of the microparticles were processed using ImageJ to determine the mean diameter of each microparticle blend. An example image is shown in Figure 5.02. The microparticles were produced using a flow rate ratio (Q_{outer}/Q_{inner}) of 20, since this value consistently yielded microparticles with diameters in the range of 300-350 µm. The size distributions obtained compare favourably with those measured for the commercially available gelatin Cultispher-S microparticles.

Table 5.01: Mean diameters of SF and SF/G particles produced by axisymmetric flow focussing (Q_{outer}/Q_{inner} = 20, Q_{inner} = 0.36 mL/hr), from 3 batches each. Data shown represents mean ± standard deviation. Values for Cultispher-S are included for comparison.

Material	Diameter (µm)	Range (µm)
SF/G 75:25	339 ± 59	201-490 (98.6%)
SF/G 50:50	347 ± 44	213-446 (99.8%)
SF/G 25:75	308 ± 39	218-428 (98.6%)
Cultispher-S	237 ± 86	108-565 (98.6%)

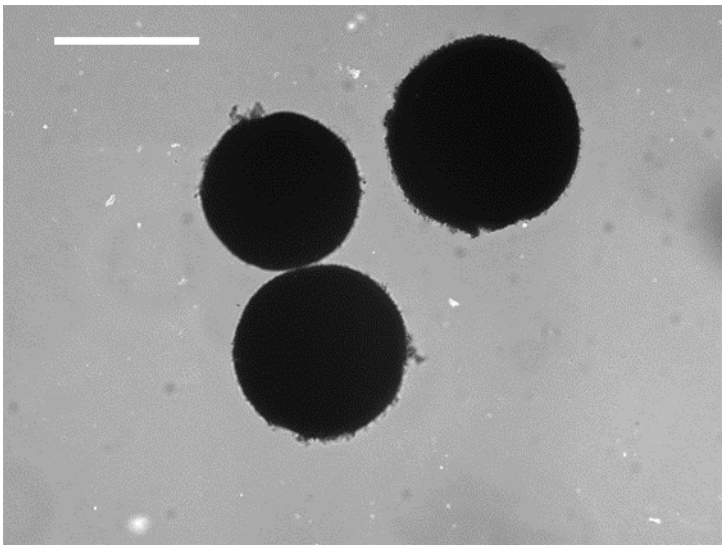

Figure 5.02: Bright field image of SF/G 25:75 microparticles produced by flow focussing. Scale bar represents 200 µm.

The microparticles were examined by SEM and representative images are shown in Figure 5.03. Microparticles produced from SF/G blends all show a distinctive textured topography.

From the images it appears as though the particles have a porous structure, although the pores are in the region of 2 μm, and thus too small for cells to migrate into or through. The topography observed in Figure 5.03 is typical of that observed for all the SF/G particles. It is also consistent with SF microparticles created by electrospraying, as described elsewhere [206].

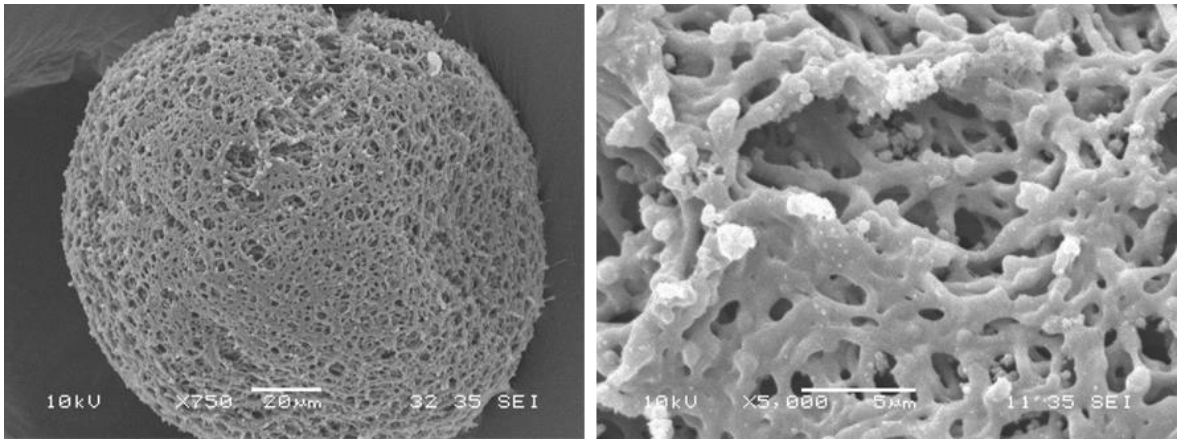

Figure 5.03: SEM images of a SF/G 75:25 microparticle produced by axisymmetric flow focusing.

5.3.3. Effect of porogens on SF microparticle structure

To see if larger pores could be created within the microparticles, the starting SF solution was blended with porogens. If the pores in the microparticles were sufficiently large, cells could be seeded into them, or migrate into them, thus producing a more homogenous cell distribution. Without cell-sized pores, cells will simply settle on the exterior of the particles.

The particles produced with porogens were examined by SEM and the results are shown in Figure 5.04. The particles are very similar to the porogen-free samples in Figure 5.03, and the structures do not show any pores of the size described above. This could be expected from samples produced using sodium chloride or PEG as a porogen, since at the low concentrations used here, they simply dissolve into the silk solution. Examples of porous SF scaffolds produced using salt leeching typically use much higher concentrations of sodium choride, and cast scaffolds into fixed moulds [190, 207]. Since the SF solution must pass through the axisymmetric flow focussing device, these supersaturated slurries are not suitable for use here, and the lower concentrations investigated do not make a significant difference to the microparticle structure.

The use of insoluble, fine calcium carbonate particles was investigated on the basis that the calcium carbonate would become encapsulated within the SF structure, and then dissolve away in an acidic solution to leave pores throughout. However, this was not observed, even at the highest concentration tested (20% w/v). This could be due to the calcium carbonate granules not being sufficiently large to leave visible pores, though as mentioned earlier, the use of large particles runs the risk of blocking the axisymmetric device, and they would also settle within the input syringe, leaving an uneven distribution within the SF solution. The use of porogens was not pursued further given these results.

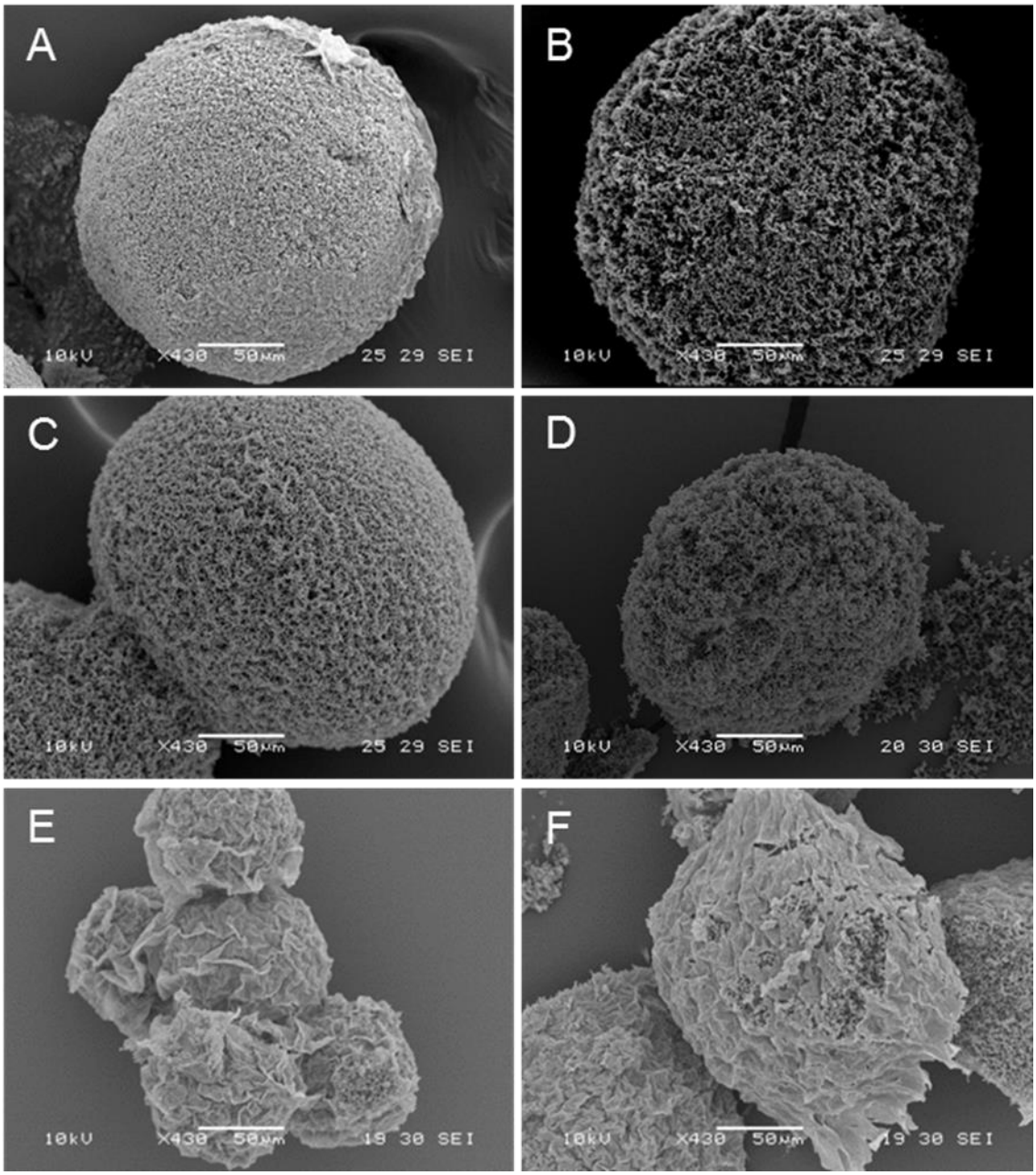

Figure 5.04: SEM images of SF microparticles made with porogens. (A) 10 % w/v PEG; (B) 1% w/v NaCl; (C) 10% w/v NaCl; (D) 5% w/v $CaCO_3$; (E) 10% w/v $CaCO_3$; (F) 20% w/v $CaCO_3$.

5.3.4. Young's moduli of SF/G materials

The Young's moduli of discs made from SF and SF/G blends were determined by compression testing, in order to see if they corresponded to the elasticity range favouring osteogenic differentiation, and to see the effect of blending the two primary materials. The results are shown in Figure 5.05. As observed for the films in Chapter 4, SF actually had the lowest Young's modulus of the materials measured, at 20 kPa. However, unlike the SF/G films, the discs cast from SF/G 50:50 and 25:75 had the highest values, at 183 kPa and 162 kPa respectively. The values obtained here are similar to those obtained for freeze-dried porous SF/G scaffolds in the literature (between approximately 60 and 160 kPa for SF/G blends). He et al. attribute the higher value of compressive modulus for SF/G 50:50 scaffolds to a more homogenous pore structure than is obtained for 25:75 or 75:25 [85].

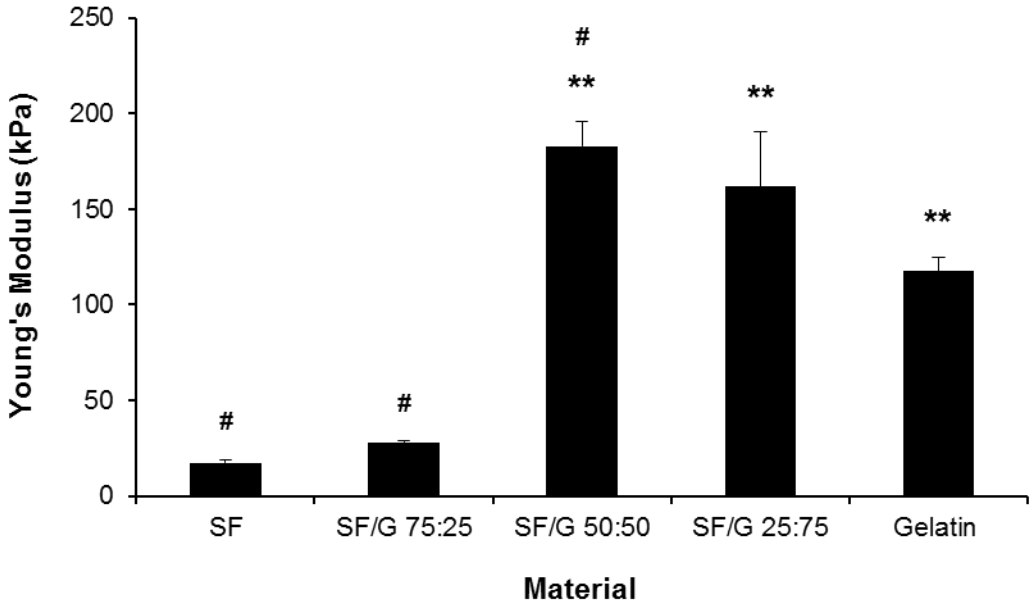

Figure 5.05: Young's modulus of SF/G gel discs determined by compression testing. Data shown represents mean + standard error (n=3). ** $p<0.01$ w.r.t SF; # $p<0.05$ w.r.t gelatin.

Engler et al. describe a substrate stiffness of 25-40 kPa as sufficiently rigid to induce osteogenic differentiation [33]. This value, much lower than the expected Young's modulus of bone itself, corresponds to the stiffness of the osteoid region of bone, which is the matrix on which MSCs transition to pre-osteoblasts [167]. Though SF and SF/G 75:25 materials sit at the lower end of this range, the blends of SF/G 50:50 and 25:75 should adequately support osteogenic differentiation according to these criteria.

Measurements were recorded using solid, centimetre-sized discs of SF and SF/G blends, since it was not logistically possible to analyse the microparticles themselves due to their small size. The discs were in a hydrated state during compression testing, unlike the dry films analysed for tensile strength in Chapter 4. This may explain why the values observed in Figure 5.05 are much lower than those in Figure 4.04 (for example, 20 kPa for wet SF discs compared to 19.8 MPa for dry SF films). Since the materials are hydrated during cell culture, the values in Figure 5.05 are likely to be more representative of the environment cells would experience.

To measure the Young's modulus of the microparticles directly, it would be possible to use atomic force microscopy (AFM). Indentation of the AFM tip into microparticles has been used to measure the elastic properties of SF microparticles, for example by Breslauer et al. who recorded an average Young's modulus of 1.5 kPa [55]. The discrepancy between this value and the value determined here could be due to the differences in structure between flow focussing-produced microparticles and moulded discs, or due to a variation in SF properties or processing steps. The results in Figure 5.05 again confirm the potential for SF/G blends as scaffolds for osteogenic tissue engineering, especially in terms of using a blend of the two materials rather than one alone.

5.3.5. Microparticle stability in solution

As a measure of stability, the mass of protein lost from SF/G 75:25 microparticles was calculated over 7 days incubation in PBS at 37°C. The results are shown in Figure 5.06. Although particles do gradually lose mass over the time period, this is only equal to 2.3% of the total mass of microparticles. The microparticles show an acceptable level of stability, and when examined visually appeared robust.

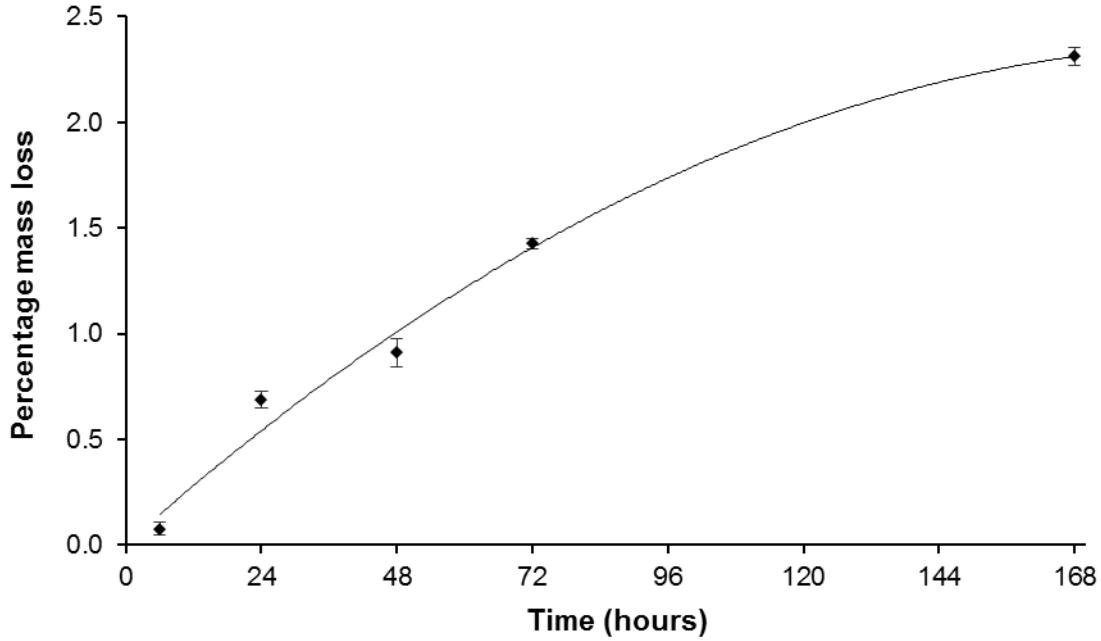

Figure 5.06: Percentage of mass lost from SF/G 75:25 microparticles in PBS over 7 days. Data shown represents mean ± standard error (n=3). $R^2 = 0.9871$.

This is consistent with results for aqueous-derived SF scaffolds obtained by Kim et al., who observed that while protease-treated aqueous-derived scaffolds degraded rapidly, untreated scaffolds maintained their structures without significant degradation [207]. The same group later reported that aqueous-derived SF scaffolds supported higher levels of osteogenesis than HFIP-derived equivalents, attributed to their different degradation rates [80].

5.3.6. Seeding 3T3 fibroblasts onto microparticles

To confirm the SF/G materials retained their ability to support cell attachment in a microparticle format, seeding experiments were carried out, initially using 3T3 fibroblasts as a model cell line (described in Section 3.1.1). The results, shown in Figure 5.07, mirror those observed for SF/G-coated TCP and for thin films of SF/G materials – in short the cells adhered poorly to SF microparticles but adhered at a much higher number to SF/G blends. As previously discussed, this is likely due to the presence of RGD residues provided by gelatin, which facilitate cell attachment through β-integrin receptors [102].

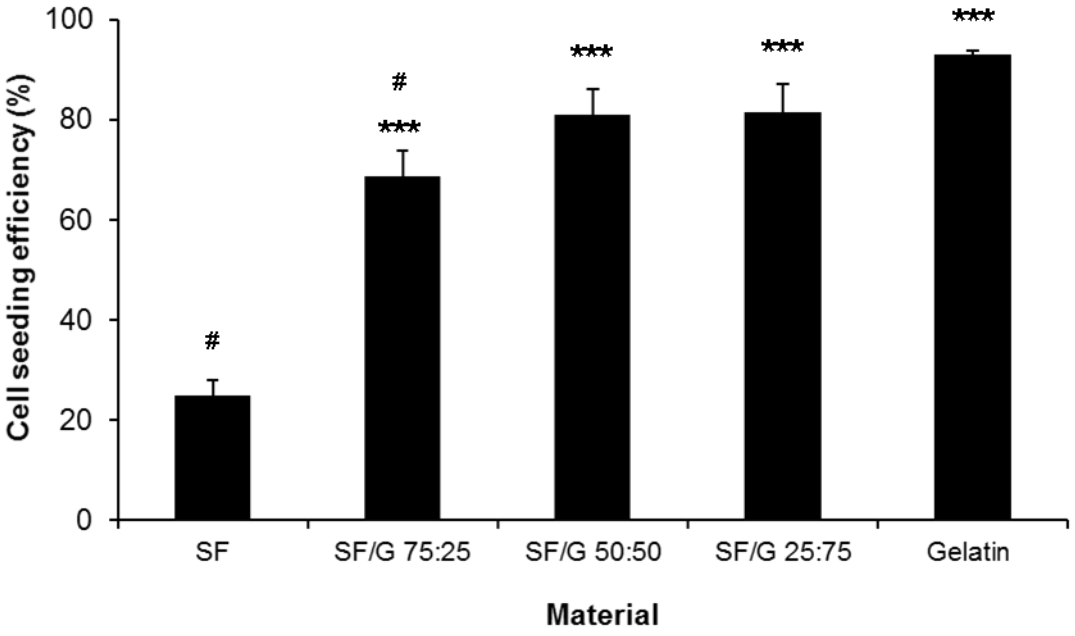

Figure 5.07: Seeding efficiency (percentage of 3T3 fibroblasts seeded adhered to microparticles) of SF, SF/G and gelatin microparticles. Data shown represents mean + standard error (n=5). *** $p<0.001$ w.r.t SF alone; # $p<0.05$ w.r.t gelatin.

Cell viability on SF/G microparticles was confirmed by LIVE/DEAD fluorescent staining, visualised by confocal microscopy. Figure 5.08 shows representative images, which all show a high level of cell viability on all the SF/G blends and on gelatin, included here as a positive control. The images are consistent with the data in Figure 5.07, showing that 3T3 fibroblasts adhere to SF/G blends at a level equivalent to gelatin.

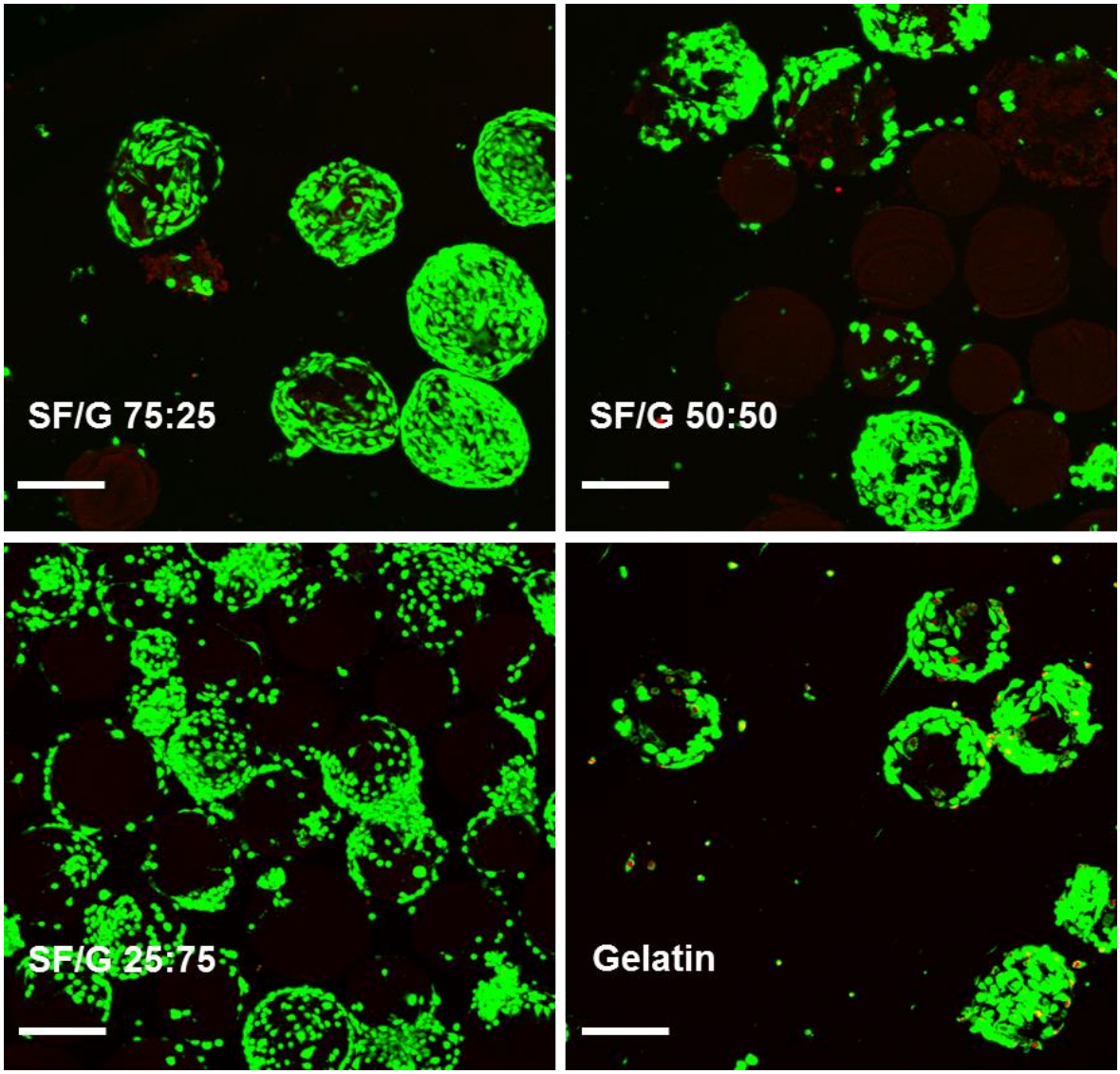

Figure 5.08: Microparticles seeded with 3T3 fibroblasts, stained with LIVE/DEAD to indicate viability after 3 days of culture. Viable cells fluoresce green, while non-viable cells fluoresce red. Scale bars represent 200 µm.

Cell adhesion onto SF/G microparticles was also investigated by SEM. In Figure 5.09 (A), cells can be seen coating the exterior of the microparticles (though they are somewhat damaged by the extensive processing steps required), while in Figure 5.09 (B), a monolayer of cells on the surface of a single particle is visible.

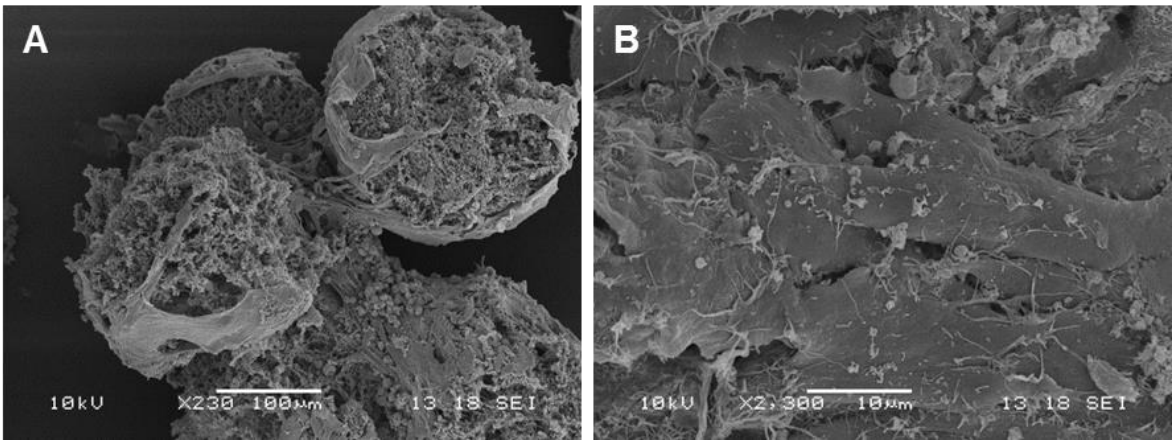

Figure 5.09: SEM images of 3T3 cells on SF/G blended microparticles. (A) SF/G 50:50; (B) SF/G 25:75.

5.3.7. Seeding rMSCs onto microparticles

Once cell attachment was confirmed using fibroblasts, the experiments were repeated using rMSCs. The seeding efficiencies are shown in Figure 5.10. The results are similar to those observed for 3T3 fibroblasts in Figure 5.07, in that cells do not adhere well to the SF microparticles and seeding efficiency is improved on SF/G blends. While for fibroblasts, the SF/G blends appear equivalent, for rMSCs, seeding efficiencies are higher on the 50:50 and 25:75 blends (i.e. those with a higher gelatin proportion). Anecdotally it is recognised that fibroblasts are relatively unselective in their adhesion to culture substrates, whereas MSCs can be more selective. This is reflected in the data shown here, where more rMSCs adhere to the substrates with a higher proportion of gelatin.

The viability of the rMSCs on the microparticles was again examined using LIVE/DEAD staining. A representative image of rMSCs seeded on SF/G 25:75 microparticles is shown in Figure 5.11. As was the case with the 3T3 fibroblasts, the rMSCs show a high level of viabilty.

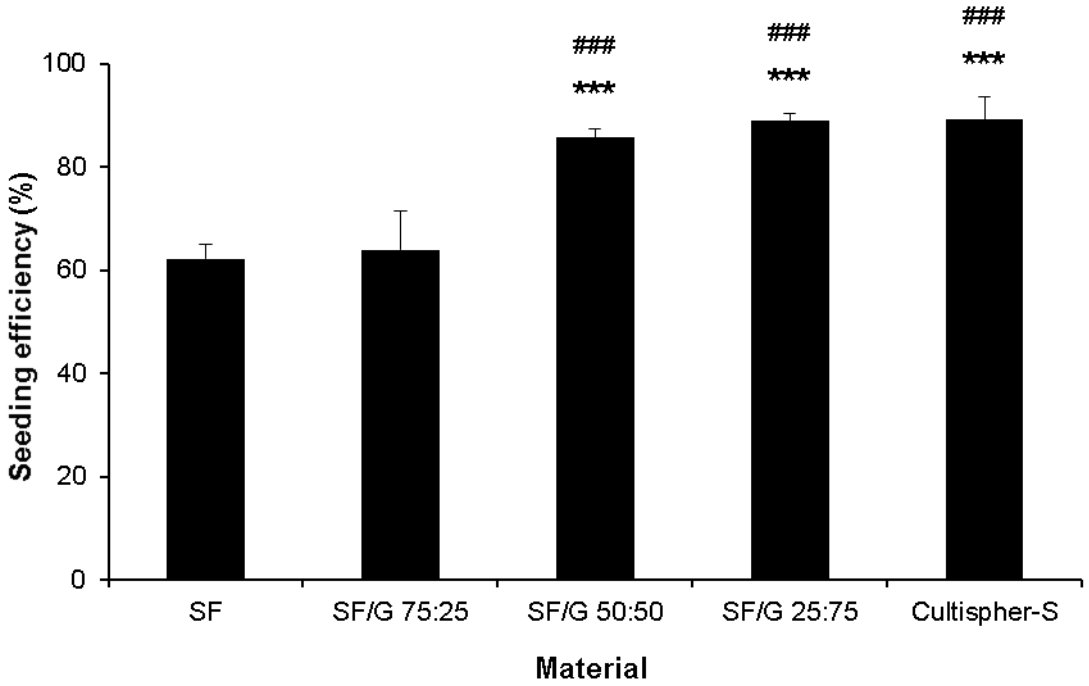

Figure 5.10: Seeding efficiency (percentage of rMSCs seeded that have adhered to microparticles) of SF, SF/G and gelatin microparticles. Data shown represents mean + standard error (n=3). ### p<0.001 w.r.t. SF; *** p<0.001 w.r.t. SF/G 75:25.

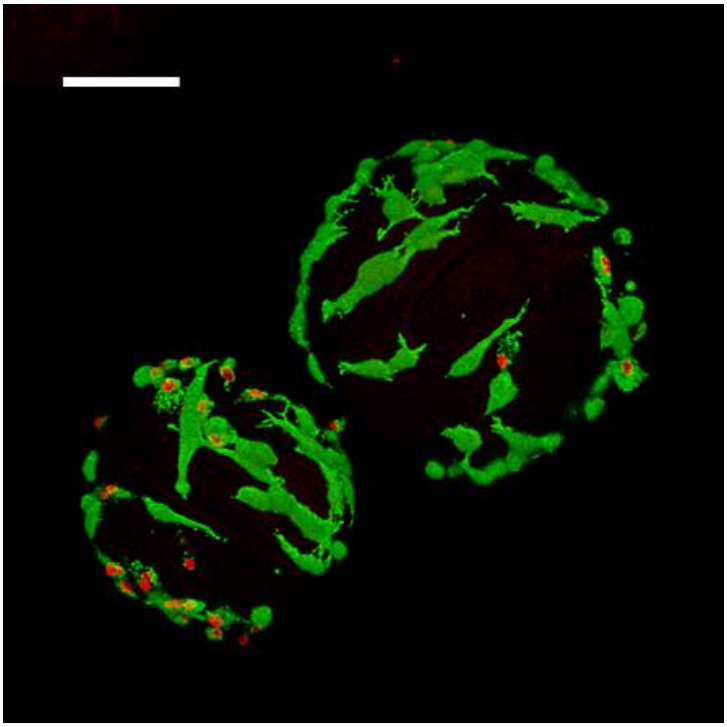

Figure 5.11: Fluorescent confocal image of rMSCs cells seeded onto SF/G 25:75 microparticles after 4 days of culture. Cells were stained with LIVE/DEAD to indicate viability. Cells stained green were viable, while cells stained red were dead. Scale bar represents 100 μm.

The rMSC adhesion to SF microparticles is higher than anticipated, with 62% of cells adhering to the microparticles, only marginally lower than the seeding efficiency observed for SF/G 75:25. This is in contrast to the results observed for 3T3 fibroblasts, in Figure 5.07, where the seeding efficiency of cells on SF microparticles was 25% and significantly lower than that of SF/G 75:25. For the remaining materials, SF/G 50:50, SF/G 25:75 and gelatin (Cultispher-S microparticles), rMSC seeding efficiencies were over 80%, as for 3T3 fibroblasts. It is not clear why the level of rMSC attachment to SF microparticles is relatively high here, especially since this was not observed in two-dimensional seeding experiments (Figure 4.08). One possibility is that rMSCs form large cell aggregates, adhering to each other in preference to the SF microparticles. If these aggregates are sufficiently large (greater than 70 μm), they would be filtered out of the solution with the microparticles while single cells and smaller aggregates are collected and counted. However, since this is a risk for all of the microparticle cultures, the presence of the cells on the microparticles was confirmed by fluorescent confocal microscopy images and SEM images for both 3T3s and rMSCs (Figures 5.08, 5.09 and 5.11).

5.3.8. Osteodifferentiation of rMSCs on SF/G microparticles

Once rMSCs had been seeded onto SF/G microparticles, the media they were suspended in was switched to osteodifferentiation media (ODM). The cultures were assayed for markers of osteogenic differentiation: ALP activity and osteopontin expression. Background staining of the SF/G materials rendered typical osteogenic assays such as Alizarin Red and Von Kossa unusable, as was the case for two-dimensional films described in Chapter 4.

Given the results obtained for cell adhesion to SF/G blends, as well as the varied Young's modulus values, the decision was made to progress into osteodifferentiation assays with the SF/G 25:75 blend only, using Cultispher-S particles as a positive control for comparison. While the rMSCs cultured on Cultispher-S microparticles showed much higher ALP activity in ODM than basal media, rMSCs cultured on SF/G 25:75 microparticles appeared to have equal levels of ALP activity in both ODM and basal media (Figure 5.12). This is consistent with results in Chapter 4, in which levels of osteogenic differentiation appeared equivalent for rMSCs on SF/G 25:75 cultured in basal media and ODM, particularly when measured by osteocalcin expression, and to a lesser extent, ALP activity. Compared to the results observed for the Cultispher-S seeded rMSCs, this may suggest that the SF/G blend supports osteogenic differentiation even in the absence of osteogenic supplements.

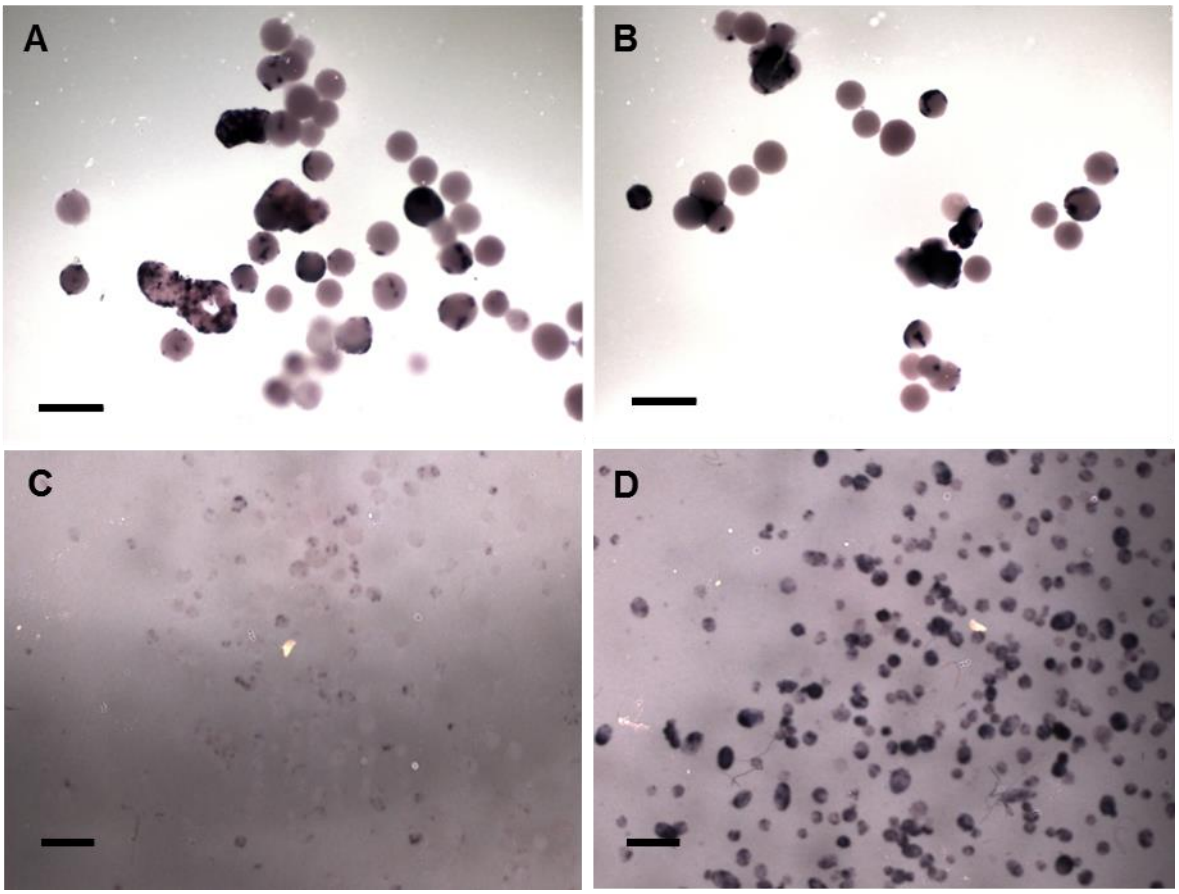

Figure 5.12: ALP activity in rMSCs cultured for 28 days on SF/G 25:75 or Cultispher-S microparticles. (A) SF/G 25:75 with basal media; (B) SF/G 25:75 with ODM; (C) Cultispher-S with basal media and (D) Cultispher-S with ODM. Scale bars represent 500 µm.

To confirm this result, osteopontin levels in the cultures were assayed. The results are shown in Figure 5.13. In contrast to the results for ALP activity in the SF/G cultures observed in Figure 5.12, osteopontin expression is much higher in ODM-cultured rMSCs than in the basal media, as would normally be expected. For rMSCs cultured on Cultispher-S microparticles, the osteopontin expression mirrors the results for ALP activity, whereby rMSCs cultured in ODM show stronger evidence of osteodifferentiation than those cultured in basal media. The expression of osteopontin in ODM-SF/G 25:75 cultures appears slightly higher than for ODM-Cultispher-S cultures, however this difference was not found to be significant. The large error bars (standard error) observed for ODM-SF/G 25:75 osteopontin expression reflect the variable results obtained here. This could be a result of the fact that osteopontin is a late marker of differentiation, and day 14 is a relatively early time point, leading to variation in cell responses. However, this large variation was not observed for the Cultispher-S seeded rMSCs, nor for the rMSCs in two-dimensional cultures (Figure 4.13). Osteopontin expression should be measured at further time points (perhaps day 21 and 28) in addition to day 14 to gain a clearer understanding of the rMSC behaviour on SF/G 25:75

microparticles. A further factor may be that the cells have not reached a confluent state by day 14. The rMSCs were seeded onto the microparticles at a concentration of 3-5 x 10^4 cells/cm^2. Successfully differentiated rMSCs have been seeded in static cultures at densities of 1-4 x 10^4 cells/cm^2 [141, 208], so the cell density on the particles is within the normal range and is unlikely to be a contributing factor here.

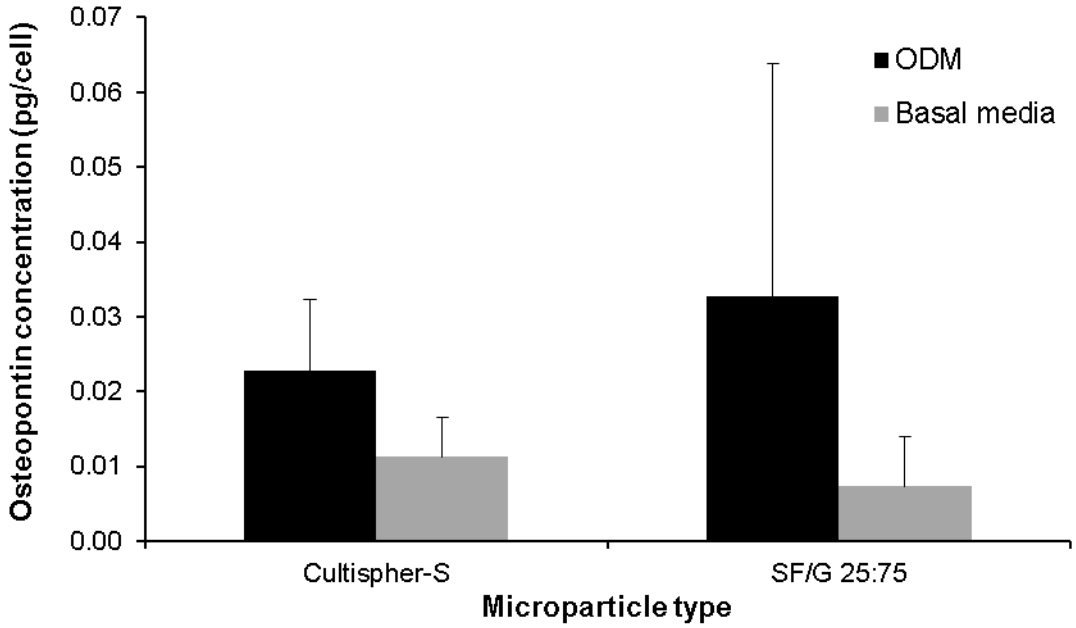

Figure 5.13: Expression of osteopontin at day 14 in cultures of rMSCs seeded on SF/G 25:75 and Cultispher-S microparticles. Data is normalised by cell number. Data shown represents mean + standard error (n=5). No significance was observed.

The observed results are consistent with several reports of osteogenic differentiation of MSCs on SF/G scaffolds. Das et al. observed increased expression of the bone markers RUNX2, ALP and osteopontin in human nasal inferior turbinate MSCs encapsulated in sonication-cross-linked SF/G scaffolds, when cultured in ODM for 14 days. These scaffolds were not stable in culture media for prolonged periods however, resulting in much lower levels of these markers at day 21 [192]. However, it could be that the faster degradation rate encourages cells to deposit their own ECM more rapidly, as was observed by Park et al. for pure SF scaffolds [80]. The osteoinductive potential of the SF/G microparticles could therefore potentially be improved by decreasing the extent of cross-linking to decrease stability. Another alternative could be the inclusion of a third material to improve differentiation. SF/G/hydroxyapatite scaffolds have been produced by Moisenovich et al. though not yet investigated for their ability to support osteodifferentiation [161].

Vorrapakdee et al. observed increased ALP activity and calcium deposition in rMSCs grown on decellularised bone scaffolds modified with SF/G, while Wongputtaraksa et al. had similar results using SF scaffolds modified with gelatin, though both these reports used Thai *Nangnoi srisaket* silk rather than *Bombyx mori* [190, 191]. Together, these reports and the data collected here suggest SF is an osteoconductive material.

5.3.9. Moulding 3T3-laden SF/G microparticles into a macroscopic tissue construct

In order to create a macroscopic solid bone construct it was necessary to mould the cell-laden SF/G microparticles together. To this end, 3T3 fibroblast-laden SF/G microparticles or Cultispher-S microparticles were placed inside small cylindrical moulds within 24 well plates (see Section 3.1.2). In theory, within the mould, the cells on adjacent microparticles should start to make adhesions to each other and other microparticles, thus effectively cross-linking the separate microparticles into one densely populated structure. This has been observed and utilised elsewhere, and the ability to mould small building blocks into a larger tissue construct is a strong motivator for using microparticles as opposed to a larger pre-formed scaffold [30].

It was possible to form a stable structure from SF/G 25:75 microparticles seeded with 3T3 fibroblasts. Once the mould was removed the structure held its shape, as evidenced by the dense arrangement of microparticles shown in Figure 5.14. A similar construct was also produced using 3T3 fibroblasts on Cultispher-S microparticles. H&E staining (described in Section 3.2.7) showed that the SF/G construct was held together by relatively large cell clumps or aggregates (Figure 5.15). The scaffold material was stained a light pink by eosin, and from this it is possible to see that the particles have a homogenous, porous structure throughout, though the pores themselves are very small, whereas the Cultispher-S particles have much larger pores producing an irregular honeycomb-type structure. The cells, nuclei stained blue by haematoxylin, appear much more disperse in the Cultispher-S structure, possibly due the greater accessible surface area for cells seeded on these particles. It appears that the Cultispher-S structure was held together primarily by individual cell-cell or cell-scaffold adhesions, whereas the SF/G structure was held together by cell aggregates.

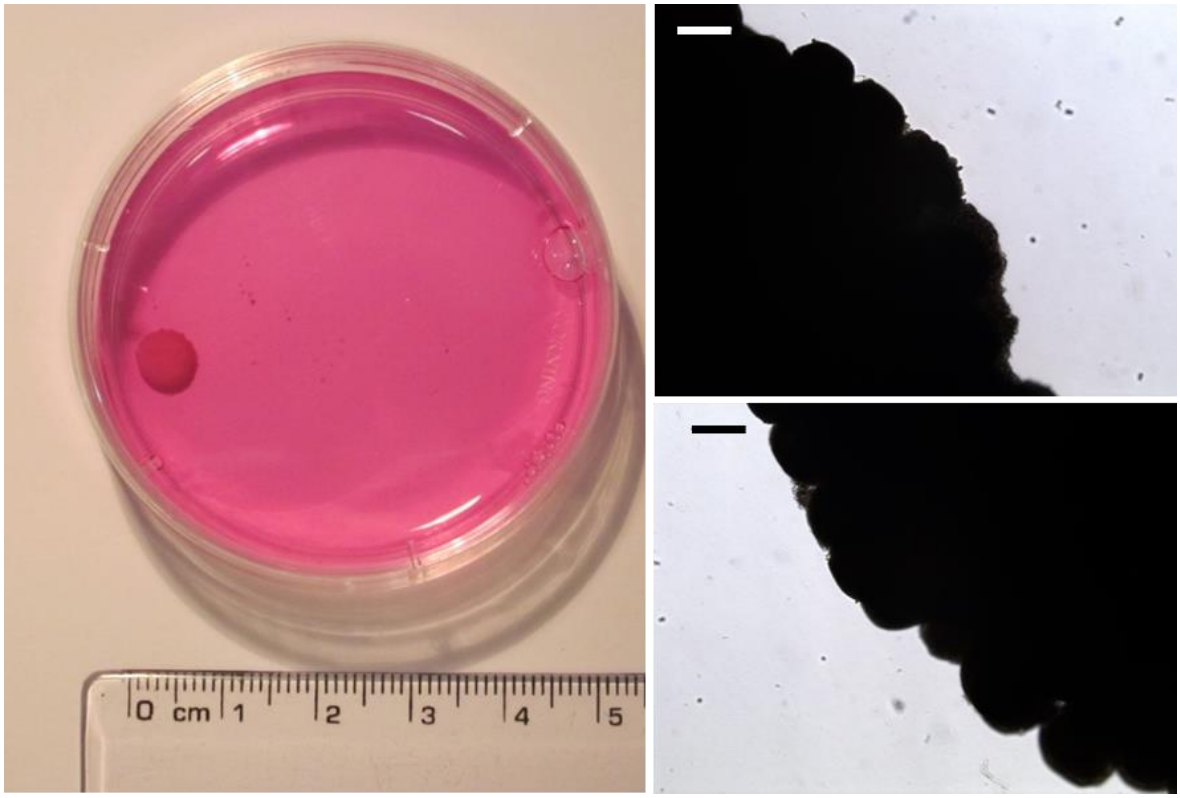

Figure 5.14: SF/G 25:75 microparticles seeded with 3T3 fibroblasts and moulded into a cylindrical disc, measuring approximately 5 x 2 mm. Right hand images show the dense structure of microparticles held together by cell-cell and cell-scaffold adhesions. Scale bars represent 200 µm.

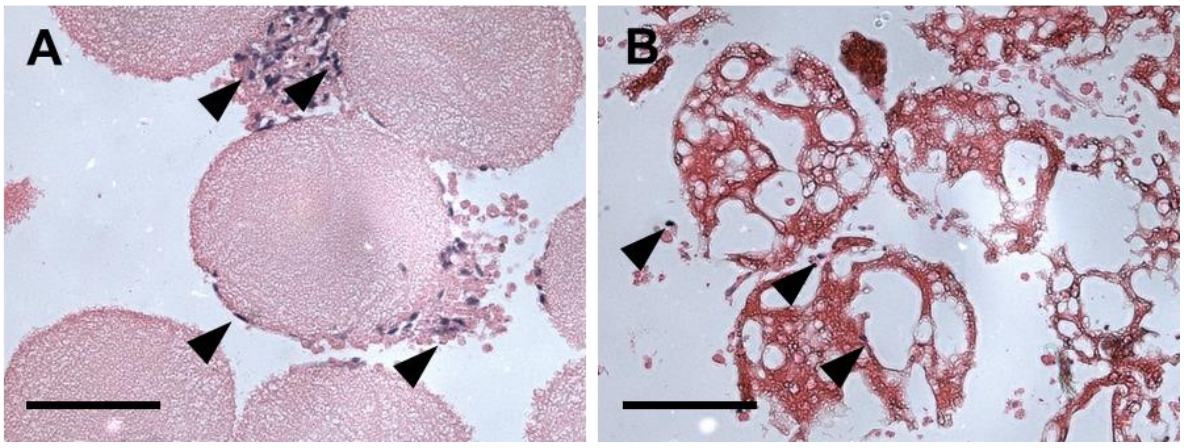

Figure 5.15: Fixed slices through constructs formed from 3T3 fibroblasts on (A) SF/G 25:75 microparticles and (B) Cultispher-S microparticles. Sections were stained with Haematoxylin and Eosin. Dark blue nuclei are indicated with arrow heads. Scale bars represent 100 µm.

Unfortunately this process was not robust enough to be repeatable, with 3T3 fibroblasts nor rMSCs, and although it worked as a proof of concept, the lack of reliability means the production of a macroscopic tissue construct using SF/G microparticles is not practical. It is

possible that further refinement could overcome this problem, by optimising parameters such as cell seeding density, microparticles per moulding volume and mould design.

Similar approaches have been successful elsewhere, frequently using commercially available microparticles and using a variety of cell types. Twal et al. coated Cultispher-G microparticles with human umbilical vein endothelial cells and human aortic smooth muscle cells before successfully moulding them into O-shaped rings, which were stacked together to produce a tubular construct [56]. Unlike the Cultispher-S structure observed in Figure 5.15, a large number of cells were seen to be located in the spaces between particles. This could be a factor of the different cell types used and their differing proliferative potential. Slower growing cells would not fill the spaces between microparticles as rapidly as quicker growing lines. The difference observed is not likely to be due to the different microparticles used, as Cultispher-G and Cultispher-S particle are both composed of porcine gelatin and differ only in their thermal stabilities.

The construction of centimetre-scale tissue constructs from Cultispher-S and Cytopore-2 microparticles in perfusion cultures has been described elsewhere [57, 209]. Although perfusion cultures prevent central tissue necrosis and prolong construct viability, they can also be responsible for 'washing out' any *de novo* ECM proteins, hindering tissue formation [42].

Matsunaga et al. were also able to mould cell-laden microparticles into a self-supporting structure, using 3T3 fibroblasts. However, the use of a very soft form of collagen (atelocollagen) resulted in rapid shrinking of the construct due to the contractive forces of the cells and degradation by proteolytic enzymes [30]. Preliminary work undertaken in this thesis investigated the preparation of collagen I microparticles using the conditions described by Matsunaga et al. However, it was not possible to reproduce microparticles of the type described, due to the slow, temperature-dependent gelation of collagen. Droplets inevitably coalesced before gelation, producing large clumps rather than discrete droplets, even when using surfactants.

This demonstrates that the development of a tissue construct using a bottom up approach depends heavily on the choice of materials and cells. In order to create such a structure using SF/G microparticles, it may be necessary to encapsulate the microparticles in a hydrogel (perhaps gelatin), essentially gluing the particles together.

5.4. Conclusions

The work in this chapter describes how microparticles were reproducibly created from SF/G 75:25, 50:50 and 25:75 blends using a custom flow focussing device. By adapting systems described in the literature, an easily-assembled device was created from unmodified commercially available parts. This system is simple to assemble and a significant advantage of its design is that, because it requires no custom modification of parts, it can be built by any group interested in its application for microparticle production (and this is not limited to SF/G materials).

Both 3T3 fibroblasts and rMSCs were successfully seeded onto SF/G microparticles in small dynamic cultures, though there is certainly potential for these systems to be scaled up: some preliminary work using stirred flasks was carried out, though not pursued. Future work should investigate optimisation of stirred flask microparticle cultures. rMSCs were shown to remain viable once seeded on SF/G microparticles and evidence of osteodifferentiation was observed, by ALP activity and expression of osteopontin, at levels equivalent to Cultispher-S cultured rMSCs.

A centimetre-scale construct was successfully created from SF/G 25:75 microparticles seeded with 3T3 fibroblasts, but unfortunately could not be reproduced using either 3T3s or rMSCs. However, SF/G microparticles could still be used for cell expansion in scaled-up cultures, or for the injectable delivery of MSCs. Using SF/G microparticles for both the expansion of MSCs and as the scaffold for their differentiation would minimise processing steps for cell-based therapies that could be delivered *in vivo* via minimally invasive techniques.

Chapter 6

Rapid production of alginate/ECM microparticles for use in tissue engineering applications

Introduction

Alginate as a biomaterial

Alginate, a brown algae-derived polysaccharide, is a useful material for cell culture because it is biocompatible, although not cell adhesive, and rapidly forms hydrogels on exposure to divalent cations (see Section 2.3.2). The ratio of guluronic to mannuronic acid residues within different types of alginate can vary and this, combined with choice of cross-linking cation, can affect the properties of the resultant hydrogel [91]. Cells do not adhere to alginate alone, but it can be modified or blended with other materials in order to improve this.

Alginate hydrogels have been used for encapsulating cells, either to act as immune barriers in cell transplantations, or for storage purposes [90, 210, 211]. They can also be used as wound dressings (e.g. Algicell™ and AlgiSite M™), utilising their high fluid uptake ability to absorb wound exudates [212]. Although unmodified alginate degrades slowly and unpredictably, oxidation of alginate produces a dialdehyde derivative that is susceptible to hydrolysis under physiological conditions [213]. Oxidation can also affect the swelling of the alginate gel, with higher levels of oxidation producing softer, less stable gels [95].

Decellularised extracellular matrix (ECM) materials

Decellularised whole organ scaffolds have been used successfully to produce functional tissue engineered organs, but are dependent on finding donor organs of an appropriate size, and face similar issues as synthetic scaffolds designed in a top down manner, such as even cell distribution upon re-seeding. However, it is possible to produce solubilised solutions of decellularised ECM components which can be used to coat cell culture vessels, or formed into hydrogels (see Section 2.3.4) [122, 214]. This provides the flexibility to produce scaffolds of a variety of sizes and shapes. The advantage of using decellularised materials rather than purified protein samples is that within the original tissue, a mixture of proteins exists in the right proportions to support cell growth, attachment, proliferation and possibly differentiation. Instead of trying to replicate the ECM artificially, decellularised tissue samples can provide an appropriate scaffold for re-population with a low risk of

immune rejection. A number of scaffolds of this type have received FDA approval for *in vivo* human applications, including Alloderm®, a collagenous matrix derived from cadaveric skin.

The specific constituents of an ECM product will depend on the starting material, although typically they include a large proportion of collagen, along with glycosaminoglycans, laminin, fibronectin, elastin, and possibly small amount of growth factors. Adequate removal of cellular material is necessary to prevent adverse host reactions to scaffolds produced from decellularised materials upon implantation. Insufficient decellularisation may result in cytocompatibility issues when cells are reintroduced to the material, or immunogenic reactions *in vivo*. Decellularisation is commonly evaluated by assaying double-stranded DNA rather than other cellular components because DNA content of a decellularised scaffold directly relates to adverse *in vivo* reactions [119]. It is also equivalent in all cell types. The criteria for decellularisation are described in Section 2.3.4.

Bottom up tissue engineering

As previously discussed (see Section 2.2.4) the method of starting with small building blocks of scaffold and cells to produce a final larger structure is considered a bottom up approach to tissue engineering. This has advantages in that it allows for even cell distribution and precise control over a hierarchical structure. Encapsulating cells within small scaffold units, such as microparticles, provides a suitable starting point for this. The mild conditions required for the rapid gelation of alginate make it ideal for cell encapsulation, without compromising viability.

6.2. Aims & Objectives

While SF/G microparticles have been shown to have some potential as osteogenic scaffolds for tissue engineering, the inability to mould these particles into a 3D structure prompted investigation into alternative materials for microparticle production. This also provided the opportunity to look at improving other characteristics of the microparticles such as production time, bioactivity and need for post-production cross-linking. Alginate was chosen due to its ease of handing and rapid gelation, while ECM proteins were selected for their ability to support cell adhesion and function.

The aims of the work in this chapter were therefore to investigate a rapid method of particle production using alginate based biomaterials, blended with cell-adhesive and bioactive extracellular matrix components.

The objectives were as follows:

- Investigate methods of rapidly producing a homogenous population of microparticles using oxidised alginate as the primary material.
- Determine the best method for the removal of cellular material from skeletal muscle samples to harvest extracellular matrix proteins.
- Establish whether the decellularised materials are capable of forming collagenous hydrogels.
- Blend extracellular matrix proteins with oxidised alginate to produce a biocompatible, cell-adhesive scaffold and establish cell seeding or cell encapsulation protocols.
- Investigate whether these materials can be moulded into a macroscopic construct.

6.3. Results & Discussion

6.3.1. Periodate oxidation of alginate

Treating alginate with sodium periodate results in the oxidation of the hydroxyl groups on carbons 2 and 3 to aldehyde groups, breaking the carbon-carbon bond in the process. Alginate itself degrades very slowly and in an uncontrolled manner, producing high molecular weight fragments that are not easily cleared *in vivo*. Partial oxidation of alginate creates the more reactive aldehyde groups (Figure 6.01), which results in higher levels of alginate hydrolysis while not significantly affecting the gelation properties of the material [143, 215].

It has been reported previously that microparticles produced from 10%-oxidised alginate were too fragile to handle, and thus a range of oxidation levels from 2.5% to 10% were investigated for their use in microparticle production [93].

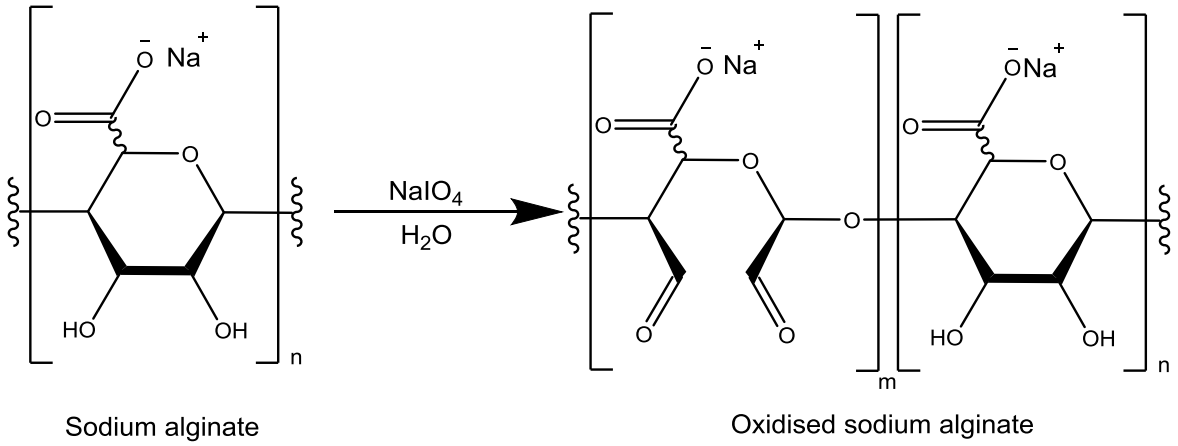

Figure 6.01: Oxidation of sodium alginate. Sodium periodate cleaves the bond between carbons 2 and 3, oxidising the hydroxyl groups to produce alginate dialdehyde [143].

The oxidation level of the alginate was quantified by measuring the amount of sodium periodate remaining in the reaction mixture after 24 hours, with the amount consumed directly proportional to the oxidation level of the alginate (Section 3.1.5). This was regularly found to be more than 98% of the initial amount, thus it was safe to assume that, for example, for a 5%-oxidised alginate, the actual level of oxidation was 4.9 – 5.0%. Gomez et al. observed than for low levels of oxidation, a high level of periodate consumption is typical of the reaction with alginate [143].

6.3.2. Measured viscosities of alginate solutions

The oxidised alginate solutions became progressively less viscous with increasing levels of oxidation. This was confirmed by dynamic rheology measurements (Table 6.01). The decrease in viscosity of oxidised samples is related to the decrease in molecular mass as a result of cleavage of the alginate backbone during oxidation [95, 215]. Gomez et al. suggest this is the result of a free radical-independent degradation. Another factor is that the stiffness of the alginate chains is decreased upon oxidisation, as the cleavage of the bond between C_2-C_3 produces a more flexible chain (Figure 6.01) [143].

The initial viscosity of an alginate is a result of the conditions under which it is extracted from seaweed. Extraction is achieved by solubilising the alginate so that it can be separated from the bulk of the seaweed. By adjusting the temperature and time of the extraction, the viscosity of the final product can be altered. Higher temperatures and longer reaction times

result in the breakdown of uronic acid chains within the structure, leading to lower viscosities [216].

The relative viscosities of the alginate solutions were of particular interest because of their effect on the production of alginate microparticles through the air flow focussing system (see Section 6.4.4.).

Table 6.01: Measured viscosity values for a selection of alginate solutions.

Alginate type	Concentration (% w/v)	Oxidation level (%)	Viscosity (Pa·s)
Low viscosity	1	-	8.62×10^{-3}
Low viscosity	5	-	1.95×10^{-1}
Low viscosity	10	-	1.23×10^{0}
Low viscosity	5	5.0	1.15×10^{-2}
Low viscosity	5	7.5	5.00×10^{-2}
Low viscosity	10	5.0	4.99×10^{-2}
Medium viscosity	1	-	9.04×10^{-2}
Medium viscosity	5	-	2.30×10^{1}
Medium viscosity	10	-	2.74×10^{3}
Medium viscosity	5	5.0	2.30×10^{-2}
Medium viscosity	10	5.0	1.90×10^{-1}
Medium viscosity	5	2.5	4.45×10^{-1}
Medium viscosity	13	2.5	6.17×10^{1}

6.3.3. Production of alginate microparticles using liquid flow focussing

The rapid gelation of alginate upon exposure to divalent cations proved unhelpful when the production of alginate microparticles was attempted using the liquid-liquid flow focussing system described in Chapter 3 (Section 3.1.9). Using alginate as the disperse phase and calcium chloride as the continuous phase resulted in rapid gelation of the alginate within the device, blocking the tubing and creating misshapen and irregular lumps of gel rather than defined spherical microparticles. Increasing concentrations of sodium salts were added to the calcium chloride continuous phase in an attempt to delay gelation by means of sodium/calcium competition but this did not prove successful.

Instead, to delay the gelation process, an internal gelation method was used. The alginate was mixed with fine, insoluble calcium carbonate particles. To ensure even and homogenous gelation, the calcium carbonate particles must be small and evenly dispersed. To encourage this, 'nano'-calcium carbonate was produced, as described by Ueno et al. [144]. This created a fine suspension that could be fed through the flow focussing device as the disperse phase. The continuous phase was replaced with acidified oil, which acted as an immiscible solvent but also reacted with the carbonate to release calcium ions, which in turn cross-linked the alginate solution:

$$2\ CH_3CO_2H + CaCO_3 \rightarrow Ca(CH_3CO_2)_2 + CO_2 + H_2O \qquad \textbf{(Equation 6.01)}$$

Although this method was used to successfully produce microparticles (shown in Figure 6.02), the microparticles produced were opaque, in contrast to alginate gels produced from direct contact with a calcium solution which are typically clear and colourless. This is typical of this process of internal gelation [217]. The opacity observed is most likely due to unreacted calcium carbonate or to the presence of small bubbles within the alginate from the released carbon dioxide. Decreasing the concentration of calcium carbonate did not improve the transparency significantly. Opacity is not an ideal characteristic of a scaffold, as it makes visualising cells much harder. The use of a processing step involving acid also means that it would not be possible to encapsulate cells within microparticles of this type without compromising cell viability. Alternative methods of particle production were therefore investigated.

However, alginate-calcium carbonate scaffolds have been investigated for the controlled release of ibuprofen, as the drug can be adsorbed to calcium carbonate particles, which act as reservoirs within the structure. In this case, release of calcium ions is controlled by the gradual hydrolysis of D-glucono-δ-lactone, which causes a decrease in pH [217]. It is possible that the alginate-calcium carbonate microparticles could be produced in the same

way. In which case, the microparticles described above could also be useful as a method of controlled drug delivery, especially with the increased surface area provided over a solid scaffold of the same volume.

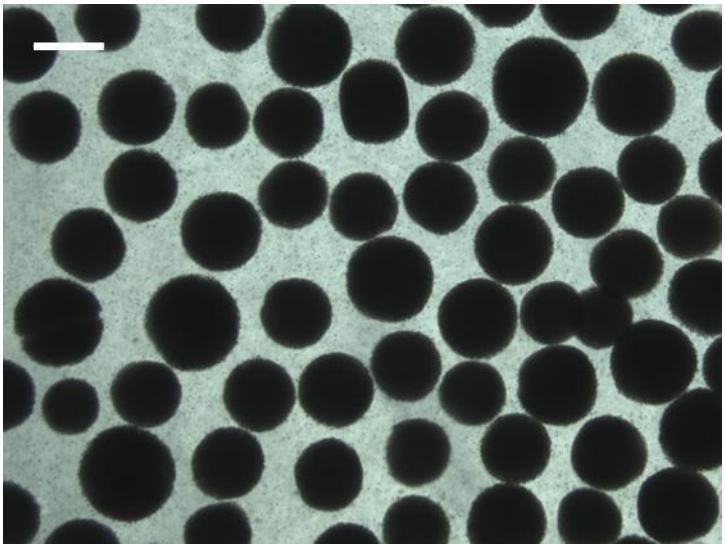

Figure 6.02: 7.5%-oxidised LV calcium alginate microparticles (2% w/v) produced using 2% w/v $CaCO_3$. Scale bar represents 200 µm.

6.3.4. Production of alginate microparticles using air flow focussing

Microparticles were produced using the air flow focussing device shown in Figure 3.04. The viscosity of the alginate solution was found to be a crucial parameter. The alginate solution needed to be very viscous to ensure a homogenous particle population. With low viscosities, the microparticles produced tended to have a very wide size distribution and were often more tear-shaped than spherical. In preliminary experiments, spherical, consistently-sized microparticles were produced using 10% w/v low viscosity (LV) alginate in the air flow focussing system. Examples of these microparticles are shown in Figure 6.03. Unlike the microparticles formed using calcium carbonate, the alginate-only microparticles were translucent, allowing for the visualisation of cells either on or in the microparticles themselves. The gentle processing conditions make this a suitable method for the encapsulation of cells, unlike the SF/G microparticles described in Chapter 5 which required soaking in methanol.

However, the unpredictable degradation of unmodified alginate makes it less attractive as a scaffold material than oxidised alginate, as previously discussed. Therefore, attempts to find an oxidised alginate solution with an equivalently high viscosity were undertaken. The

oxidised LV alginates all showed very low viscosities and so a very high concentration would have been required to attain the necessary viscosity. Low level oxidation of medium viscosity (MV) alginate was therefore considered a more practical approach. To generate a solution of 2.5%-oxidised MV alginate, the minimum volume of PBS required to dissolve a known mass of the solid was determined, producing a solution at 13% w/v. However, the viscosity of this solution was measured at 61.7 Pa·s, much higher than the 10% w/v LV alginate at 1.23 Pa·s (Table 6.01). The decision was therefore taken to use the 2.5%-oxidised MV alginate at a concentration of 10% w/v for air flow focussing. This improved its ease of handling, and also allowed for the blending of the alginate solution with solutions containing extracted ECM proteins without excessive decrease in the viscosity.

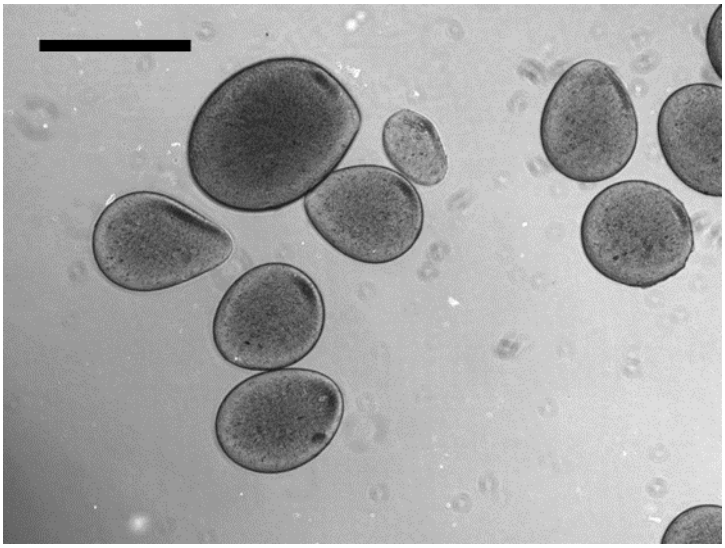

Figure 6.03: Calcium alginate microparticles produced in the air flow focussing system, from 10% w/v LV alginate. Scale bar represents 500 μm.

The use of a co-axial air flow to create beads or microparticles is well-reported in the literature. Though the equipment and precise set-ups vary, the principal is the same throughout [48, 93, 218]. The system used in this work is described in Section 3.1.9. The air flow acts to disrupt the flow of alginate to produce small droplets, which are cross-linked by collection in a calcium chloride or barium chloride bath. Having defined the concentration and oxidation level of the alginate solution, the key parameters that affect the output are:

- The distance between the end of the alginate nozzle/needle and the collection bath.
- The air flow rate disrupting the alginate solution.
- The rate of alginate flow [219].

While electrospraying is a similar, alternative method, air flow focussing holds less risk for the operator and requires less specialist equipment. Air flow focussing also provides more control over microparticle size than the formation of an emulsion, another alternative technique, and is also less damaging to cells.

6.3.5. Analysis of decellularisation techniques and products

While alginate allows for the rapid production of microparticles, its lack of bioactivity means cells do not adhere to it and can become quiescent when entrapped inside it [220]. In order to provide ECM proteins and bioactive signals to cells, decellularised skeletal muscle was produced for combination with alginate. However, as discussed, decellularisation must be carefully quantified to prevent immune rejections *in vivo.* Removal of cellular material from porcine skeletal muscle (PSM) was assessed by investigating levels of DNA within the treated samples. Although histological stains are not a quantitative method of examining decellularisation, they still prove useful. Sections of untreated PSM, SDS-treated PSM and Triton X-100/EDTA-treated PSM were stained with H&E and Hoechst 33342. This technique was not suitable for the homogenised sample as it was produced in a liquid form.

Figure 6.04 shows the stained sections. In 6.04(A), the untreated sample, cell nuclei are clearly visible around the outside of muscle bundles, and individual muscle fibres can be observed within the bundles. In both 6.04(B), the SDS-treated sample, and 6.04(C), Triton X-100/EDTA-treated PSM, the tissue has clearly been degraded by the decellularisation treatment. However, it is possible to see some intact nuclei within each section. In Figure 6.05, the sections have been stained with Hoechst to illuminate cell nuclei. There is clearly a large number of nuclei in the untreated sample, and there also appear to be a number of intact nuclei within the Triton X-100/EDTA-treated PSM. In the SDS-treated PSM sample, it is harder to distinguish any clear nuclei, suggesting a higher level of decellularisation in this sample.

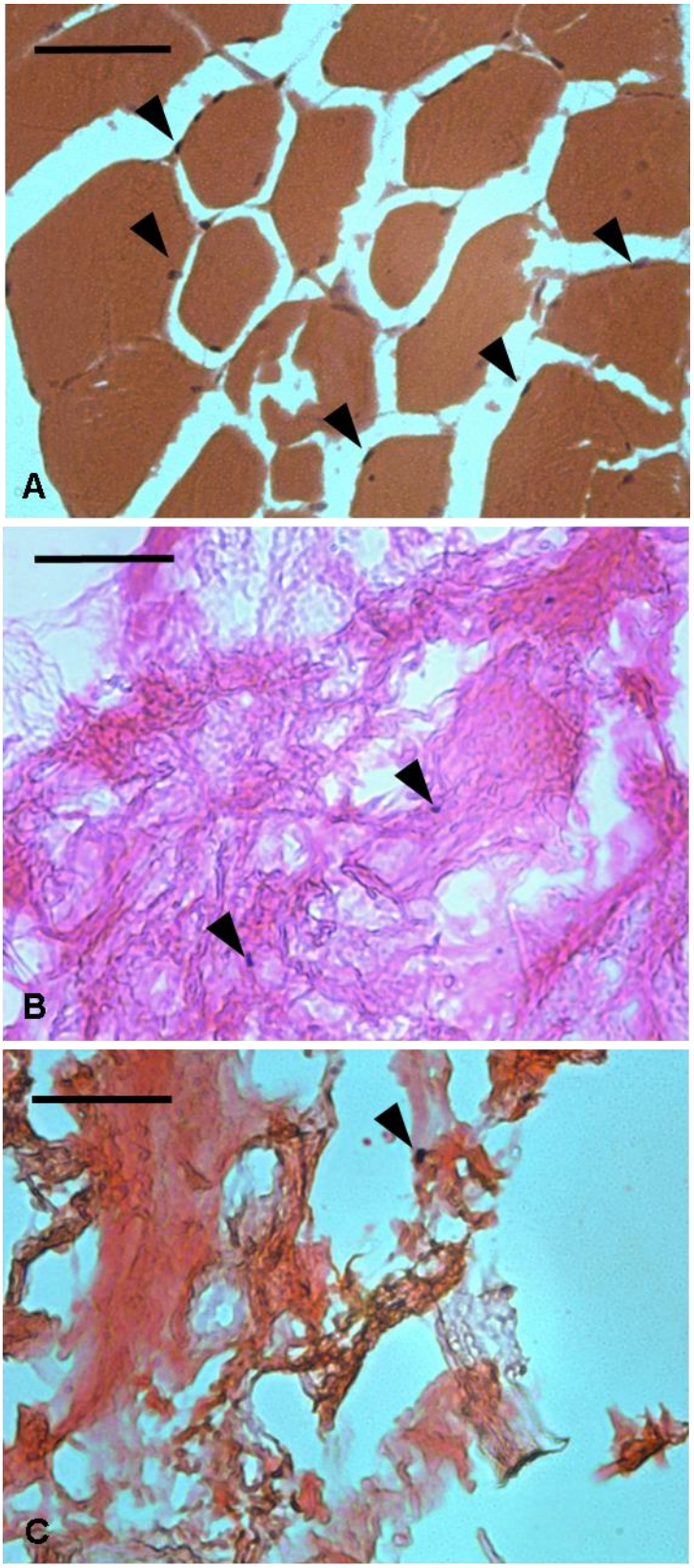

Figure 6.04: H&E stained sections of (A) untreated PSM, (B) SDS-treated PSM and (C) Triton X-100/EDTA treated PSM. Arrow heads indicate cell nuclei. Scale bars represent 50 µm.

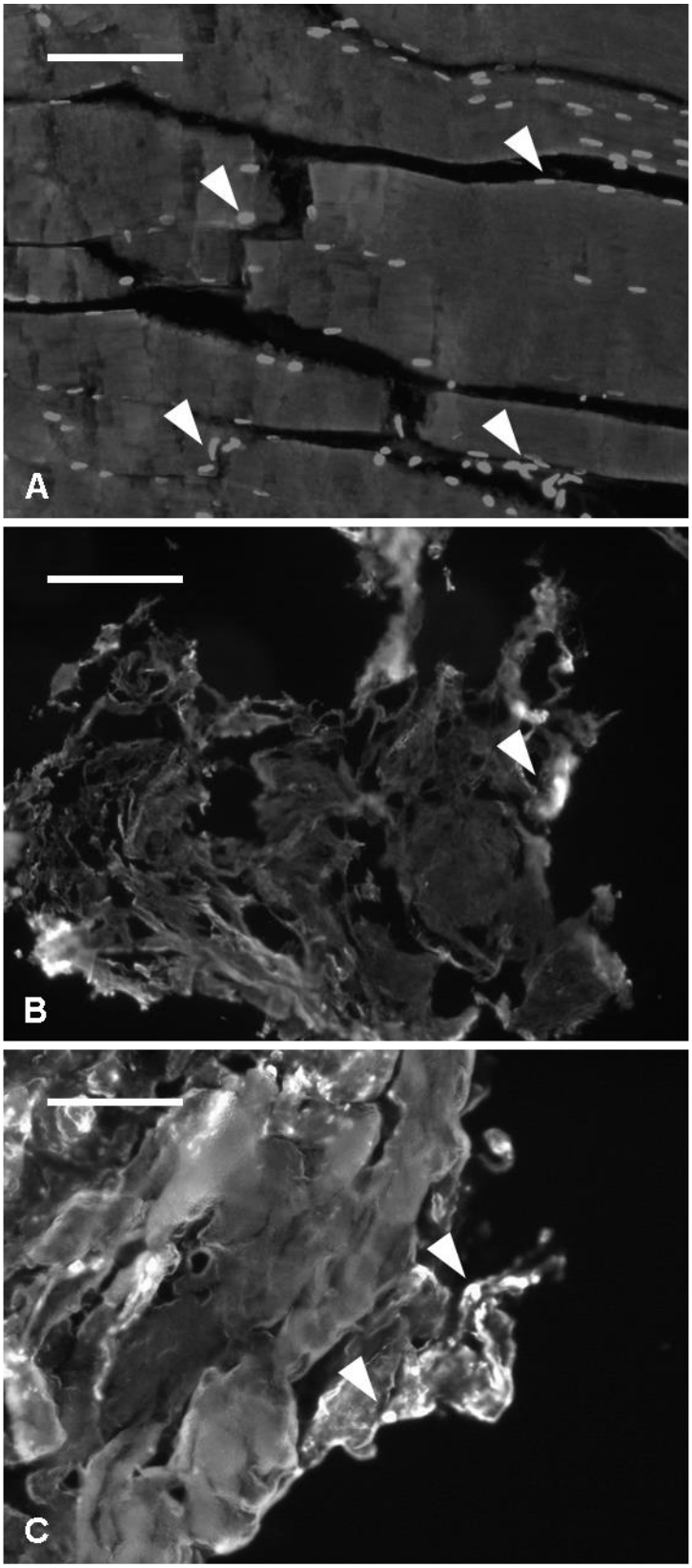

Figure 6.05: Hoechst-stained sections of (A) untreated PSM, (B) SDS-treated PSM and (C) Triton X-100/EDTA treated PSM. Arrow heads indicate fluorescently stained cell nuclei. Scale bars represent 100 µm.

The DNA content of samples of untreated PSM, SDS-treated PSM, Triton X-100/EDTA-treated PSM and homogenised/solubilised PSM was quantified as described in Section 3.2.7. The results are shown in Figure 6.06. As expected, the SDS-treated PSM contains significantly less DNA than the untreated sample. The value of 36.5 ng DNA/mg suggests a sufficient level of decellularisation according to the criteria described by Crapo et al. [104]. However, the Triton X-100/EDTA-treated sample is shown to still contain a high level of DNA (131.54 ng/mg), implying this protocol is not efficiently removing cellular material from the sample. The homogenised samples contained on average 48.5 ng of DNA per milligram of freeze-dried solution, just under the upper limit for successful decellularisation. It is possible that optimising the protocol could reduce this further below the threshold of 50 ng/mg. The levels of DNA in samples of this type were not reported in the original paper by Abberton et al. [145].

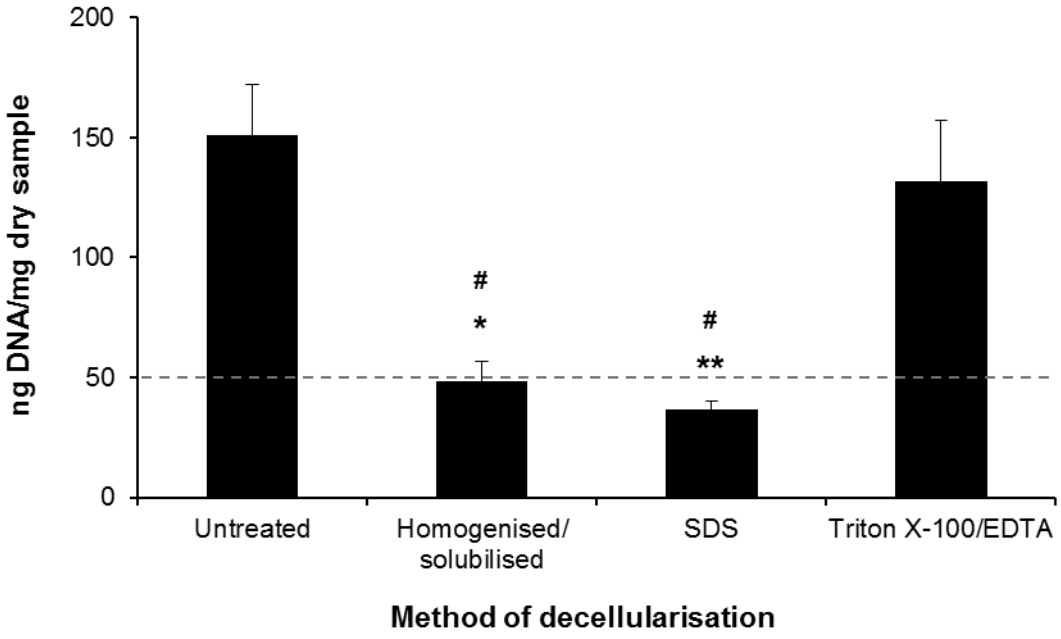

Figure 6.06: DNA levels in untreated PSM, SDS-treated PSM, Triton X-100/EDTA-treated PSM and homogenised/solubilised PSM, as determined by the PicoGreen assay. The dashed line indicates 50 ng/mg, the threshold level for successful decellularisation. Data shown represents mean + standard error (n=3). *p< 0.05 with respect to Untreated, ** p<0.01 w.r.t. Untreated; # p<0.05 w.r.t. Triton X-100/EDTA.

From the data shown here, it is apparent that the Triton X-100/EDTA procedure does not adequately remove cellular material from samples of PSM. The paper reporting this method only assessed DNA removal by H&E staining, and did not use a quantitative method of analysis [121]. The results obtained here suggest that H&E staining alone is not sufficient to confirm the removal of cellular material, since in Figure 6.04, the effectiveness of the

Triton X-100/EDTA method and the SDS method seem equivalent. However, the quantitative DNA results in Figure 6.06 strongly counter that. The SDS treatment and the homogenisation/solubilisation method appear to remove more cellular material than the Triton X-100/EDTA, but to confirm this, gel electrophoresis should be used to investigate the length of remaining DNA fragments.

Three methods were investigated here but there are multiple reports of different protocols, with different variations and combinations of decellularising agents [105, 221, 222]. The variety of results suggests that the efficacy of a particular method also depends on the starting tissue. This emphasises the importance of quantifying DNA remaining within a decellularised sample, especially for use *in vivo* where remaining DNA is likely to promote an immunogenic reaction [120].

One of the objectives of this work was to determine whether the decellularised muscle products would form self-supporting gels, as this would influence the amount and concentration of alginate necessary as a supporting matrix. The solubilised SDS-treated PSM sample did not form a gel, in contrast to instances described in the literature [214, 223, 224]. Even after neutralisation and 24 hours incubation at 37°C, the solution remained fluid. This could be due to the low protein concentration of the sample, which was determined by the BCA assay as 2.25 mg/mL. Though collagen alone would be expected to form a weak gel at concentrations of this range, it is likely the sample contained a large proportion of other proteins less prone to gelation. The inability of the product to gel could also be due to the denaturing effect of SDS on proteins, which results in the loss of tertiary structure [225]. The use of this product was therefore not pursued.

The protein content of the homogenised/solubilised PSM solution ranged between 7.0 and 11.4 mg/mL in different batches. Aliquots of the solution were found to gel at physiological conditions, after approximately 1 hour at 37°C, as reported by Abberton et al. [145] (Figure 6.07). This is likely to be due to a large proportion of collagen within the extract. However, the gels produced were soft and fragile, despite observed syneresis. The product was therefore deemed more suitable for blending with a stronger scaffold material such as alginate than for use alone.

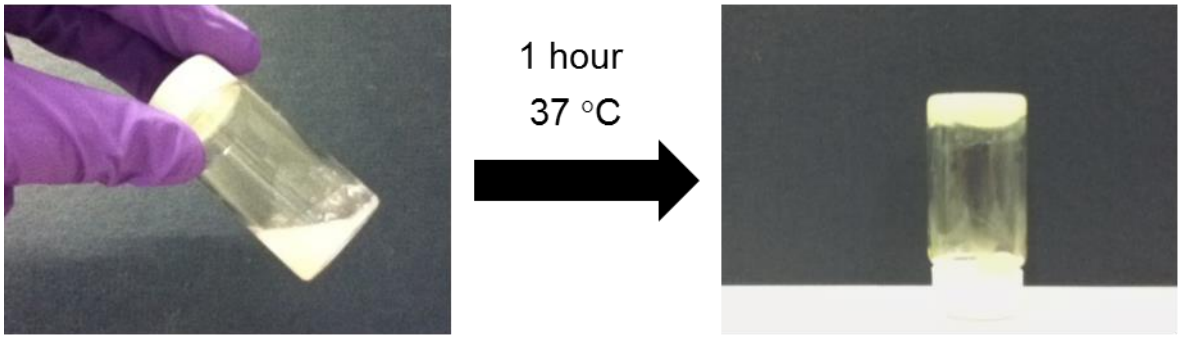

Figure 6.07: Homogenised/solubilised product of decellularisation. The product is initially in a liquid form. After 1 hour incubation at 37°C, it forms a gel stable to inversion.

The product was analysed by SDS-PAGE, and the results are summarised in Figure 6.08. The results are consistent with those obtained by Abberton et al., showing bands that correspond to the masses of collagen I, laminin α4 and α1 chains, as well as entactin [145].

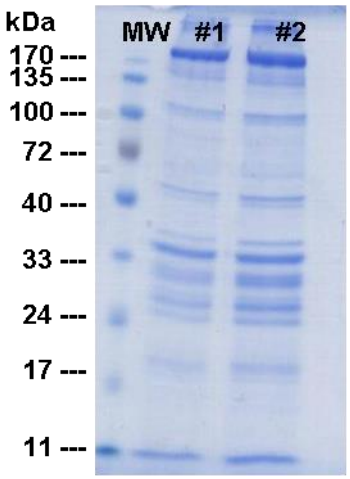

Visible bands (kDa)	Possible protein
~35	Degradation products
~50	Biglycans
~100	Collagen I
~140	Entactin
180-200	Laminin α1 & α4

Figure 6.08: An SDS-PAGE of homogenised/solubilised samples (#1, #2) with a molecular weight ladder (MW) for reference. The most prominent bands are summarised with the proteins likely to be responsible.

To test the cytocompatibility of the product, 3T3 fibroblasts were seeded on multiwell plates coated with either the decellularised product or collagen. After three days, cell metabolism was assessed with the MTS assay. The results are shown in Figure 6.09. 3T3 fibroblasts showed equivalent levels of metabolic activity between untreated TCP and the decellularised product and collagen coated surfaces. This strongly suggests that the decellularised product is biocompatible and supports cell attachment and growth.

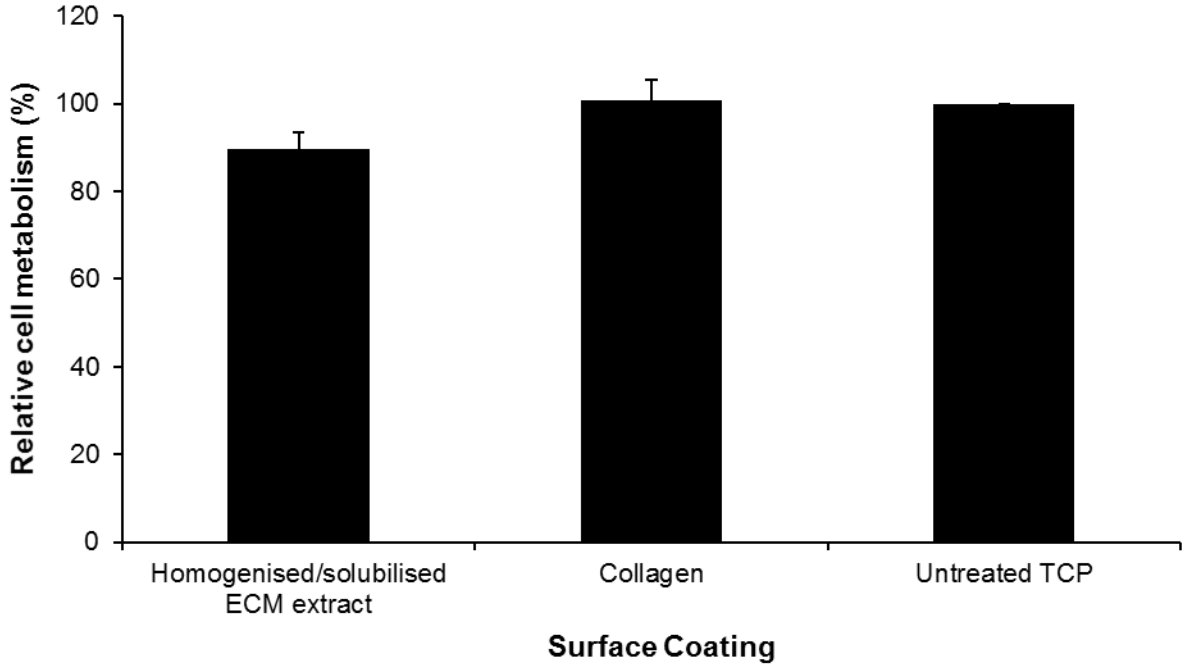

Figure 6.09: 3T3 fibroblast metabolism assessed 3 days after seeding expressed as a percentage of the signal obtained for the control, untreated TCP. Higher values suggest higher cell adhesion to the substrate in question. Data shown represents mean + standard error (n=4). No significant differences were observed.

6.3.6. Production of alginate/ECM protein microparticles

The homogenised/solubilised PSM protein solution was blended 1:1 with 2.5%-oxidised MV alginate and fed into the air flow focussing system to produce the microparticles shown in Figure 6.10. These microparticles showed some size variation but were generally consistently sized with a mean diameter of 321 ± 82 μm (mean ± standard deviation). However, the microparticles had a mottled appearance, suggesting that the homogenised/solubilised proteins might have precipitated out of solution and were not consistently mixed with the alginate solution. These microparticles look very similar to examples of alginate microparticles encapsulating decellularised ECM powders, produced by Mazzitelli et al., who showed the inclusion of the ECM powders in the (un-oxidised) alginate microparticles resulted in improved encapsulated Sertoli cell viability compared to

cells encapsulated in alginate alone [115]. The fact the ECM extract was in powdered form rather than solubilised did not seem to have any effect, although it is still the case that the ECM constituents are not evenly distributed which could lead to uneven cell distribution and viabilities within the microparticles.

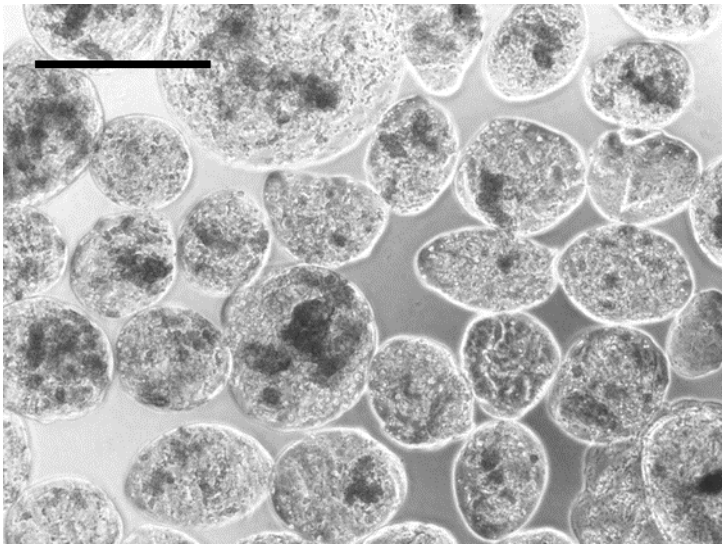

Figure 6.10: Microparticles produced from 2.5%-oxidised calcium alginate and homogenised/solubilised PSM solution. The final oxidised alginate concentration was 5% w/v; the final protein concentration was 0.35% w/v. Scale bar represents 500 µm.

6.3.7. Cell encapsulation within alginate-blended microparticles

As previously discussed, alginate alone does not interact with cells to support adhesion or proliferation and simply acts as an inert scaffold. An aim of the work in this chapter was to combine alginate with decellularised ECM extracts, but as shown above, the homogenised/solubilised ECM solution appeared to precipitate in the oxidised alginate particles. In order to provide cells with a homogenous environment, with protein evenly distributed throughout, commercially available collagen was adopted as a model protein. As collagen is the major structural protein in mammalian tissues, it is also likely to be the major constituent of any ECM extract. 2.5%-oxidised MV alginate (10% w/v) was therefore blended in a 1:1 ratio with a commercially available collagen solution, producing the microparticles shown in Figure 6.11. Blending oxidised alginate with lysine residue-containing proteins such as gelatin or collagen can lead to the cross-linking of the two components by formation of a Schiff base, between the amine group provided by the protein and the available aldehyde, providing stability to the blend [92, 226].

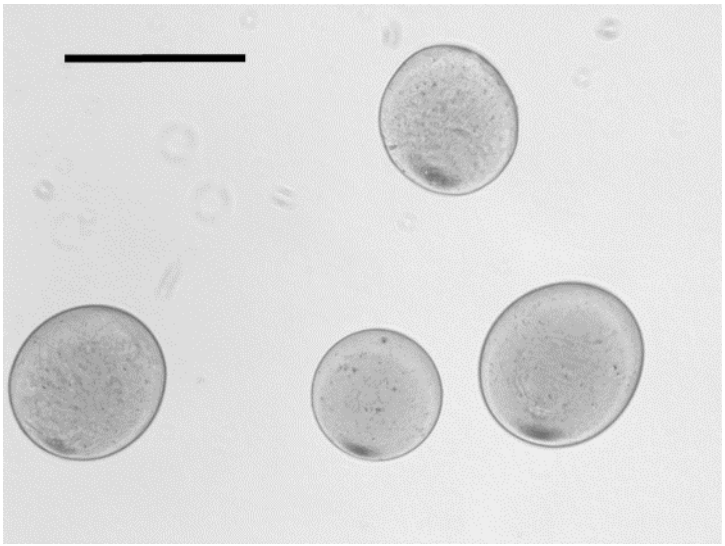

Figure 6.11: Microparticles produced from 2.5%-oxidised calcium alginate (final concentration 5% w/v) and collagen (final concentration 0.15 % w/v). Scale bar represents 500 µm.

To establish the feasibility of encapsulating cells within oxidised alginate/ECM microparticles, rMSCs were re-suspended in collagen solution and then blended with oxidised alginate. The resultant solution was used to produce microparticles, shown in Figure 6.12. The translucent nature of the microparticles makes it possible to see the cells without the need for fluorescent staining. This is a strong advantage over commercially available microparticles like Cultispher-S. Unlike the microparticles blended with the decellularised ECM extract, the oxidised alginate/collagen microparticles show no evidence of precipitated proteins.

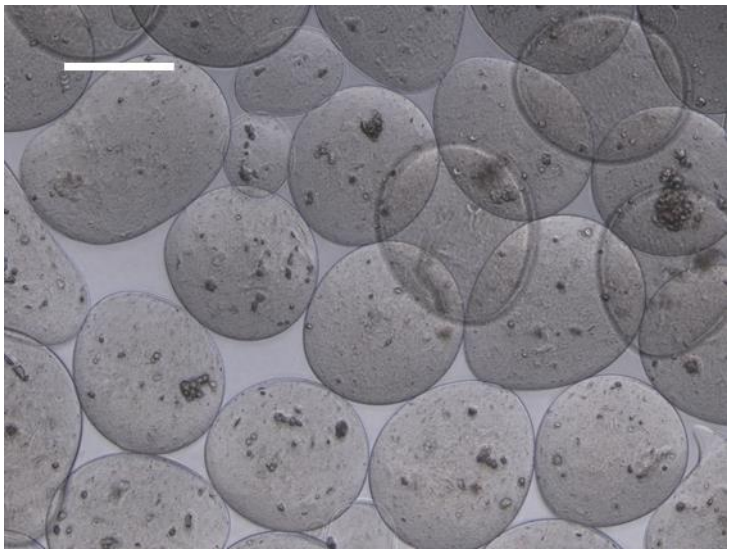

Figure 6.12: rMSCs encapsulated in oxidised calcium alginate/collagen microparticles. Scale bar represents 200 µm.

However, in calcium chloride solution these oxidised alginate/collagen microparticles had a mean diameter of 329 μm, but expanded upon transfer into DMEM, swelling to an average of 529 μm, a 60% increase. This swelling is possibly due to exchanges between the calcium ions in the alginate with other cations in the cell media, such as sodium. This weakens the structure of the cross-linked alginate and allows swelling to occur. Oxidised alginates are also recognised to be more highly hydrated than their unmodified components, possibly contributing to this effect [95].

To improve the stability of alginate-based microparticles in cell culture media, the use of barium chloride as a divalent cation source was investigated. It has been reported that the use of Ba^{2+} to cross-link alginate gels can increase the resultant stability, as barium ions have a higher affinity for alginate than calcium ions [91]. However, barium can act as an inhibitor of potassium ion channels above 10 mM and so should be used at low concentrations to avoid this toxicity [227]. Though the benefit of using Ba^{2+} in place of Ca^{2+} can depend on the ratio of guluronic acid to mannuronic acid within the alginate (not defined for the alginate used), an increase in stability was observed for barium alginate microparticles in DMEM, suggesting the alginate used here had a high proportion of guluronic acid residues. The mean diameter of the barium alginate/collagen microparticles increased upon the transfer of the microparticles into DMEM but this was limited to a 13% increase.

Cardiomyocyte cells have been encapsulated within barium alginate/collagen microparticles, cross-linked by an initial exposure to 50 mM barium chloride with no detrimental effects on cell viability [228]. However, to stay well below toxicity limits, in this work a solution of 10 mM barium chloride was used.

Maintenance of cell viability in the oxidised alginate/collagen microparticles was assessed by fluorescent staining (Section 3.2.2). The results are shown in Figure 6.13. At both days 3 and 7 post-encapsulation, the rMSCs remain predominately viable. A higher proportion of rMSCs appear viable at day 7, which could be a result of the individual particles measured, though representative samples were chosen. It is more likely that by day 7, viable cells have proliferated, resulting in a higher proportion of viable cells. Measuring total cell number at these time points would help establish whether this was the case.

High cell viability is consistent with reports suggesting alginate and alginate/protein blends can adequately support cell growth and proliferation. Bai et al. cultured cardiomyocytes in electrosprayed alginate/collagen microparticles for periods of up to 180 days, and observed high cell viability, along with the development of a contractile phenotype [228]. It has also been shown that oxidised alginate/gelatin scaffolds can help maintain the function of

hepatocytes, avoiding de-differentiation while supporting proliferation for a period of four weeks [92]. Wright et al. also observed that the inclusion of collagen IV in oxidised alginate gels increased the viability of encapsulated limbal epithelial cells, while Sang et al. found that the use of alginate/collagen gels resulted in increased proliferation over collagen gels alone [95, 229]. Generally, the inclusion of gelatin, collagen or other ECM proteins in alginate gels improves cell adhesion, viability and proliferation [115, 230].

A number of groups also used alginate to improve the mechanical properties of collagen gels, either increasing the Young's modulus of the combined alginate/collagen gels, making the gels more resistant to plastic deformation, or using alginate to allow more rapid gelation and control over the final gel shape [226, 231, 232].

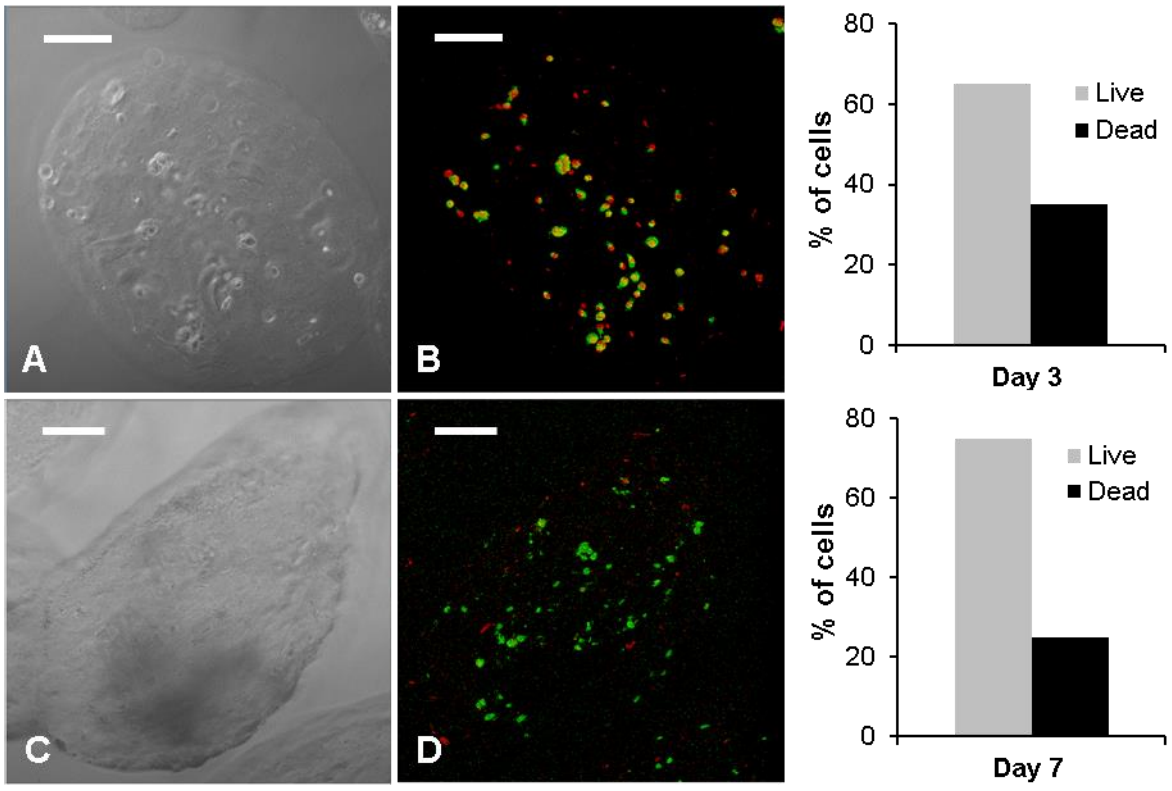

Figure 6.13: Confocal images of encapsulated rMSCs in oxidised alginate/collagen microparticles. Microparticles are shown at 3 days (A and B) and 7 days (C and D). Cells are stained with LIVE/DEAD to indicate viability. Viable cells fluoresce green, while non-viable cells fluoresce red. Graphs represent the proportion of viable to non-viable cells at each time point (n=1). Scale bars represent 100 µm.

6.3.8. Osteodifferentiation of encapsulated cells

Osteodifferentiation of rMSCs encapsulated within oxidised alginate/collagen microparticles was assessed to determine whether this scaffold type was suitable for bone tissue

engineering. Differentiation was assessed by ALP activity and osteopontin expression (Section 3.2.3). ALP activity is indicated by the purple deposits within the microparticles as shown in Figure 6.14. There does not appear to be a large difference in ALP activity between rMSCs cultured in either basal media or ODM. However from these results it would appear the oxidised alginate/collagen microparticles do support osteodifferentiation.

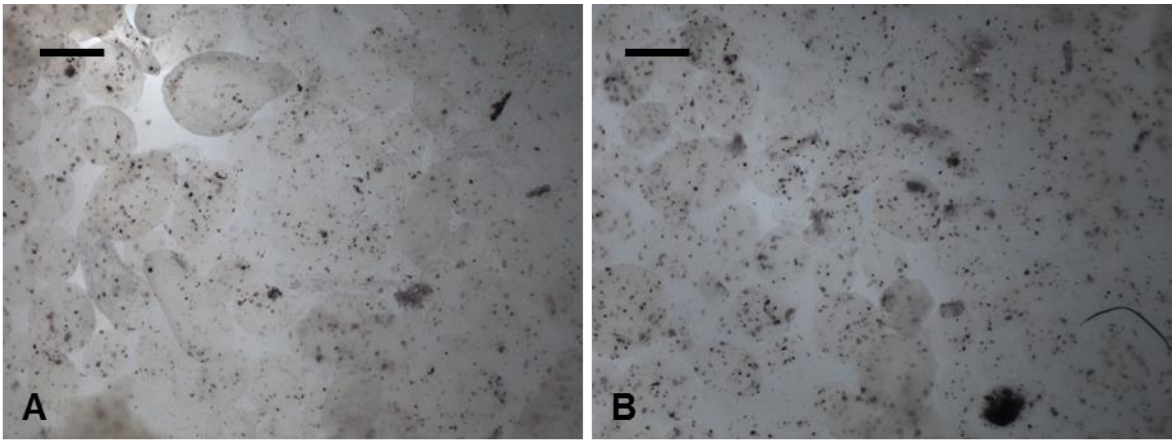

Figure 6.14: rMSCs encapsulated in alginate/collagen microparticles. Cells were cultured for 14 days in A) basal media; or B) ODM. The samples were assayed for ALP activity, indicated by purple deposits within the microparticles. Scale bars represent 500 μm.

The levels of secreted osteopontin were assessed to confirm these results (Section 3.2.3) and can be seen in Figure 6.15. Very small quantities of osteopontin were expressed by both rMSCs in ODM and basal media. The low values observed (compared to expression from rMSCs culture on SF/G 25:75 microparticles, Figure 5.15), could be due to expressed protein remaining encapsulated within the alginate/collagen microparticles rather than freely diluted in the culture media.

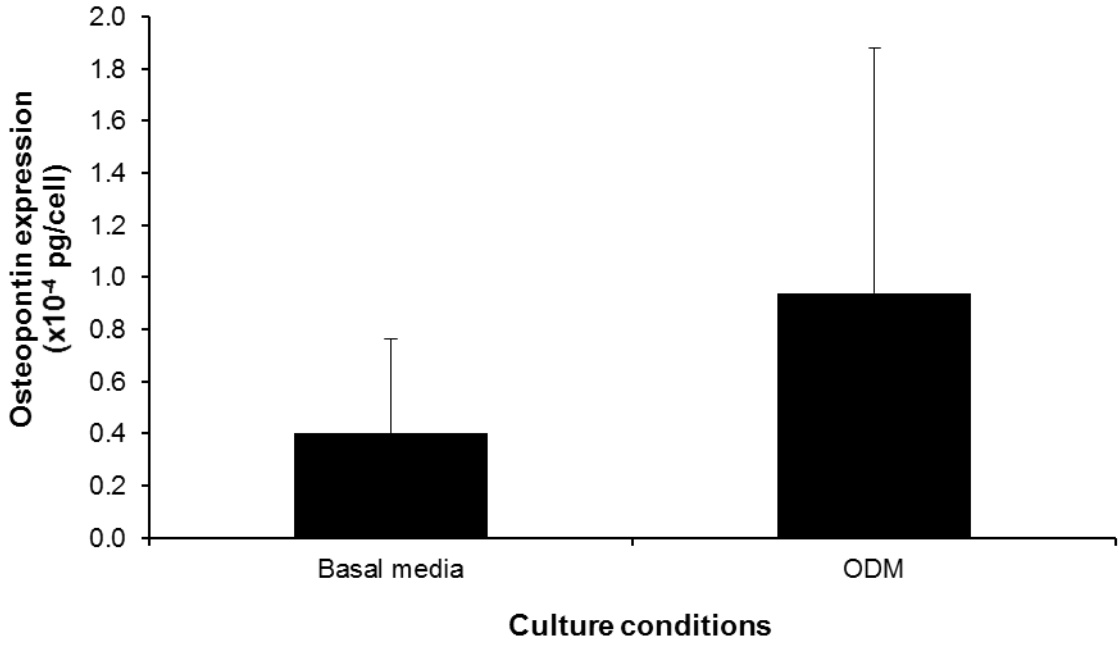

Figure 6.15: Expression of osteopontin at day 14 in cultures of rMSCs encapsulated in oxidised alginate/collagen microparticles. Data was normalised by cell number. Data shown represents mean + standard error (n=3). No significance was observed.

Future experiments should investigate dissolving the oxidised alginate/collagen microparticles, for example by use of a chelation agent such as EDTA, before assaying the sample for protein expression. It would also be desirable to assay samples for other osteogenic bone markers, such as calcium deposition or osteocalcin expression, and examining the cultures at later time points, up to 28 days.

The ability of oxidised alginate/collagen materials to support osteodifferentiation has not been widely reported, though cardiogenesis and chondrogenesis on these blends have been separately reported [228, 233, 234]. However, the results here suggest oxidised alginate/collagen materials can adequately support osteogenic differentiation, though further analysis and investigation is required.

6.4. Conclusions

Having established that the method for microparticle production described in Chapter 5, axisymmetric flow focussing, was not suitable for alginate, oxidised alginate and alginate-blended materials, an alternative system was developed. An air flow focussing system was constructed to rapidly produce oxidised alginate microparticles. This system was found to be highly dependent on the viscosity of the alginate solution used. As with the axisymmetric

flow focussing device, the air flow focussing device was constructed using unmodified commercially available fittings, and so can be reproduced by any interested party.

Collecting alginate droplets directly into a gelling bath of calcium or barium chloride allowed for rapid gelation of the resulting beads. It was observed that the use of barium chloride provided improved stability of the gels in culture medium over calcium chloride for the alginate used here.

The decellularisation of skeletal muscle samples was investigated as a method of producing an alternative scaffold material, and although a number of methods were considered, only one (homogenisation and solubilisation of skeletal muscle) proved suitable for the production of a gel-forming material. However, the softness of the resultant gel meant it was impractical for use alone, but may yet prove useful as a supplement to blended scaffolds. The gel product of the homogenisation/solubilisation process described was composed of a high proportion of collagen, and thus, oxidised alginate/collagen blended gels were investigated for their ability to support the proliferation and differentiation of encapsulated cells. The use of an oxidised alginate/collagen blend for osteogenic differentiation of MSCs has not been previously described. It was shown that the oxidised alginate/collagen materials supported cell viability and the osteogenic differentiation of rMSCs. Future work should look into the potential benefits of using decellularised ECM proteins compared to collagen alone, and whether cell-laden oxidised alginate/collagen or alginate/decellularised ECM microparticles can be seeded externally with cells to allow moulding into a macroscopic tissue construct of the type described in Chapter 5.

Chapter 7

Design of a hollow fibre perfused bioreactor for the development of pseudo-vascularised tissue constructs

7.1. Introduction

Bioreactors for tissue engineering

Bioreactors are used to support cell growth and proliferation in three-dimensional cultures, by providing oxygen, nutrients, and appropriate stimuli to cell-seeded scaffolds. The use of microparticles, or even porous sponge-like scaffolds, provides much higher surface areas in smaller volumes than the equivalent two-dimensional culture systems, therefore making the expansion of cells in these systems much more efficient.

For the culture of tissue constructs, there are a number of bioreactor types that can be used, of varying levels of complexity. The properties of some of these are summarised in Table 7.01. For a fuller description of various bioreactor types, refer to Section 2.4.

Table 7.01: Advantages and disadvantages of selected bioreactor design types for the culture of cell/scaffold tissue constructs.

Bioreactor type	Advantages	Disadvantages
Stirred tank/spinner flask	Simple to assemble and use; shear stress may positively affect osteogenesis of MSCs [127].	Construct size limited, as shear stresses increase with the increased stir rate required for larger constructs [125].
Perfusion chamber	Can be used to seed cells through scaffold initially [129]; shear stress may increase osteogenesis of MSCs.	Media flow may wash out newly formed ECM; sample must fit chamber exactly to ensure media flows through and not around the construct [42].
Hollow fibre bioreactor	Very large surface area available; cells can be seeded on or in fibres; cells on fibre exterior are decoupled from shear stress [132].	Not generally integrated with scaffolds; cell harvest can be difficult to achieve efficiently [235].
Rotating wall bioreactor	Low shear stress and low turbulence environment [125].	Oxygen delivery to cell aggregates and constructs is by diffusion only, limiting scale up [125].

Tissue constructs and the importance of vascularisation

Tissue constructs have been built, from cell-laden microparticles in a bottom up approach, using perfusion chamber bioreactors [57, 58]. Perfusion chambers prevent necrosis by providing media flow through the scaffold, but may wash out *de novo* ECM components [42]. The use of a hollow fibre to perfuse the culture, isolating shear stress from oxygen and nutrient delivery, could prevent this whilst maintaining viability.

Construct viability can be improved and maintained for longer periods of time using the bioreactors discussed, by preventing necrosis of central regions and therefore allowing larger construct sizes to be grown. However, on implantation *in vivo*, unless nutrient flow is maintained the construct may become necrotic as angiogenesis and vasculogenesis may not occur rapidly. If a construct is designed with an in-built pseudo-vasculature system, this would allow for anastomosis upon implantation and therefore rapid integration with the host vasculature.

While some groups have taken the somewhat laborious approach of building microchannels by the piece-by-piece assembly of individual hollow rings, others have utilised more elegant approaches [236-238]. Miller et al. printed 3D grids from carbohydrate glass (i.e. sugars), then moulded cell-laden gels around the structure which began to dissolve on exposure to cell culture media, leaving behind a hollow, interconnected network through which media was perfused [239]. A similar approach has been used to create collagen scaffolds with capillary-like networks, by moulding collagen around gelatin hydrogel rods – the gelatin dissolves as the collagen solidifies at 37 °C [240]. A simpler approach is to mould scaffolds around biodegradable hollow fibres, which reduces the processing steps as the fibres do not need to be removed. They could also be seeded internally and externally with endothelial and smooth muscle cells, respectively, before encasing in a scaffold structure, in order to replicate the vascular phenotype. Highly permeable, biodegradable PLA hollow fibres have been designed with this application in mind [241].

7.2. Aims & Objectives

Previous chapters have shown that microparticles can be produced from both silk fibroin/gelatin (SF/G) and alginate/extracellular matrix protein blends. The SF/G microparticles were shown to support cell adhesion on their exterior, and evidence of the osteodifferentiation of rMSCs was observed. Meanwhile, the gentle conditions necessary for the production of alginate/ECM microparticles allowed for the encapsulation of cells

within the microparticles, also supporting osteodifferentiation of rMSCs. The original aim of using microparticles as a scaffold type was the ability to rapidly mould them together to produce a relatively large tissue construct (as in Figure 2.02). Preliminary results suggested that the SF/G microparticles had some potential for building up structures in this way. However, as previously discussed (Section 2.2.4), larger constructs are hindered by lack of vasculature and central areas will become necrotic if cells are further than 200 μm from a source of oxygen [242].

The aim of the work in this chapter is therefore to create a bioreactor system to allow the generation of a macroscopic construct from cell-laden microparticles with a pseudo-vascular structure. The objectives were defined as follows:

- Design a hollow fibre bioreactor system for moulding cell-laden microparticles into a three-dimensional construct.
- Examine whether the use of the hollow fibre system can improve construct viability over a non-perfused control.
- Create and characterise a centimetre-scale bone tissue construct using rMSC-laden microparticles moulded within the bioreactor.

7.3. Results & Discussion

7.3.1. Design of a hollow fibre/microparticle bioreactor

To investigate whether cell-laden microparticles could be moulded around a perfused hollow fibre, a prototype bioreactor was developed. It was designed so that a permeable hollow fibre would pass through a chamber or mould containing the microparticles, and thus support cell growth and proliferation (and therefore the formation of a cell linked construct). A schematic of the hollow fibre bioreactor can be seen in Figure 7.01.

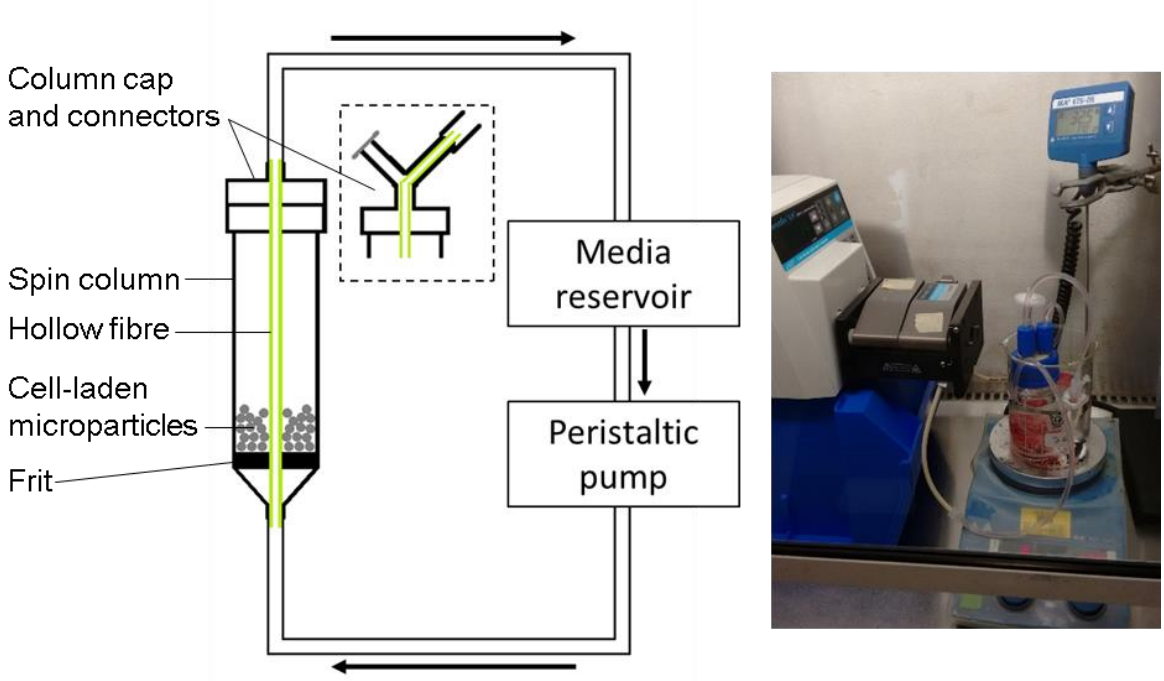

Figure 7.01: Schematic of bioreactor set up for cell culture experiments. The dashed box shows the alternative fittings to allow sampling from within the chamber. Arrows indicate the direction of media flow. A photograph of the set-up is shown on the right.

Since these experiments were preliminary investigations, it was deemed practical to design the hollow fibre bioreactor on a small scale. Protein extraction spin columns were chosen for the outer body of the hollow fibre chamber due to their size (approximate volume of 1 mL) and convenient design – open at both ends with a Luer lock fitting cap. This allowed for a hollow fibre to be threaded through the column easily, and the whole chamber can easily be connected onwards using a Luer-barb connector.

To ensure consistency in the permeability of the fibre, commercially available KrosFlo® Implant Membranes were used. These are PVDF hollow fibres, designed for the implantation of cells within animal models. The fibres can be sterilised by autoclaving, and resist cell adhesion. This would prevent cells coating the fibre and creating a monolayer which would hinder diffusion to the rest of the chamber. The molecular weight cut off of the tubing is 500 kDa, high enough to readily allow the diffusion of BSA (approximately 70 kDa), a major component of foetal bovine serum (FBS) in cell culture media. However, this cut off is low enough to isolate mycoplasma, viruses and bacteria, protecting cells from any potential contaminants in the media (though aseptic cell culture techniques should prevent this occurring in the first place).

The fibres were threaded through the spin columns and fixed at both ends to ensure that media flow into the hollow fibre chamber was only through the hollow fibre wall. Flow

through the fibre was against the direction of gravity so that the fibre was entirely full of media with no bubbles (which would minimise the contact of the media with the wall and therefore minimise the potential surface area for media diffusion).

The chamber was connected to platinum-cured silicone tubing at each end to allow for gas exchange between the media and the atmosphere. Silicone tubing is low protein binding, and platinum curing reduces the amount of chemicals that can be leeched from it [128]. However, it has relatively low mechanical durability, so PharMed® BPT peristaltic tubing was connected in line, via the pump and the cell culture media reservoir, to create a closed circuit around the hollow fibre bioreactor chamber. The PharMed tubing was chosen for its ability to withstand the stress of the peristaltic pump over a week. The use of a peristaltic pump allowed for the continuous circulation of media through the system.

Due to the size of the equipment, the hollow fibre system could not be assembled within the atmosphere-controlled incubators available for use. The cells grown for culture in the hollow fibre bioreactor were therefore adapted to grow in carbon dioxide-independent media. This media uses a buffering system of mono- and dibasic sodium phosphate and glycerol 2-phosphate (instead of sodium bicarbonate), so that carbon dioxide is not required for buffering and cells can be grown under atmospheric conditions.

Each bioreactor chamber with hollow fibre was discarded after a single use, as the component parts were relatively cheap and easily replaced. This also removed the need to thoroughly clean and sterilise the chambers between uses, minimising the risks of cross-culture contamination. The small size of the bioreactor chamber meant that the inclusion of inline monitoring for pH and dissolved oxygen was not practical, although further refinement of the design should look to include a mechanism for this.

At this stage, scale-up of the system was not a priority for design, but it would be theoretically possible to run a number of the bioreactor chambers in parallel. Alternatively, the chamber itself could be expanded, and with the inclusion of additional fibres, larger constructs could potentially be formed.

7.3.2. Diffusion of protein through the hollow fibre bioreactor

The purpose of moulding microparticles around a hollow fibre was to improve delivery of nutrients and oxygen to central regions of the final construct, with the aim of improving cell viability. To test whether cell culture components, including large molecules such as serum proteins, would diffuse across the hollow fibre wall into the cell chamber, preliminary

experiments were carried out using BSA. As mentioned above, BSA is a major component of FBS (accounting for over 60% of the protein content) [243]. A solution of BSA was pumped through the bioreactor and samples were taken from within the chamber at hourly time points during the day (Section 3.1.3). The results are shown in Figure 7.02.

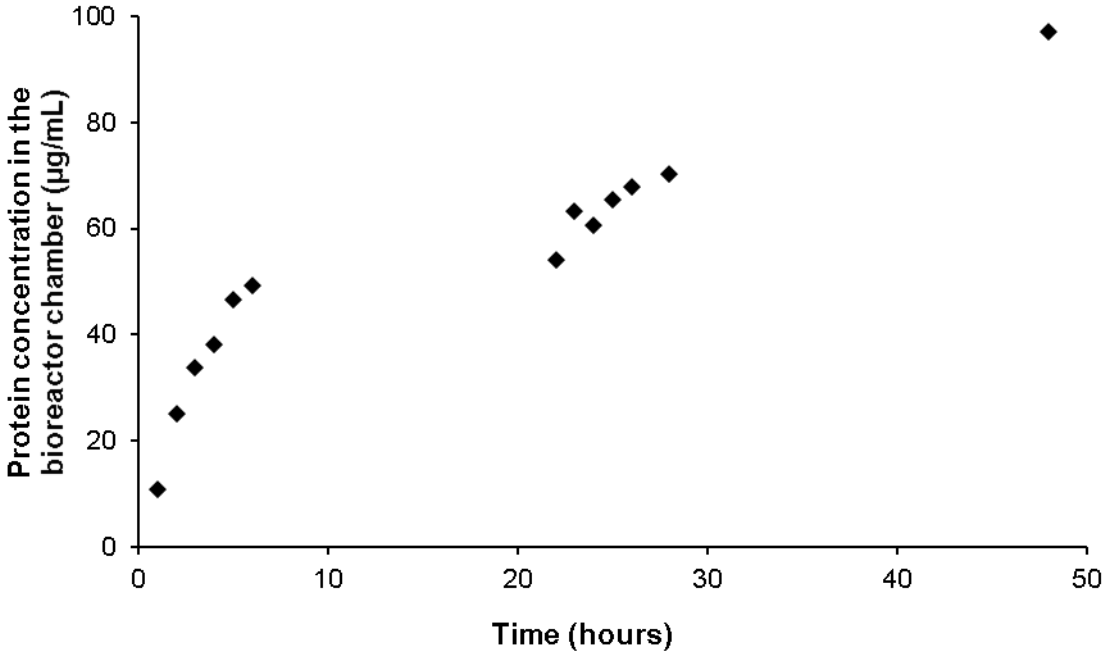

Figure 7.02: Diffusion of BSA through hollow fibre into bioreactor chamber. Data shown represents mean values (n=2).

Initially, BSA diffused into the chamber rapidly, though this rate slowly plateaued. The highest measurement was obtained at 48 hours, thought at 97.1 µg/mL, this is only 24% of the concentration within the fibre. The slowing rate of diffusion could be a result of the build-up of protein on the inside of the fibre and through the pores. This process, of the reversible accumulation of solutes at a membrane, is known as concentration polarisation, and over longer periods of time can lead to irreversible adsorption and fouling of the membrane [244]. This would significantly decrease diffusion through the hollow fibre membrane, and in this scenario, deprive cells of their nutrient supply. It is possible this effect could be minimised by periodically reversing the direction of flow to dislodge any accumulated protein.

7.3.3. Cell viability with the hollow fibre bioreactor

3T3 fibroblasts were seeded onto Cultispher-S microparticles before transferral into the hollow fibre chamber, or a sealed Eppendorf of approximately the same size, which functioned as a control system. After 7 days of culture, the cell viability within the samples was assessed using fluorescent LIVE/DEAD staining and a metabolic activity assay. The results are shown in Figures 7.03 and 7.04. It is immediately apparent that the 3T3 fibroblasts grown around the hollow fibre have maintained a higher level of viability. In Figure 7.03, 72.4% of visible cells cultured in the hollow fibre bioreactor are viable, compared to only 34.3% of cells grown in the control system.

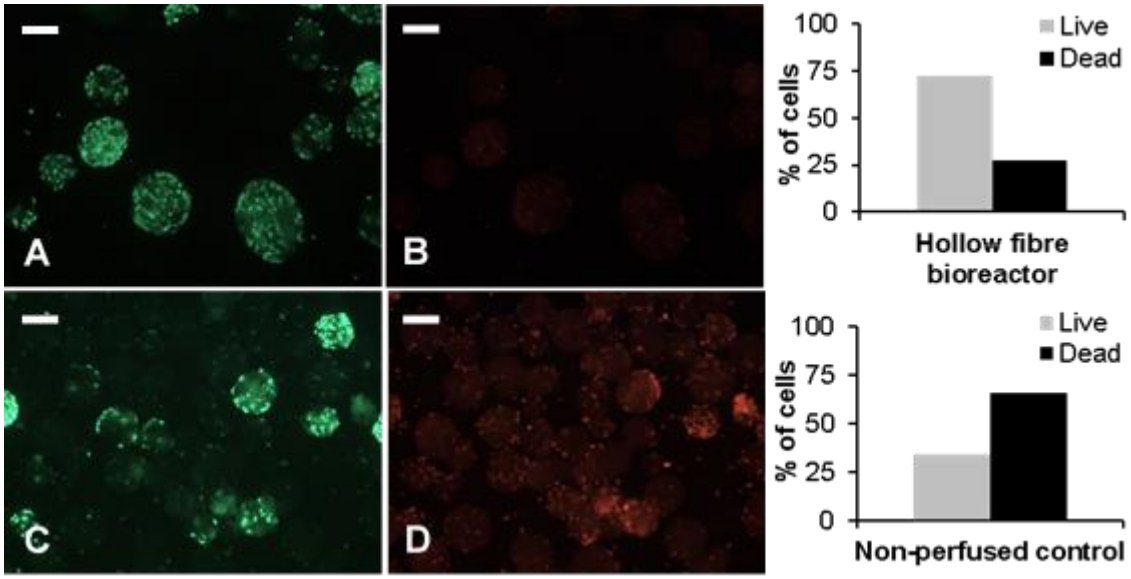

Figure 7.03: 3T3 fibroblasts on Cultispher-S microparticles, stained fluorescently for viability after 7 days of culture. Cells were cultured in (A, B) the hollow fibre bioreactor or (C, D) the non-perfused control system (n=1). Live cells fluoresce green while red cells are dead. Scale bars represents 200 µm. The graphs show proportions of visible cells in representative images.

This is reflected also in Figure 7.04, in which 3T3 fibroblast metabolism is shown to be much higher than in the hollow fibre bioreactor than in the non-perfused control. This is likely due to the reduced number of viable cells in the control system, but nonetheless strongly suggests the hollow fibre bioreactor is a useful and functional system for maintaining the viability and function of cells seeded on microparticles in a low shear environment.

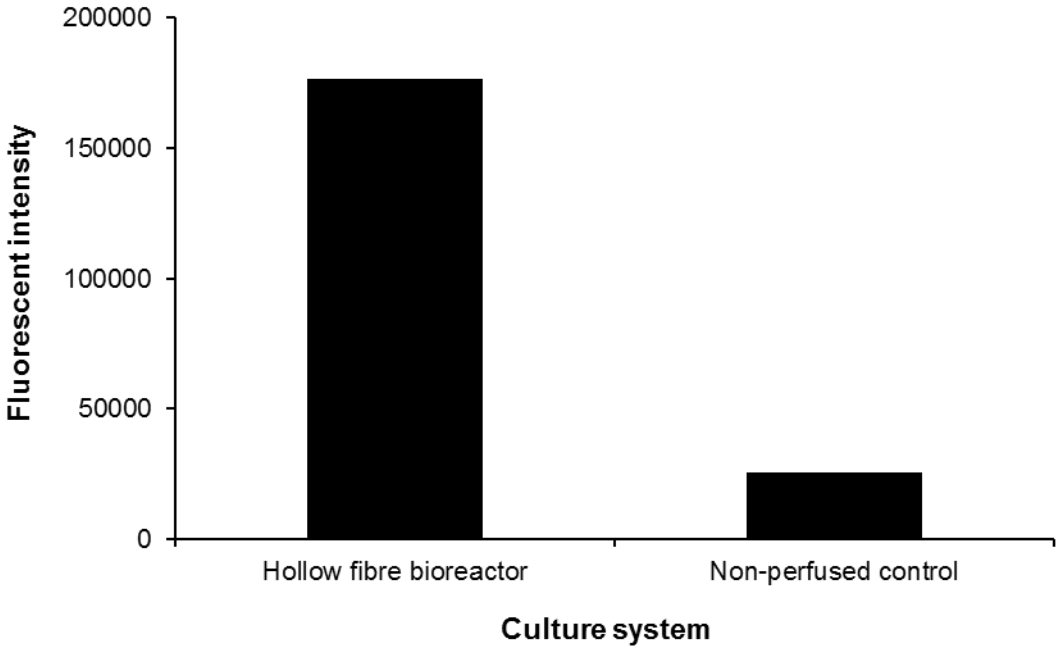

Figure 7.04: Relative metabolic activity of Cultispher-S seeded 3T3 fibroblasts in the hollow fibre bioreactor and non-perfused control system. Metabolism was measure by reduction of resazurin after 7 days of culture. Data shown represents one individual experiment.

The results using 3T3 fibroblasts were confirmed using the cells of interest here, rMSCs. The proportion of viable cells is shown in Figure 7.05. Again the population from the hollow fibre bioreactor shows a higher proportion of viable cells than the control system, at 78.8% and 63.1% viabilities respectively. This difference is less pronounced than that which was observed in Figure 7.03 for 3T3 fibroblasts (1.25 times more viable cells in the hollow fibre bioreactor than in the control using rMSCs, compared to 2.11 times using 3T3 fibroblasts). 3T3 fibroblasts are faster growing cells, and as such have higher energy requirements and oxygen consumption rates. While the specific oxygen consumption rate of 3T3 fibroblasts has been reported to be in the region 0.22 picomoles O_2/cell/hour, MSCs have shown much lower rates of 8.1 femtomoles O_2/cell/hour [245, 246]. It is therefore likely that the 3T3 fibroblasts were more affected by the lack of oxygen and nutrients in the control system than the rMSCs. rMSCs also exhibited very slow growth in two-dimensional culture in the carbon dioxide-independent media required for growth in the bioreactor, further emphasising this effect.

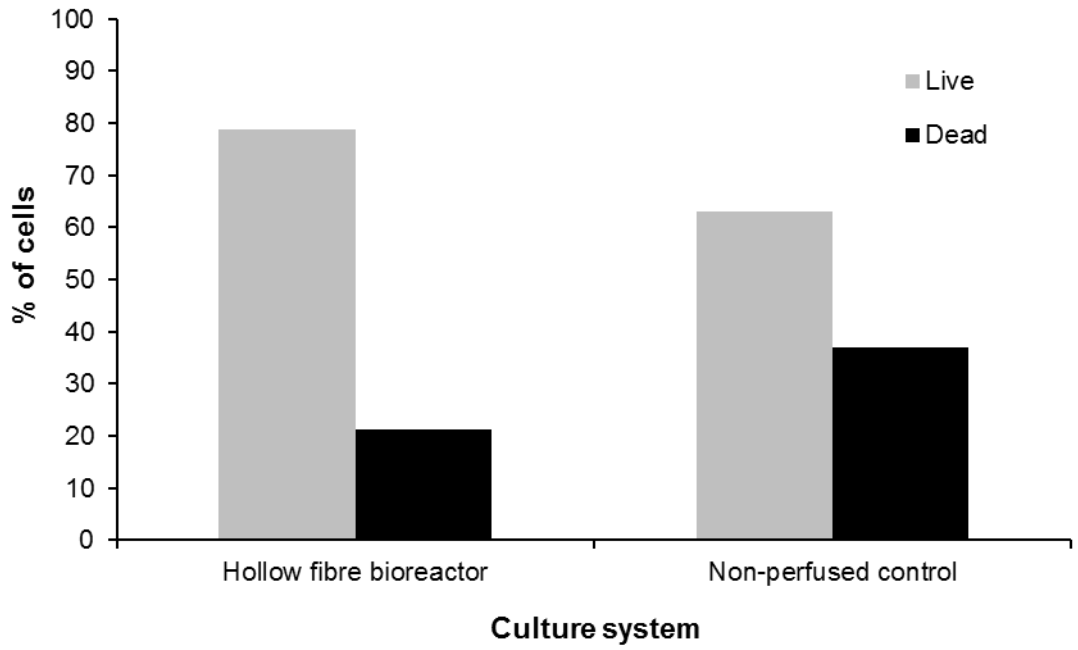

Figure 7.05: Proportion of viable rMSCs in the hollow fibre bioreactor and non-perfused control system after 7 days. Viability was determined by fluorescent staining and quantified. Data shown represents one individual experiment.

7.3.4. Cell expansion within the bioreactor

Equal numbers of cells were seeded within the hollow fibre and non-perfused control systems. After 7 days of culture within the systems, the cultures were extracted, washed, and analysed for DNA content to establish cell number. For both 3T3 fibroblasts (Figure 7.06) and rMSCs (Figure 7.07), higher cell numbers were obtained from the hollow fibre bioreactor, strongly suggesting again that this system supports cell proliferation compared to the control system. As discussed in the previous section, the difference is more pronounced in the 3T3 fibroblast cultures, likely due to their more rapid growth. The overall number of cells is also higher in the 3T3 fibroblast cultures, possibly also a reflection of the higher growth rate in these cells. It could be a reflection of the difference in initial cell adhesion to the microparticles (though this was shown in Chapter 5 to be 93% for 3T3 fibroblasts and 89% for rMSCs, a relatively small discrepancy).

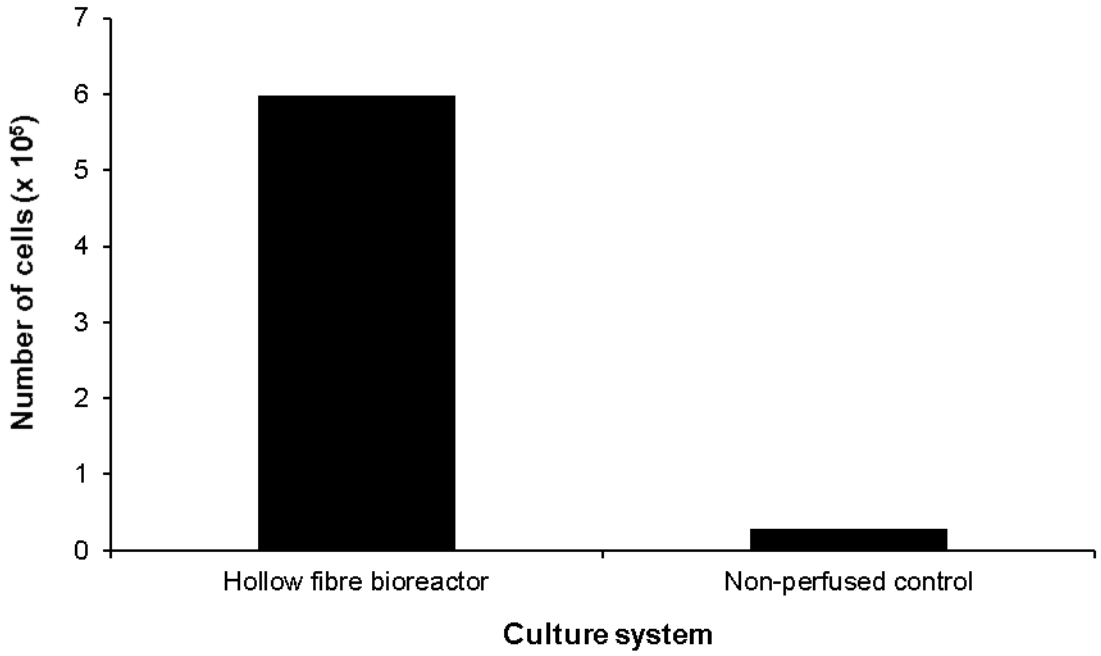

Figure 7.06: Number of 3T3 fibroblasts harvested from the hollow fibre bioreactor and non-perfused control system after 7 days. Cell number was determined by Hoechst staining of cell lysate. The initial cell number was 1.88 x 10^5 cells. Data shown represents one individual experiment.

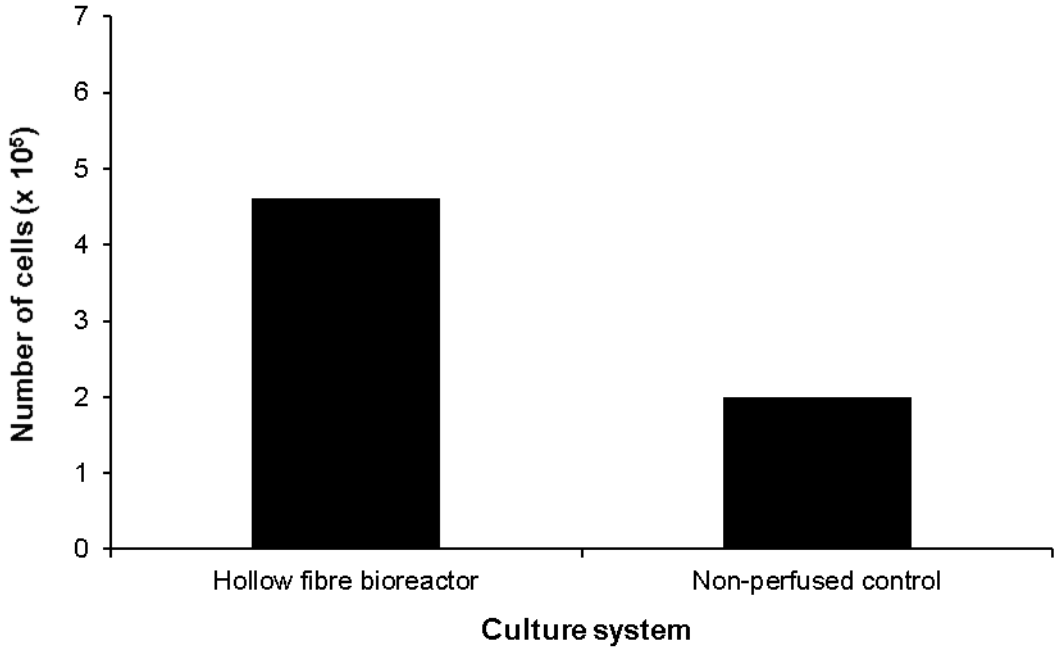

Figure 7.07: Number of rMSCs harvested from the hollow fibre bioreactor and non-perfused control system after 7 days. Cell number was determined by Hoechst staining of cell lysate. The initial cell number was 1.88 x 10^5 cells. Data shown represents one individual experiment.

7.3.5. Formation of tissue construct within the bioreactor

Literature reports of cell-Cultispher-S constructs suggest that culturing the microparticles within a small mould, with microparticles in close proximity to each other, is sufficient to induce the formation of a stable structure by means of cell-bridging [56, 57]. This was not observed in this thesis despite the promising preliminary results described in Chapter 5. No stable construct was formed using the hollow fibre bioreactor, though on occasion loose structures were formed, as shown in Figure 7.08. These were not stable to manipulation, and disintegrated upon contact with buffer solution. This is in contrast to literature reports of constructs formed by cell-cell bridging, which were stable to manipulation and handling [56, 57]. However, in both of these reports, cells were cultured on microparticles for up to 28 days before moulding, allowing a high cell density to develop. Comparing results, it seems likely that the cell densities achieved in this work were not high enough to support the formation of a stable cell-bridged structure and future work should look to address this.

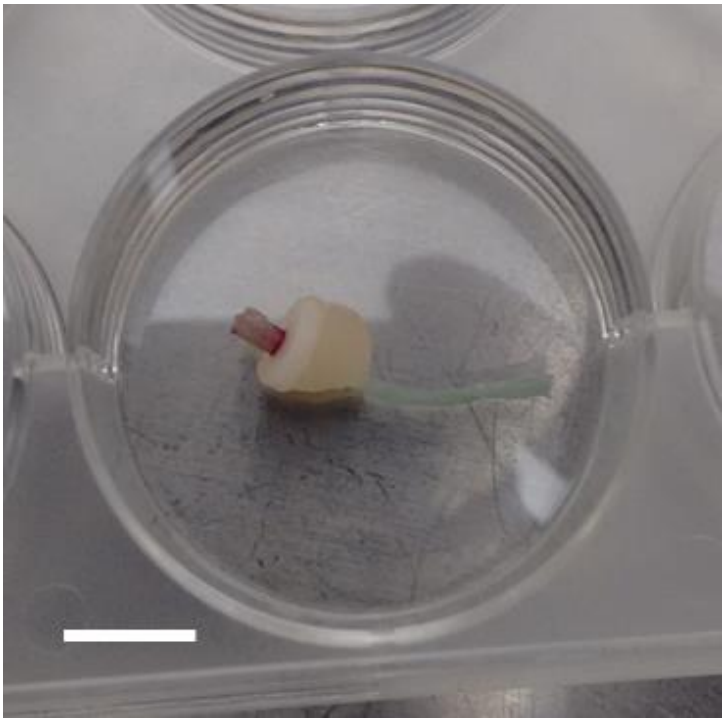

Figure 7.08: rMSC-laden Cultispher-S microparticles loosely adhered together immediately following removal from the hollow fibre bioreactor. The microparticles are resting on the filter frit and surrounding the hollow fibre. Scale bar represents 10 mm.

Unfortunately the lack of structure of the product meant that information about cell viability within different regions of the hollow fibre bioreactor could not be obtained. Future work could investigate the possibility of fixing the particles into a structure through use of a

hydrogel such as collagen, or fibrin glue, though this would change diffusion through the structure itself. MSCs have been encapsulated within Matrigel® in hollow fibre bioreactors with some success, and the incorporation of microparticles could reinforce the structure to produce a stronger construct [247].

It would be expected that areas close to the fibre, and on the top of the microparticle layer, would contain more viable cells, due to their close or direct contact with media. However, the proliferation of cells close to a nutrient or oxygen source can itself create a barrier to diffusion [241]. Information about cell distribution within the chamber would therefore prove useful to understand whether this is occurring in this system. Scaling up the size of the chamber to theoretically produce larger constructs could be coupled with the introduction of more fibres, and so to see patterns of cell distribution within a more complex system would also be valuable.

7.3.6. Evidence of osteodifferentiation within the bioreactor

To examine whether the rMSCs cultured within the bioreactor underwent osteogenic differentiation, expression of osteopontin in the media was measured from within the cell chamber, rather than from the media reservoir. The results are shown in Figure 7.09. The expression of osteopontin appears to be slightly higher in the non-perfused control system than in the hollow fibre bioreactor, though no statistical tests can be performed until the experiment is repeated. The slight difference in expression could be due to the fact that only media from the inner chamber of the hollow fibre bioreactor was assayed. Potentially, osteopontin may have diffused out of the chamber through the hollow fibre and into the media reservoir, and was thus not measured in this experiment. Repeats of this experiment should assay the bulk media in addition to the sample from the hollow fibre chamber sample to rectify this.

The non-perfused control would be expected to have a much lower oxygen concentration than the hollow fibre bioreactor, though this was not measured directly. Hypoxia has been reported to increase the osteogenic differentiation of rMSCs and human periodontal ligament stem cells, and this effect could be responsible for the unexpectedly high level of osteopontin expression in the control system [248, 249]. The oxygen concentrations in these experiments were reported as 5% and 2% respectively. Defining this as a hypoxic environment may be inaccurate however, as the percentage of oxygen within the MSC bone marrow niche has been estimated at between 2 and 9%. Oxygen levels in this range may be better described as providing physiological normoxia [250].

However, where the oxygen concentration is set at less than 1%, in what is a truly hypoxic environment, the osteogenic potential of human MSCs is decreased [251, 252]. The ability to measure the oxygen concentration within the bioreactor chamber would therefore be highly desirable for bone tissue engineering applications, though use of a probe sensor at this small scale would be impractical. Small LED sensors, colorimetric methods such as the indigo carmine reaction, or titration using the Winkler method, could prove useful for measuring the dissolved oxygen concentration in the media at defined time points.

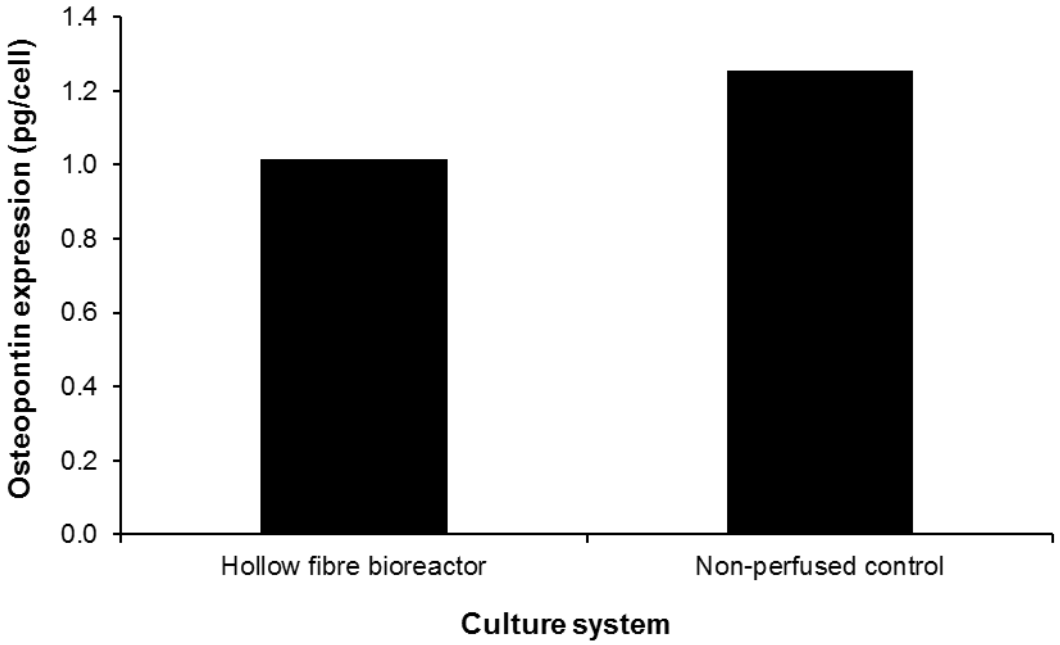

Figure 7.09: Osteopontin expression from rMSCs cultured in either the hollow fibre bioreactor or control system for 7 days. Data shown represents one individual experiment.

The osteopontin expression levels for both samples are much higher than those observed for rMSCs in previous experiments, for example in Figure 5.15, where osteopontin expression (by rMSCs on SF/G or Cultispher-S microparticles) is in the range of 0.02 pg/cell, compared to 1.0 pg/cell here, shown in Figure 7.09. This higher value could be due to the fact that the media in the hollow fibre chamber and the control system was not changed directly, causing osteopontin to accumulate over the 7 days of culture, whereas in the SF/G microparticle experiments, media was changed completely 4 days before assaying.

Despite the fact the media used was not supplemented with osteogenic additives, the carbon dioxide-independent media already contained one of the ODM supplements, glycerol 2-phosphate, as part of its buffering system. Though the concentration in the media is unknown, it is possible this could have had an osteogenic effect on the rMSCs. Further

experiments should investigate other markers of differentiation such as expression of bone sialoprotein, alkaline phosphatase, osteocalcin and deposition of calcium over a range of time points to confirm these preliminary results. The effect of using supplemented ODM instead of basal media should also be investigated, as this would be expected to increase the rate of osteogenic differentiation.

Osteocytes *in vivo* exist in fluid cavities, where loading of the joints and bones causes increases in pressure as well as shear flow over the cells. There is some evidence that mimicking this hydrostatic pressure by compression can increase osteogenic differentiation [125, 253, 254]. Future refinement of the bioreactor described here should consider the application of mechanical loading as a means to better replicate the native bone cell niche and improve cellular outcomes, such as proliferation and matrix deposition.

7.4. Future work

As a proof of principle design, the bioreactor described here worked to show that cell viability within a dense arrangement of microparticles was increased by the inclusion of a central hollow fibre. This was observed for both 3T3 fibroblasts and rMSCs. However, neither cell type promoted the formation of a stable tissue construct. The design of the system could be altered to promote this, for example by surrounding the cell-laden microparticles in a hydrogel (for example, gelatin or alginate) to fix the structure together. In terms of the bioreactor itself, a number of adjustments to the design could be made to enhance its function.

As a first step, it would be desirable to situate the bioreactor system in an atmosphere-controlled incubator. This would allow cells to be grown in their preferred media, which should positively impact on viability and proliferation. In order to measure the cell behaviour within the reactor during culture, it would be useful to have an accessible port to the main bioreactor chamber to allow for media sampling. Media samples could be analysed for glucose and lactate concentration as a proxy for cell number. As previously discussed, it would be very useful to measure oxygen concentrations within the bioreactor chamber, and so future designs of the bioreactor should include either inline oxygen sensors on the input and output tubing of the reactor, or a small probe within the chamber itself. Though the current bioreactor design used only off-the-shelf parts and fittings, the design would benefit from a custom chamber part in order to facilitate the changes suggested here. Optimising the design to allow for the easy removal of the chamber contents would also be beneficial, especially for the removal of a solid construct.

As hydrostatic pressure has been shown to positively influence osteogenic differentiation, a mechanism to provide this stimuli could be considered for the bioreactor. One possibility would be mimicking a syringe, using a plunger as the top of the reactor that could be slightly compressed to create small pressure increases. The frequency and size of these stimuli would need careful consideration. Co-cultures of different cell types could also be investigated to improve the physiological relevance of the resultant product. The use of microparticles would allow for the spatial arrangement of different cell types, for example in defined layers.

Further characterisation of the bioreactor and fibre, such as permeation rate of media through the fibre or a mass balance of the system, would be valuable to determine how efficiently cells are fed by the system and allow for optimisation of flow rates.

7.5. Conclusions

In this chapter, a bioreactor system was designed for the culture of cell-laden microparticles, utilising a hollow fibre to act as pseudo-vasculature while protecting cells from the shear stress of media flow. The bioreactor was shown to successfully maintain increased cell viability and function over a 7 day period, compared to a control system without a perfused fibre. Future work should include the culture of cells within the bioreactor for longer periods of time, as well as further refinement of the design as discussed above. While the initial experiments described here used Cultispher-S microparticles, results obtained in Chapter 5 suggested that osteodifferentiation of rMSCs could be improved by the use of SF/G microparticles, and so their use within the bioreactor should be investigated. Equally, the use of alginate/ECM-encapsulated cells may provide a more homogenous cell distribution valuable in creating a bone tissue construct.

Though microparticles were cultured within the bioreactor successfully, evidence of the formation of a stable construct was lacking, and so this aim was not achieved. However, the system could be used with alternative scaffold types, or gels moulded within the chamber, to investigate whether they would be more successful. It is possible that optimisation of cell seeding and culture time before moulding could positively influence this outcome. The simple design of the bioreactor is such that it would allow for a variety of scaffold types to be cultured within the perfused chamber, in the form of microparticles or gels, or indeed both.

Chapter 8

Conclusions & future work

8.1. Conclusions

The use of SF and SF/G blends as biomaterials was studied by assessing biocompatibility and cell response to two-dimensional films. It became apparent that while cell adhesion to SF films alone was generally poor, blending with gelatin significantly improved cell adhesion, and also increased the Young's moduli of the dry films. The poor cell adhesion to SF-only films was in contrast to many literature reports, though the source of silk could be an important factor here and should be taken into account in future work. MSCs were successfully extracted from rat bone marrow and shown to be capable of osteogenic, adipogenic and (sparingly) chondrogenic differentiation. SF/G films supported the osteogenic differentiation of these rMSCs, and were shown to be capable of undergoing mineralisation under physiological conditions, confirming the suitability of SF/G blended materials as osteogenic scaffolds for tissue engineering.

SF/G materials were translated from two to three dimensions by the production of porous microparticles. A flow focussing device was used to produce these microparticles, utilising two co-flowing immiscible streams to generate consistently sized microparticles. The device described here did not require the customisation of any parts or fittings and therefore it should be easily assembled by any research group interested in producing microparticles, without requiring custom modifications. This is a clear advantage over many such devices described in the literature which are built from custom pieces or 3D-printed in-house. Though the solvent system was optimised here for use with SF and SF/G blends, it could equally be adapted for use with different polymers and solvents.

The cell behaviour on SF/G microparticles mimicked the behaviour previously observed on two-dimensional films. Cell adhesion increased with the addition of gelatin. Unlike the films, however, the blending of SF and gelatin increased the Young's modulus of hydrated discs to values greater than either SF or gelatin alone. Osteogenic differentiation of rMSCs was supported on SF/G 25:75 microparticles, evidenced by expression of active ALP and osteopontin. The moulding of cell-laden microparticles into a centimetre-scale structure was observed, though not repeated.

The use of oxidised alginate as a supporting matrix for less mechanically stable ECM extracts was investigated in Chapter 6. While the liquid-liquid flow focussing device described in Chapter 5 was adapted to work with alginate solutions, a more rapid production

method was developed using an air flow to disrupt the stream of alginate, propelling droplets directly into a gelling bath. This system provided a more rapid, simpler means of producing alginate microparticles, and should be translatable for any solution that can be rapidly cross-linked in this way.

ECM proteins were extracted from skeletal muscle samples using three alternative methods. Homogenising and solubilising the skeletal muscle produced a gel-forming solution with sufficiently low DNA levels to confirm decellularisation. SDS treatment also adequately removed cellular material from the samples but the products did not form hydrogels, likely due to protein denaturation by the detergent itself. The use of SDS in decellularisation methods should be minimised to avoid damaging the ECM proteins. The third method investigated, using Triton X-100/EDTA did not adequately remove cellular components from the samples. Oxidised alginate and the gel-forming ECM extract were mixed and processed into microparticles but the protein component appeared to precipitate rather than blending uniformly through the microparticles. Oxidised alginate/collagen microparticles were therefore produced as a model of alginate/ECM blends and were shown to support encapsulated cell viability and osteogenic differentiation.

Finally, in Chapter 7, a prototype bioreactor was designed to culture microparticles around a media-perfused hollow fibre in order to maintain cell viability in a centimetre scale construct. Cell viability in the hollow fibre bioreactor was much improved over the non-perfused control. More cells were harvested from the hollow fibre bioreactors than from the control systems, but no stable construct was formed in the bioreactor chamber. However, these preliminary results demonstrate the potential of hollow fibre bioreactors to support the maintenance and growth of microparticle-seeded cells.

8.2. Future work

The initial aims of this work were to investigate the use of silk fibroin, alginate, and ECM derived proteins as scaffold materials - in particular, for the production of microparticles. The motivation for this was the potential to mould cell-laden microparticles into a larger construct, around hollow fibres, to create a viable, macroscopic bone tissue construct. While microparticles were successfully produced, moulding the particles together was not achieved and thus a solid tissue construct was not generated in this work. However, the cell behaviour on the materials was promising and thus optimising cell densities or using an alternative cell type might allow for the formation of a cell-bridged construct.

8.2.1. Short-term targets

In the short term, it would be valuable to look at optimising cell seeding densities and mould design in order to achieve the formation of a cell-bridged construct, as described in the literature. As discussed in Chapter 7, the application of hydrostatic pressure may be useful to increase the osteogenic differentiation of rMSCs within the bioreactor, and this may also have the effect of encouraging cell-cell and cell-scaffold adhesions by pushing cell-laden microparticles into closer contact within the bioreactor chamber. Alternatively, it might be the case that the scaffolds created here are more appropriate for non-osteogenic applications and this should be considered. The length of time the cells are cultured on microparticles may also be a crucial factor in promoting aggregation, as the production of new ECM by the cells would allow for ECM-cell adhesions across neighbouring particles. Time-dependent aggregation should be investigated, as should the production of new ECM by rMSCs (for example type 1 collagen and fibronectin).

If moulding the microparticles together through cell bridging is not achievable, it may be valuable to investigate using hydrogels to act as a glue to fix particles together. Hydrogels which rapidly solidify, such as gelatin or alginate, could be added to a mould after the microparticles to create a solid structure. This would still allow for the formation of layered, or hierarchical structures, though diffusion of media through the structure would be impeded.

While rMSCs have been a useful model, in order to produce a clinically relevant model, efforts should be made to make the switch to using human cells. Human MSCs have been isolated from bone marrow, umbilical cord blood and adipose tissue. Umbilical cord blood can be obtained without harm to the mother or new-born, and MSCs harvested from it have been shown to possess a high proliferative capacity, though some groups have found that MSCs cannot be isolated from cord blood reliably [14, 255]. Adipose tissue, usually collected in non-invasive liposuction procedures, is an attractive alternative source of MSCs as it provides an abundant source of multipotent MSCs. Where liposuction is performed cosmetically, the aspirate would usually be discarded and thus harvest of MSCs from this material would make effective use of this waste material.

Once a source of human MSCs had been determined, osteogenic differentiation of the human MSCs on three-dimensional SF/G materials should be fully confirmed, by ALP activity, expression of osteopontin, osteocalcin, or bone sialoprotein. These could be quantified through the use of ELISAs, Western blotting or PCR. Since the common stains for mineralisation were found to stain the SF/G scaffolds under control conditions, mineralisation could be examined by EDX.

In reference to the work investigating the use of alginate/ECM microparticles, the results obtained using alginate/collagen materials should be compared to alginate blended with the ECM extracted from skeletal muscle. This ECM extract should first be subjected to gel electrophoresis to confirm that any remaining DNA fragments are less than 200 base pairs in length, to fulfil the final condition of the decellularisation criteria. As discussed, human lipoaspirate material is a waste product but in addition to the extraction of MSCs, the ECM itself has been used to produce scaffolds for tissue engineering [105, 113]. This approach could be investigated as it provides a potentially autologous source of ECM proteins as well as making full use of the lipoaspirate.

Following encapsulation of MSCs within the alginate/ECM microparticles, external seeding of cells should be investigated. Use of an endothelial cell line, such as HUVECs, on the exterior of the particles could allow for the formation of connected vascular structures between adjacent microparticles once moulded or fixed together. This could begin the process of creating a vascularised structure, especially when used in conjunction with a perfused flow bioreactor.

8.2.2. Medium to long term targets

In the medium to long term, the bioreactor designed in Chapter 7 should be optimised for the long term culture of tissue constructs. This may include a method of inducing hydrostatic pressure to optimise osteogenic differentiation, as well as the inclusion of in-line oxygen sensors to ensure cells are maintained in a physiological normoxic environment. Adjustment of the design to allow easier removal of the final construct would also be beneficial. The bioreactor could be expanded in size, with the inclusion of additional hollow fibres, to produce larger constructs. Flow rates should be more carefully optimised to ensure oxygen delivery throughout the entire chamber.

The resultant constructs, whether formed from cell-bridged microparticles or hydrogel-encapsulated microparticles, should be characterised by cell distribution, cell viability, differentiation characteristics and mechanical properties. To investigate whether the inclusion of a hollow fibre in the structure hastens anastomosis, preliminary *in vivo* studies could study the integration of constructs with host vasculature.

Alternatively, the un-moulded microparticles could be utilised as an injectable therapy for filling irregularly shaped bone defects. The culture of cell-laden microparticles should be scaled up to more efficiently produce larger cultures. This could be achieved through the

use of spinner flasks, or even bench top stirred tank bioreactors, though alternative systems such as the rotating wall vessel bioreactor should also be considered.

Although the primary focus of the work in this thesis has been the differentiation of MSCs down an osteogenic pathway, it may also be worth considering other cell lineages. For example, the proposed alginate/adipose ECM scaffolds may prove more useful for soft tissue engineering, with applications as cosmetic fillers or in volumetric tissue loss.

There is also potential for the scaffolds to act as drug delivery reservoirs. By incorporating drugs, growth factors, or therapeutic proteins in the scaffold, gradual release over time could be achieved. Depending on the choice of drug or protein, this could provide an antibacterial effect to prevent infections, a chemotactic effect to recruit particular cells, or a proliferative effect to encourage cell growth. The ability to precisely control the location and 3D relationship between different microparticles, laden with different biomolecules or cell types, would be very useful, and the use of such microparticles in a 3D printing approach could help achieve this.

References

1. Shegarfi, H. and O. Reikeras, *Review article: bone transplantation and immune response.* J Orthop Surg (Hong Kong), 2009. **17**(2): p. 206-11.
2. Drury, J.L. and D.J. Mooney, *Hydrogels for tissue engineering: scaffold design variables and applications.* Biomaterials, 2003. **24**(24): p. 4337-4351.
3. NHS Blood and Transplant *Success Rates* Organ Donation, [cited 2015 January 14th]; Available from: http://www.organdonation.nhs.uk/about_transplants/success_rates/
4. Kirouac, D.C. and P.W. Zandstra, *The Systematic Production of Cells for Cell Therapies.* Cell Stem Cell, 2008. **3**(4): p. 369-381.
5. Muschler, G.F., C. Boehm, and K. Easley, *Aspiration to Obtain Osteoblast Progenitor Cells from Human Bone Marrow: The Influence of Aspiration Volume**. Vol. 79. 1997. 1699-1709.
6. Wikimedia Commons, *Tissue engineering english*. [cited 2015 07/05/2015]; Licensed under CC BY 3.0 via Wikimedia Commons]. Available from: http://commons.wikimedia.org/wiki/File:Tissue_engineering_english.jpg#/media/File:Tissue_engineering_english.jpg
7. Polak, J.M. and A.E. Bishop, *Stem Cells and Tissue Engineering: Past, Present, and Future.* Annals of the New York Academy of Sciences, 2006. **1068**(1): p. 352-366.
8. Von Der Mark, K., et al., *Relationship between cell shape and type of collagen synthesised as chondrocytes lose their cartilage phenotype in culture.* Nature, 1977. **267**(5611): p. 531-532.
9. Martin, M.J., et al., *Human embryonic stem cells express an immunogenic nonhuman sialic acid.* Nat Med, 2005. **11**(2): p. 228-32.
10. Klimanskaya, I., et al., *Human embryonic stem cells derived without feeder cells.* The Lancet. **365**(9471): p. 1636-1641.
11. Swistowski, A., et al., *Xeno-Free Defined Conditions for Culture of Human Embryonic Stem Cells, Neural Stem Cells and Dopaminergic Neurons Derived from Them.* PLoS ONE, 2009. **4**(7): p. e6233.
12. Vats, A., et al., *Embryonic stem cells and tissue engineering: delivering stem cells to the clinic.* Journal of the Royal Society of Medicine, 2005. **98**(8): p. 346-350.
13. Barry, F.P. and J.M. Murphy, *Mesenchymal stem cells: clinical applications and biological characterization.* International Journal of Biochemistry & Cell Biology, 2004. **36**(4): p. 568-584.
14. Kern, S., et al., *Comparative Analysis of Mesenchymal Stem Cells from Bone Marrow, Umbilical Cord Blood, or Adipose Tissue.* STEM CELLS, 2006. **24**(5): p. 1294-1301.
15. Zuk, P.A., et al., *Human adipose tissue is a source of multipotent stem cells.* Molecular Biology of the Cell, 2002. **13**(12): p. 4279-4295.
16. Gimble, J.M. and F. Guilak, *Adipose-derived adult stem cells: isolation, characterization, and differentiation potential.* Cytotherapy, 2003. **5**(5): p. 362-369.
17. Novosel, E.C., C. Kleinhans, and P.J. Kluger, *Vascularization is the key challenge in tissue engineering.* Advanced Drug Delivery Reviews, 2011. **63**(4-5): p. 300-311.
18. Badylak, S.F., *The extracellular matrix as a biologic scaffold material.* Biomaterials, 2007. **28**(25): p. 3587-3593.
19. Gentili, C. and R. Cancedda, *Cartilage and bone extracellular matrix.* Curr Pharm Des, 2009. **15**(12): p. 1334-48.
20. Faculty of Biological Sciences, *Bone*. The Histology Guide, 2003 [cited 2015 29/0/2015]; Available from: http://www.histology.leeds.ac.uk/bone/bone.php
21. Agrawal, C.M. and R.B. Ray, *Biodegradable polymeric scaffolds for musculoskeletal tissue engineering.* Journal of Biomedical Materials Research, 2001. **55**(2): p. 141-150.

22. Hunt, N.C. and L.M. Grover, *Cell encapsulation using biopolymer gels for regenerative medicine.* Biotechnology Letters, 2010. **32**(6): p. 733-742.
23. Ferreira, L.S., et al., *Bioactive hydrogel scaffolds for controllable vascular differentiation of human embryonic stem cells.* Biomaterials, 2007. **28**(17): p. 2706-2717.
24. Ruoslahti, E., *RGD and other recognition sequences for integrins.* Annual Review of Cell and Developmental Biology, 1996. **12**: p. 697-715.
25. Hubbell, J.A., et al., *Endothelial Cell-Selective Materials for Tissue Engineering in the Vascular Graft Via a New Receptor.* Nat Biotech, 1991. **9**(6): p. 568-572.
26. Zhang, M., et al., *Immobilization of anti-CD31 antibody on electrospun poly(epsilon-caprolactone) scaffolds through hydrophobins for specific adhesion of endothelial cells.* Colloids and Surfaces B-Biointerfaces, 2011. **85**(1): p. 32-39.
27. Hsu, F.Y., et al., *The collagen-containing alginate/poly(L-lysine)/alginate microcapsules.* Artificial Cells Blood Substitutes and Immobilization Biotechnology, 2000. **28**(2): p. 147-154.
28. Tsai, S.W., et al., *Gel beads composed of collagen reconstituted in alginate.* Biotechnology Techniques, 1998. **12**(1): p. 21-23.
29. Dixon, J.E., et al., *Combined hydrogels that switch human pluripotent stem cells from self-renewal to differentiation.* Proceedings of the National Academy of Sciences, 2014. **111**(15): p. 5580-5585.
30. Matsunaga, Y.T., Y. Morimoto, and S. Takeuchi, *Molding Cell Beads for Rapid Construction of Macroscopic 3D Tissue Architecture.* Advanced Materials, 2011. **23**(12): p. H90-H94.
31. Hou, T., et al., *In vitro evaluation of a fibrin gel antibiotic delivery system containing mesenchymal stem cells and vancomycin alginate beads for treating bone infections and facilitating bone formation.* Tissue Eng Part A, 2008. **14**(7): p. 1173-82.
32. Nicodemus, G.D. and S.J. Bryant, *Cell encapsulation in biodegradable hydrogels for tissue engineering applications.* Tissue Engineering Part B-Reviews, 2008. **14**(2): p. 149-165.
33. Engler, A.J., et al., *Matrix elasticity directs stem cell lineage specification.* Cell, 2006. **126**(4): p. 677-689.
34. Bajaj, P., et al., *3D biofabrication strategies for tissue engineering and regenerative medicine.* Annu Rev Biomed Eng, 2014. **16**: p. 247-76.
35. Gunatillake, P.A. and R. Adhikari, *Biodegradable synthetic polymers for tissue engineering.* European Cells & Materials, 2003. **5**(January-June Cited May 23, 2003): p. 1-16.
36. Lee, K.Y. and D.J. Mooney, *Hydrogels for tissue engineering.* Chemical Reviews, 2001. **101**(7): p. 1869-1879.
37. Detsch, R. and A.R. Boccaccini, *The role of osteoclasts in bone tissue engineering.* J Tissue Eng Regen Med, 2015. **9**(10): p. 1133-49.
38. Hadjidakis, D.J. and I.I. Androulakis, *Bone Remodeling.* Annals of the New York Academy of Sciences, 2006. **1092**(1): p. 385-396.
39. Tessmar, J.K. and A.M. Gopferich, *Matrices and scaffolds for protein delivery in tissue engineering.* Advanced Drug Delivery Reviews, 2007. **59**(4-5): p. 274-291.
40. Murphy, W.L., et al., *Sustained release of vascular endothelial growth factor from mineralized poly(lactide-co-glycolide) scaffolds for tissue engineering.* Biomaterials, 2000. **21**(24): p. 2521-2527.
41. Perets, A., et al., *Enhancing the vascularization of three-dimensional porous alginate scaffolds by incorporating controlled release basic fibroblast growth factor microspheres.* Journal of Biomedical Materials Research Part A, 2003. **65A**(4): p. 489-497.
42. Urciuolo, F., et al., *Building a Tissue In Vitro from the Bottom Up: Implications in Regenerative Medicine.* Methodist DeBakey Cardiovascular Journal, 2013. **9**(4): p. 213-217.

43. Botchwey, E.A., et al., *Bone tissue engineering in a rotating bioreactor using a microcarrier matrix system.* Journal of Biomedical Materials Research, 2001. **55**(2): p. 242-253.
44. Nilsson, K., *Microcarrier Cell Culture.* Biotechnology and Genetic Engineering Reviews, 1988. **6**(1): p. 404-439.
45. Czermak, P., R. Pörtner, and A. Brix, *Special Engineering Aspects*, in *Cell and Tissue Reaction Engineering*2009, Springer-Verlag Berlin Heidelberg. p. 83-172.
46. Choi, Y.S., S.N. Park, and H. Suh, *The effect of PLGA sphere diameter on rabbit mesenchymal stem cells in adipose tissue engineering.* J Mater Sci Mater Med, 2008. **19**(5): p. 2165-71.
47. Percell, *Percell Products*. [cited 10/11/2011; Available from: http://www.percell.se/products.htm
48. Tebb, T.A., et al., *Development of porous collagen beads for chondrocyte culture.* Cytotechnology, 2006. **52**(2): p. 99-106.
49. Skardal, A., et al., *The generation of 3-D tissue models based on hyaluronan hydrogel-coated microcarriers within a rotating wall vessel bioreactor.* Biomaterials, 2010. **31**(32): p. 8426-8435.
50. Rivest, C., et al., *Microscale hydrogels for medicine and biology: Synthesis, characteristics and applications.* Journal of Mechanics of Materials and Structures, 2007. **2**(6): p. 1103-1119.
51. Dendukuri, D., et al., *Continuous-flow lithography for high-throughput microparticle synthesis.* Nat Mater, 2006. **5**(5): p. 365-369.
52. Kim, S.Y., et al., *Formulation of Biologically-Inspired Silk-Based Drug Carriers for Pulmonary Delivery Targeted for Lung Cancer.* Sci Rep, 2015. **5**: p. 11878.
53. Tan, W.H. and S. Takeuchi, *Monodisperse Alginate Hydrogel Microbeads for Cell Encapsulation.* Advanced Materials, 2007. **19**(18): p. 2696-2701.
54. Utada, A.S., et al., *Monodisperse double emulsions generated from a microcapillary device.* Science, 2005. **308**(5721): p. 537-541.
55. Breslauer, D.N., S.J. Muller, and L.P. Lee, *Generation of Monodisperse Silk Microspheres Prepared with Microfluidics.* Biomacromolecules, 2010. **11**(3): p. 643-647.
56. Twal, W.O., et al., *Cellularized microcarriers as adhesive building blocks for fabrication of tubular tissue constructs.* Ann Biomed Eng, 2014. **42**(7): p. 1470-81.
57. Chen, M.Q., et al., *A modular approach to the engineering of a centimeter-sized bone tissue construct with human amniotic mesenchymal stem cells-laden microcarriers.* Biomaterials, 2011. **32**(30): p. 7532-7542.
58. Luo, H., et al., *Fabrication of viable centimeter-sized 3D tissue constructs with microchannel conduits for improved tissue properties through assembly of cell-laden microbeads.* Journal of Tissue Engineering and Regenerative Medicine, 2014. **8**(6): p. 493-504.
59. Adhirajan, N., N. Shanmugasundaram, and M. Babu, *Gelatin microspheres cross-linked with EDC as a drug delivery system for doxycyline: development and characterization.* Journal of Microencapsulation, 2007. **24**(7): p. 647-59.
60. Unger, R.E., et al., *Endothelialization of a non-woven silk fibroin net for use in tissue engineering: growth and gene regulation of human endothelial cells.* Biomaterials, 2004. **25**(21): p. 5137-5146.
61. Wang, Y., et al., *Stem cell-based tissue engineering with silk biomaterials.* Biomaterials, 2006. **27**(36): p. 6064-6082.
62. Stoppel, W.L., et al., *Clinical Applications of Naturally Derived Biopolymer-Based Scaffolds for Regenerative Medicine.* Ann Biomed Eng, 2014.
63. Yang, S.F., et al., *The design of scaffolds for use in tissue engineering. Part 1. Traditional factors.* Tissue Engineering, 2001. **7**(6): p. 679-689.
64. International Sericulture Commission, *Types of Silk*. Silk Industry, [cited 2015 29/04/15]; Available from: http://inserco.org/en/types_of_silk

65. Hardy, J.G. and T.R. Scheibel, *Composite materials based on silk proteins.* Progress in Polymer Science, 2010. **35**(9): p. 1093-1115.
66. Kaewprasit, K., et al., *Physico-chemical properties and in vitro response of silk fibroin from various domestic races.* Journal of Biomedical Materials Research Part B: Applied Biomaterials, 2014. **102**(8): p. 1639-1647.
67. Yoshido, A., et al., *The Bombyx mori Karyotype and the Assignment of Linkage Groups.* Genetics, 2005. **170**(2): p. 675-685.
68. Altman, G.H., et al., *Silk-based biomaterials.* Biomaterials, 2003. **24**(3): p. 401-416.
69. Rockwood, D.N., et al., *Materials fabrication from Bombyx mori silk fibroin.* Nature Protocols, 2011. **6**(10): p. 1612-1631.
70. Zhou, C.-Z., et al., *Silk fibroin: Structural implications of a remarkable amino acid sequence.* Proteins: Structure, Function, and Bioinformatics, 2001. **44**(2): p. 119-122.
71. Ko, F., *Engineering Properties of Spider Silk Fibers*, in *Natural Fibers, Plastics and Composites*, F.T. Wallenberger and N. Weston, Editors. 2004, Kluwer Academic Publishers. p. 29.
72. DermaSilk, *THE HYPOALLERGENIC SILK*. Healthcare Professionals, [cited 2015 13/05/2015]; Available from: http://www.dermasilk.com.au/content.php?view=HEALTHCARE_PROFESSIONALS
73. Meinel, L., et al., *The inflammatory responses to silk films in vitro and in vivo.* Biomaterials, 2005. **26**(2): p. 147-155.
74. Lv, Q., et al., *Preparation and characterization of PLA/fibroin composite and culture of HepG2 (human hepatocellular liver carcinoma cell line) cells.* Composites Science and Technology, 2007. **67**(14): p. 3023-3030.
75. Gotoh, Y., M. Tsukada, and N. Minoura, *Effect of the chemical modification of the arginyl residue in Bombyx mori silk fibroin on the attachment and growth of fibroblast cells.* Journal of Biomedical Materials Research, 1998. **39**(3): p. 351-357.
76. Altman, G.H., et al., *Silk matrix for tissue engineered anterior cruciate ligaments.* Biomaterials, 2002. **23**(20): p. 4131-4141.
77. Bhardwaj, N., S. Chakraborty, and S.C. Kundu, *Freeze-gelled silk fibroin protein scaffolds for potential applications in soft tissue engineering.* International Journal of Biological Macromolecules, 2011. **49**(3): p. 260-267.
78. Meinel, L., et al., *Engineering cartilage-like tissue using human mesenchymal stem cells and silk protein scaffolds.* Biotechnology and Bioengineering, 2004. **88**(3): p. 379-391.
79. Cao, Y. and B. Wang, *Biodegradation of Silk Biomaterials.* International Journal of Molecular Sciences, 2009. **10**(4): p. 1514-1524.
80. Park, S.-H., et al., *Relationships between degradability of silk scaffolds and osteogenesis.* Biomaterials, 2010. **31**(24): p. 6162-6172.
81. Baimark, Y., M. Srisa-ard, and P. Srihanam, *Morphology and thermal stability of silk fibroin/starch blended microparticles.* Express Polymer Letters, 2010. **4**(12): p. 781-789.
82. Chung, T.-W., C.-H. Chang, and C.-W. Ho, *Incorporating chitosan (CS) and TPP into silk fibroin (SF) in fabricating spray-dried microparticles prolongs the release of a hydrophilic drug.* Journal of the Taiwan Institute of Chemical Engineers, 2011. **43**(4): p. 592-597.
83. Kotsaeng, N., et al., *Preparation and Characterization of Poly(D,L-lactide) and Silk Fibroin Nanocomposite Microparticles for Potential Use in Tissue Engineering*, in *Smart Materials*. 2008. p. 725-728.
84. Chomchalao, P., et al., *Fibroin and fibroin blended three-dimensional scaffolds for rat chondrocyte culture.* Biomed Eng Online, 2013. **12**: p. 28.
85. He, J., et al., *Bottom-up generation of 3D silk fibroin–gelatin microfluidic scaffolds with improved structural and biological properties.* Materials Letters, 2012. **78**: p. 102-105.

86. Tiyaboonchai, W., et al., *Preparation and Characterization of Blended Bombyx mori Silk Fibroin Scaffolds.* Fibers and Polymers, 2011. **12**(3): p. 324-333.
87. Yang, Z., et al., *In vitro and in vivo characterization of silk fibroin/gelatin composite scaffolds for liver tissue engineering.* Journal of Digestive Diseases, 2012. **13**(3): p. 168-178.
88. Chung, T.-W. and Y.-L. Chang, *Silk fibroin/chitosan-hyaluronic acid versus silk fibroin scaffolds for tissue engineering: promoting cell proliferations in vitro.* Journal of Materials Science-Materials in Medicine, 2010. **21**(4): p. 1343-1351.
89. Lai, G.-J., et al., *Composite chitosan/silk fibroin nanofibers for modulation of osteogenic differentiation and proliferation of human mesenchymal stem cells.* Carbohydrate Polymers, 2014. **111**(0): p. 288-297.
90. Chen, B., et al., *A novel alternative to cryopreservation for the short-term storage of stem cells for use in cell therapy using alginate encapsulation.* Tissue Eng Part C Methods, 2013. **19**(7): p. 568-76.
91. Mørch, Ý.A., I. Donati, and B.L. Strand, *Effect of Ca2+, Ba2+, and Sr2+ on Alginate Microbeads.* Biomacromolecules, 2006. **7**(5): p. 1471-1480.
92. Balakrishnan, B. and A. Jayakrishnan, *Self-cross-linking biopolymers as injectable in situ forming biodegradable scaffolds.* Biomaterials, 2005. **26**(18): p. 3941-3951.
93. Zhou, H.Z. and H.H.K. Xu, *The fast release of stem cells from alginate-fibrin microbeads in injectable scaffolds for bone tissue engineering.* Biomaterials, 2011. **32**(30): p. 7503-7513.
94. Balakrishnan, B., et al., *Periodate oxidation of sodium alginate in water and in ethanol–water mixture: a comparative study.* Carbohydrate Research, 2005. **340**(7): p. 1425-1429.
95. Wright, B., et al., *Oxidized alginate hydrogels as niche environments for corneal epithelial cells.* J Biomed Mater Res A, 2014. **102**(10): p. 3393-400.
96. Ramshaw, J.A.M., J.A. Werkmeister, and V. Glattauer, *Collagen-based Biomaterials.* Biotechnology and Genetic Engineering Reviews, 1995. **13**: p. 335-382.
97. Mathieu, M., et al., *Induction of mesenchymal stem cell differentiation and cartilage formation by cross-linker-free collagen microspheres.* Eur Cell Mater, 2014. **28**: p. 82-96; discussion 96-7.
98. Peterson, A.W., et al., *Vasculogenesis and Angiogenesis in Modular Collagen-Fibrin Microtissues.* Biomater Sci, 2014. **2**(10): p. 1497-1508.
99. Achilli, M. and D. Mantovani, *Tailoring Mechanical Properties of Collagen-Based Scaffolds for Vascular Tissue Engineering: The Effects of pH, Temperature and Ionic Strength on Gelation.* Polymers, 2010. **2**(4): p. 664-680.
100. Solorio, L., et al., *Gelatin microspheres crosslinked with genipin for local delivery of growth factors.* J Tissue Eng Regen Med, 2010. **4**(7): p. 514-23.
101. Grover, C.N., et al., *Crosslinking and composition influence the surface properties, mechanical stiffness and cell reactivity of collagen-based films.* Acta Biomaterialia, 2012. **8**(8): p. 3080-3090.
102. Davis, G.E., *Affinity of integrins for damaged extracellular matrix: αvβ3 binds to denatured collagen type I through RGD sites.* Biochemical and Biophysical Research Communications, 1992. **182**(3): p. 1025-1031.
103. Young, S., et al., *Gelatin as a delivery vehicle for the controlled release of bioactive molecules.* Journal of Controlled Release, 2005. **109**(1-3): p. 256-274.
104. Crapo, P.M., T.W. Gilbert, and S.F. Badylak, *An overview of tissue and whole organ decellularization processes.* Biomaterials, 2011. **32**(12): p. 3233-3243.
105. Young, D.A., et al., *Injectable hydrogel scaffold from decellularized human lipoaspirate.* Acta Biomaterialia, 2010. **7**(3): p. 1040-1049.
106. Hodde, J., *Naturally occurring scaffolds for soft tissue repair and regeneration.* Tissue Engineering, 2002. **8**(2): p. 295-308.
107. Hodde, J.P., et al., *Vascular endothelial growth factor in porcine-derived extracellular matrix.* Endothelium-New York, 2001. **8**(1): p. 11-24.

108. Badylak, S., et al., *Morphologic Study of Small Intestinal Submucosa as a Body Wall Repair Device.* Journal of Surgical Research, 2002. **103**(2): p. 190-202.
109. Macchiarini, P., et al., *Clinical transplantation of a tissue-engineered airway.* The Lancet, 2008. **372**(9655): p. 2023-2030.
110. Freytes, D.O., et al., *Preparation and rheological characterization of a gel form of the porcine urinary bladder matrix.* Biomaterials, 2008. **29**(11): p. 1630-1637.
111. Choi, J.S., et al., *Human extracellular matrix (ECM) powders for injectable cell delivery and adipose tissue engineering.* Journal of Controlled Release, 2009. **139**(1): p. 2-7.
112. Hou, Q., P.A. De Bank, and K.M. Shakesheff, *Injectable scaffolds for tissue regeneration.* Journal of Materials Chemistry, 2004. **14**(13): p. 1915-1923.
113. Choi, J.S., et al., *Decellularized extracellular matrix derived from human adipose tissue as a potential scaffold for allograft tissue engineering.* Journal of Biomedical Materials Research Part A, 2011. **97A**(3): p. 292-299.
114. Turner, A.E.B. and L.E. Flynn, *Design and Characterization of Tissue-Specific Extracellular Matrix-Derived Microcarriers.* Tissue Engineering Part C-Methods, 2011. **18**(3): p. 186-197.
115. Mazzitelli, S., et al., *Production and characterization of engineered alginate-based microparticles containing ECM powder for cell/tissue engineering applications.* Acta Biomaterialia, 2010. **7**(3): p. 1050-1062.
116. Seif-Naraghi, S.B., et al., *Design and Characterization of an Injectable Pericardial Matrix Gel: A Potentially Autologous Scaffold for Cardiac Tissue Engineering.* Tissue Engineering Part A, 2010. **16**(6): p. 2017-2027.
117. Singelyn, J.M., et al., *Naturally derived myocardial matrix as an injectable scaffold for cardiac tissue engineering.* Biomaterials, 2009. **30**(29): p. 5409-5416.
118. Gilbert, T.W., T.L. Sellaro, and S.F. Badylak, *Decellularization of tissues and organs.* Biomaterials, 2006. **27**(19): p. 3675-3683.
119. Keane, T.J., et al., *Consequences of ineffective decellularization of biologic scaffolds on the host response.* Biomaterials, 2011. **33**(6): p. 1771-1781.
120. Badylak, S.F., D. Taylor, and K. Uygun, *Whole-Organ Tissue Engineering: Decellularization and Recellularization of Three-Dimensional Matrix Scaffolds.* Annual Review of Biomedical Engineering, 2011. **13**(1): p. 27-53.
121. Stern, M.M., et al., *The influence of extracellular matrix derived from skeletal muscle tissue on the proliferation and differentiation of myogenic progenitor cells ex vivo.* Biomaterials, 2009. **30**(12): p. 2393-2399.
122. DeQuach, J.A., et al., *Simple and high yielding method for preparing tissue specific extracellular matrix coatings for cell culture.* Plos One, 2010. **5**(9).
123. Wolf, M.T., et al., *Polypropylene surgical mesh coated with extracellular matrix mitigates the host foreign body response.* Journal of Biomedical Materials Research Part A, 2013: p. n/a-n/a.
124. Flynn, L.E., *The use of decellularized adipose tissue to provide an inductive microenvironment for the adipogenic differentiation of human adipose-derived stem cells.* Biomaterials, 2010. **31**(17): p. 4715-4724.
125. El Haj, A.J. and S.H. Cartmell, *Bioreactors for bone tissue engineering.* Proc Inst Mech Eng H, 2010. **224**(12): p. 1523-32.
126. Gardel, L.S., et al., *Use of Perfusion Bioreactors and Large Animal Models for Long Bone Tissue Engineering.* Tissue Engineering Part B: Reviews, 2013. **20**(2): p. 126-146.
127. Sikavitsas, V.I., G.N. Bancroft, and A.G. Mikos, *Formation of three-dimensional cell/polymer constructs for bone tissue engineering in a spinner flask and a rotating wall vessel bioreactor.* Journal of Biomedical Materials Research, 2002. **62**(1): p. 136-148.
128. Bancroft, G.N., V.I. Sikavitsas, and A.G. Mikos, *Design of a flow perfusion bioreactor system for bone tissue-engineering applications.* Tissue Eng, 2003. **9**(3): p. 549-54.

129. Martin, I., D. Wendt, and M. Heberer, *The role of bioreactors in tissue engineering.* Trends in Biotechnology, 2004. **22**(2): p. 80-86.
130. Yourek, G., et al., *Shear stress induces osteogenic differentiation of human mesenchymal stem cells.* Regenerative Medicine, 2010. **5**(5): p. 713-724.
131. Liu, L., W. Yuan, and J. Wang, *Mechanisms for osteogenic differentiation of human mesenchymal stem cells induced by fluid shear stress.* Biomechanics and Modeling in Mechanobiology, 2010. **9**(6): p. 659-670.
132. Wung, N., et al., *Hollow fibre membrane bioreactors for tissue engineering applications.* Biotechnology Letters, 2014. **36**(12): p. 2357-2366.
133. Roberts, I., et al., *Scale-up of human embryonic stem cell culture using a hollow fibre bioreactor.* Biotechnology Letters, 2012. **34**(12): p. 2307-2315.
134. Nold, P., et al., *Good manufacturing practice-compliant animal-free expansion of human bone marrow derived mesenchymal stroma cells in a closed hollow-fiber-based bioreactor.* Biochemical and Biophysical Research Communications, 2013. **430**(1): p. 325-330.
135. Akhyari, P., et al., *Mechanical stretch regimen enhances the formation of bioengineered autologous cardiac muscle grafts.* Circulation, 2002. **106**(12 Suppl 1): p. I137-42.
136. Niklason, L.E., et al., *Functional arteries grown in vitro.* Science, 1999. **284**(5413): p. 489-93.
137. Zhang, L. and C. Chan, *Isolation and Enrichment of Rat Mesenchymal Stem Cells (MSCs) and Separation of Single-colony Derived MSCs.* Journal of Visualized Experiments : JoVE, 2010(37): p. 1852.
138. Chang, J., et al., *Optimization of culture of mesenchymal stem cells: a comparison of conventional plate and microcarrier cultures.* Cell Proliferation, 2012. **45**(5): p. 430-437.
139. International, C., *Mesenchymal Stem Cell Adipogenesis Kit*, in *Cat.No SCR020*2005.
140. Solchaga, L.A., K.J. Penick, and J.F. Welter, *Chondrogenic differentiation of bone marrow-derived mesenchymal stem cells: tips and tricks.* Methods Mol Biol, 2011. **698**: p. 253-78.
141. Zaminy, A., et al., *Osteogenic differentiation of rat mesenchymal stem cells from adipose tissue in comparison with bone marrow mesenchymal stem cells: melatonin as a differentiation factor.* Iran Biomed J, 2008. **12**(3): p. 133-41.
142. Murphy, W.L. and D.J. Mooney, *Bioinspired Growth of Crystalline Carbonate Apatite on Biodegradable Polymer Substrata.* Journal of the American Chemical Society, 2002. **124**(9): p. 1910-1917.
143. Gomez, C.G., M. Rinaudo, and M.A. Villar, *Oxidation of sodium alginate and characterization of the oxidized derivatives.* Carbohydrate Polymers, 2007. **67**(3): p. 296-304.
144. Ueno, Y., et al., *Drug-incorporating calcium carbonate nanoparticles for a new delivery system.* Journal of Controlled Release, 2005. **103**(1): p. 93-98.
145. Abberton, K.M., et al., *Myogel, a novel, basement membrane-rich, extracellular matrix derived from skeletal muscle, is highly adipogenic in vivo and in vitro.* Cells Tissues Organs, 2008. **188**(4): p. 347-358.
146. Rago, R., J. Mitchen, and G. Wilding, *DNA fluorometric assay in 96-well tissue culture plates using Hoechst 33258 after cell lysis by freezing in distilled water.* Analytical Biochemistry, 1990. **191**(1): p. 31-34.
147. Terada, S., et al., *Preparation of silk protein sericin as mitogenic factor for better mammalian cell culture.* Journal of Bioscience and Bioengineering, 2005. **100**(6): p. 667-671.
148. Silva, R., B. Fabry, and A.R. Boccaccini, *Fibrous protein-based hydrogels for cell encapsulation.* Biomaterials, 2014(0).
149. Santin, M., et al., *In vitro evaluation of the inflammatory potential of the silk fibroin.* Journal of Biomedical Materials Research, 1999. **46**(3): p. 382-389.

150. Minoura, N., M. Tsukada, and M. Nagura, *Physico-chemical properties of silk fibroin membrane as a biomaterial.* Biomaterials, 1990. **11**(6): p. 430-434.
151. Greenwald, D., et al., *Mechanical Comparison of 10 Suture Materials before and after in Vivo Incubation.* Journal of Surgical Research, 1994. **56**(4): p. 372-377.
152. Lam, J., et al., *Generation of Osteochondral Tissue Constructs with Chondrogenically and Osteogenically Pre-differentiated Mesenchymal Stem Cells Encapsulated in Bilayered Hydrogels.* Acta Biomaterialia, 2013(0).
153. Minoura, N., et al., *Attachment and growth of cultured fibroblast cells on silk protein matrices.* Journal of Biomedical Materials Research, 1995. **29**(10): p. 1215-1221.
154. Inouye, K., et al., *Use of Bombyx mori silk fibroin as a substratum for cultivation of animal cells.* Journal of Biochemical and Biophysical Methods, 1998. **37**(3): p. 159-164.
155. Sofia, S., et al., *Functionalized silk-based biomaterials for bone formation.* Journal of Biomedical Materials Research, 2001. **54**(1): p. 139-148.
156. Marolt, D., et al., *Bone and cartilage tissue constructs grown using human bone marrow stromal cells, silk scaffolds and rotating bioreactors.* Biomaterials, 2006. **27**(36): p. 6138-6149.
157. Singh, N., et al., *Directing Chondrogenesis of Stem Cells with Specific Blends of Cellulose and Silk.* Biomacromolecules, 2013. **14**(5): p. 1287-1298.
158. Taddei, P., et al., *Silk Fibroin/Gelatin Blend Films Crosslinked with Enzymes for Biomedical Applications.* Macromolecular Bioscience, 2013. **13**(11): p. 1492-1510.
159. Yang, L., et al., *Gelatin modified ultrathin silk fibroin films for enhanced proliferation of cells.* Biomed Mater, 2015. **10**(2): p. 025003.
160. Orlova, A.A., et al., *Relationship between Gelatin Concentrations in Silk Fibroin-Based Composite Scaffolds and Adhesion and Proliferation of Mouse Embryo Fibroblasts.* Bulletin of Experimental Biology and Medicine, 2014. **158**(1): p. 88-91.
161. Moisenovich, M.M., et al., *Composite Scaffolds Containing Silk Fibroin, Gelatin, and Hydroxyapatite for Bone Tissue Regeneration and 3D Cell Culturing.* Acta Naturae, 2014. **6**(1): p. 96-101.
162. LeGeros, R.Z., *Properties of osteoconductive biomaterials: calcium phosphates.* Clin Orthop Relat Res, 2002(395): p. 81-98.
163. Lin, L., K.L. Chow, and Y. Leng, *Study of hydroxyapatite osteoinductivity with an osteogenic differentiation of mesenchymal stem cells.* J Biomed Mater Res A, 2009. **89**(2): p. 326-35.
164. Yang, M., et al., *Nucleation of Hydroxyapatite on Antheraea pernyi (A. pernyi) Silk Fibroin Film.* Bio-Medical Materials and Engineering, 2014. **24**(1): p. 731-740.
165. Kokubo, T. and H. Takadama, *How useful is SBF in predicting in vivo bone bioactivity?* Biomaterials, 2006. **27**(15): p. 2907-2915.
166. Choi, Y., et al., *Silk fibroin particles as templates for mineralization of calcium-deficient hydroxyapatite.* Journal of Biomedical Materials Research Part B: Applied Biomaterials, 2012. **100B**(8): p. 2029-2034.
167. Nemir, S. and J.L. West, *Synthetic Materials in the Study of Cell Response to Substrate Rigidity.* Annals of Biomedical Engineering, 2010. **38**(1): p. 2-20.
168. Discher, D.E., P. Janmey, and Y.-l. Wang, *Tissue Cells Feel and Respond to the Stiffness of Their Substrate.* Science, 2005. **310**(5751): p. 1139-1143.
169. Sharma, R.I. and J.G. Snedeker, *Biochemical and biomechanical gradients for directed bone marrow stromal cell differentiation toward tendon and bone.* Biomaterials, 2010. **31**(30): p. 7695-7704.
170. Kweon, H., et al., *Physical properties of silk fibroin/chitosan blend films.* Journal of Applied Polymer Science, 2001. **80**(7): p. 928-934.
171. Bigi, A., et al., *Mechanical and thermal properties of gelatin films at different degrees of glutaraldehyde crosslinking.* Biomaterials, 2001. **22**(8): p. 763-768.
172. Domke, J. and M. Radmacher, *Measuring the Elastic Properties of Thin Polymer Films with the Atomic Force Microscope.* Langmuir, 1998. **14**(12): p. 3320-3325.

173. Amaral, M., et al., *Densification route and mechanical properties of Si3N4–bioglass biocomposites.* Biomaterials, 2002. **23**(3): p. 857-862.
174. Bhushan, B., *Nanoscale Mechanical Properties*, in *Springer Handbook of Nanotechnology*, B. Bhushan, Editor. 2010, Springer Science & Business Media. p. 1131.
175. Vehoff, T., et al., *Mechanical Properties of Spider Dragline Silk: Humidity, Hysteresis, and Relaxation.* Biophysical Journal, 2007. **93**(12): p. 4425-4432.
176. Gil, E.S., et al., *Mechanical Improvements to Reinforced Porous Silk Scaffolds.* Journal of Biomedical Materials Research. Part a, 2011. **99**(1): p. 16-28.
177. Plaza, G.R., et al., *Effect of water on Bombyx mori regenerated silk fibers and its application in modifying their mechanical properties.* Journal of Applied Polymer Science, 2008. **109**(3): p. 1793-1801.
178. Yao, A., W. Huang, and H. Rubin, *Growth in high serum concentrations leads to rapid deadaptation of cells previously adapted to growth in an extremely low concentration of serum.* Proc Natl Acad Sci U S A, 1991. **88**(21): p. 9422-5.
179. Lotfy, A., et al., *Characterization of Mesenchymal Stem Cells Derived from Rat Bone Marrow and Adipose Tissue: A Comparative Study.* International Journal of Stem Cells, 2014. **7**(2): p. 135-142.
180. Gnecchi, M. and L.G. Melo, *Bone marrow-derived mesenchymal stem cells: isolation, expansion, characterization, viral transduction, and production of conditioned medium.* Methods Mol Biol, 2009. **482**: p. 281-94.
181. Yoshimura, H., et al., *Comparison of rat mesenchymal stem cells derived from bone marrow, synovium, periosteum, adipose tissue, and muscle.* Cell and Tissue Research, 2007. **327**(3): p. 449-462.
182. Nichol, J.W., et al., *Cell-laden microengineered gelatin methacrylate hydrogels.* Biomaterials, 2010. **31**(21): p. 5536-5544.
183. Kang, H.-W., Y. Tabata, and Y. Ikada, *Fabrication of porous gelatin scaffolds for tissue engineering.* Biomaterials, 1999. **20**(14): p. 1339-1344.
184. Pal, K., A.K. Banthia, and D.K. Majumdar, *Polymeric Hydrogels: Characterization and Biomedical Applications.* Designed Monomers and Polymers, 2009. **12**(3): p. 197-220.
185. Bini, E., D.P. Knight, and D.L. Kaplan, *Mapping Domain Structures in Silks from Insects and Spiders Related to Protein Assembly.* Journal of Molecular Biology, 2004. **335**(1): p. 27-40.
186. Christenson, R.H., *Biochemical Markers of Bone Metabolism: An Overview.* Clinical Biochemistry, 1997. **30**(8): p. 573-593.
187. Huang, Z., et al., *The sequential expression profiles of growth factors from osteoprogenitors to osteoblasts in vitro.* Tissue Eng, 2007. **13**(9): p. 2311-20.
188. Hauschka, P.V., et al., *Osteocalcin and matrix Gla protein: vitamin K-dependent proteins in bone*. Vol. 69. 1989. 990-1047.
189. Birmingham, E., et al., *Osteogenic differentiation of mesenchymal stem cells is regulated by osteocyte and osteoblast cells in a simplified bone niche.* Eur Cell Mater, 2012. **23**: p. 13-27.
190. Wongputtaraksa, T., et al., *Surface modification of Thai silk fibroin scaffolds with gelatin and chitooligosaccharide for enhanced osteogenic differentiation of bone marrow-derived mesenchymal stem cells.* Journal of Biomedical Materials Research Part B: Applied Biomaterials, 2012. **100B**(8): p. 2307-2315.
191. Vorrapakdee, R., et al., *Modification of human cancellous bone using Thai silk fibroin and gelatin for enhanced osteoconductive potential.* Journal of Materials Science: Materials in Medicine, 2013. **24**(3): p. 735-744.
192. Das, S., et al., *Bioprintable, cell-laden silk fibroin-gelatin hydrogel supporting multilineage differentiation of stem cells for fabrication of three-dimensional tissue constructs.* Acta Biomater, 2015. **11**: p. 233-46.
193. Meinel, L., et al., *Silk implants for the healing of critical size bone defects.* Bone, 2005. **37**(5): p. 688-698.

194. Augst, A., et al., *Effects of chondrogenic and osteogenic regulatory factors on composite constructs grown using human mesenchymal stem cells, silk scaffolds and bioreactors.* Journal of the Royal Society Interface, 2008. **5**(25): p. 929-939.
195. Rockwood, D.N., et al., *Ingrowth of human mesenchymal stem cells into porous silk particle reinforced silk composite scaffolds: An in vitro study.* Acta Biomaterialia, 2011. **7**(1): p. 144-151.
196. Tibbitt, M.W. and K.S. Anseth, *Hydrogels as extracellular matrix mimics for 3D cell culture.* Biotechnology and Bioengineering, 2009. **103**(4): p. 655-663.
197. Pampaloni, F., E.G. Reynaud, and E.H.K. Stelzer, *The third dimension bridges the gap between cell culture and live tissue.* Nat Rev Mol Cell Biol, 2007. **8**(10): p. 839-845.
198. Haycock, J., *3D Cell Culture: A Review of Current Approaches and Techniques*, in *3D Cell Culture*, J.W. Haycock, Editor. 2011, Humana Press. p. 1-15.
199. Justice, B.A., N.A. Badr, and R.A. Felder, *3D cell culture opens new dimensions in cell-based assays.* Drug Discovery Today, 2009. **14**(1–2): p. 102-107.
200. Storm, M.P., et al., *Three-dimensional culture systems for the expansion of pluripotent embryonic stem cells.* Biotechnology and Bioengineering, 2010. **107**(4): p. 683-695.
201. Lan, Y., et al., *Preparation and characterisation of vancomycin-impregnated gelatin microspheres/silk fibroin scaffold.* J Biomater Sci Polym Ed, 2014. **25**(1): p. 75-87.
202. Baimark, Y., et al., *Preparation of Porous Silk Fibroin Microparticles by a Water-in-Oil Emulsification-Diffusion Method.* Journal of Applied Polymer Science, 2010. **118**(2): p. 1127-1133.
203. Morimoto, Y., W.H. Tan, and S. Takeuchi, *Three-dimensional axisymmetric flow-focusing device using stereolithography.* Biomedical Microdevices, 2009. **11**(2): p. 369-377.
204. Terray, A. and S.J. Hart, *"Off-the-shelf" 3-D microfluidic nozzle.* Lab on a Chip, 2010. **10**(13): p. 1729-1731.
205. Dendukuri, D. and P.S. Doyle, *The Synthesis and Assembly of Polymeric Microparticles Using Microfluidics.* Advanced Materials, 2009. **21**(41): p. 4071-4086.
206. Wang, L., et al., *Preparation of Silk Fibroin Microspheres.* Advanced Materials Research, 2011. **236-238**: p. 1902-1905.
207. Kim, U.-J., et al., *Three-dimensional aqueous-derived biomaterial scaffolds from silk fibroin.* Biomaterials, 2005. **26**(15): p. 2775-2785.
208. Fafián-Labora, J., et al., *Influence of age on rat bone-marrow mesenchymal stem cells potential.* Scientific Reports, 2015. **5**: p. 16765.
209. Adams, D.J. and P.D. Topham, *Peptide conjugate hydrogelators.* Soft Matter, 2010. **6**(16): p. 3707-3721.
210. Cabané, P., et al., *Allotransplant of Microencapsulated Parathyroid Tissue in Severe Postsurgical Hypoparathyroidism: A Case Report.* Transplantation Proceedings, 2009. **41**(9): p. 3879-3883.
211. Veriter, S., et al., *In vivo selection of biocompatible alginates for islet encapsulation and subcutaneous transplantation.* Tissue Eng Part A, 2010. **16**(5): p. 1503-13.
212. Balakrishnan, B., et al., *Evaluation of an in situ forming hydrogel wound dressing based on oxidized alginate and gelatin.* Biomaterials, 2005. **26**(32): p. 6335-6342.
213. Kim, W.S., et al., *Adipose Tissue Engineering Using Injectable, Oxidized Alginate Hydrogels.* Tissue Engineering Part A, 2012. **18**(7-8): p. 737-743.
214. Wolf, M.T., et al., *A hydrogel derived from decellularized dermal extracellular matrix.* Biomaterials, 2012(0).
215. Bouhadir, K.H., et al., *Degradation of Partially Oxidized Alginate and Its Potential Application for Tissue Engineering.* Biotechnology Progress, 2001. **17**(5): p. 945-950.
216. McHugh, D.J., *Production and Utilization of Products from Commercial Seaweeds*, ed. D.J. McHugh. Vol. 288. 1987: FAO Fish. Tec. Pap.

217. Wang, C., et al., *Alginate–calcium carbonate porous microparticle hybrid hydrogels with versatile drug loading capabilities and variable mechanical strengths.* Carbohydrate Polymers, 2008. **71**(3): p. 476-480.
218. Khanna, O., et al., *Generation of Alginate Microspheres for Biomedical Applications.* Journal of Visualized Experiments : JoVE, 2012(66): p. 3388.
219. Vecchiatini, R., et al., *Effect of dynamic three-dimensional culture on osteogenic potential of human periodontal ligament-derived mesenchymal stem cells entrapped in alginate microbeads.* J Periodontal Res, 2014.
220. Chen, B., et al., *A Novel Alternative to Cryopreservation for the Short-Term Storage of Stem Cells for Use in Cell Therapy Using Alginate Encapsulation.* Tissue Engineering Part C: Methods, 2012. **19**(7): p. 568-576.
221. Brown, B.N., et al., *Comparison of three methods for the derivation of a biologic scaffold composed of adipose tissue extracellular matrix.* Tissue engineering. Part C, Methods, 2011. **17**(4): p. 411-421.
222. Akhyari, P., et al., *The Quest for an Optimized Protocol for Whole-Heart Decellularization: A Comparison of Three Popular and a Novel Decellularization Technique and Their Diverse Effects on Crucial Extracellular Matrix Qualities.* Tissue Engineering Part C-Methods, 2011. **17**(9): p. 915-926.
223. Medberry, C.J., et al., *Hydrogels derived from central nervous system extracellular matrix.* Biomaterials, 2013. **34**(4): p. 1033-1040.
224. Wolf, M.T., et al., *Biologic scaffold composed of skeletal muscle extracellular matrix.* Biomaterials, 2012. **33**(10): p. 2916-25.
225. Bhuyan, A.K., *On the mechanism of SDS-induced protein denaturation.* Biopolymers, 2010. **93**(2): p. 186-199.
226. Hu, Y., et al., *Modification of collagen with a natural derived cross-linker, alginate dialdehyde.* Carbohydrate Polymers, 2014. **102**(0): p. 324-332.
227. Zimmermann, U., et al., *Hydrogel-based non-autologous cell and tissue therapy.* Biotechniques, 2000. **29**(3): p. 564-72, 574, 576 passim.
228. Bai, X.P., et al., *Fabrication of engineered heart tissue grafts from alginate/collagen barium composite microbeads.* Biomed Mater, 2011. **6**(4): p. 045002.
229. Sang, L., et al., *Fabrication and evaluation of biomimetic scaffolds by using collagen–alginate fibrillar gels for potential tissue engineering applications.* Materials Science and Engineering: C, 2011. **31**(2): p. 262-271.
230. Lawson, M.A., et al., *Adhesion and growth of bone marrow stromal cells on modified alginate hydrogels.* Tissue Eng, 2004. **10**(9-10): p. 1480-91.
231. Perez, R.A., et al., *Utilizing core-shell fibrous collagen-alginate hydrogel cell delivery system for bone tissue engineering.* Tissue Eng Part A, 2014. **20**(1-2): p. 103-14.
232. Lee, H.-j., S.-H. Ahn, and G.H. Kim, *Three-Dimensional Collagen/Alginate Hybrid Scaffolds Functionalized with a Drug Delivery System (DDS) for Bone Tissue Regeneration.* Chemistry of Materials, 2012. **24**(5): p. 881-891.
233. Balakrishnan, B., et al., *Self-crosslinked oxidized alginate/gelatin hydrogel as injectable, adhesive biomimetic scaffolds for cartilage regeneration.* Acta Biomaterialia, 2014. **10**(8): p. 3650-3663.
234. Zheng, L., et al., *Evaluation of novel in situ synthesized nano-hydroxyapatite/collagen/alginate hydrogels for osteochondral tissue engineering.* Biomed Mater, 2014. **9**(6): p. 065004.
235. Usuludin, S.B., X. Cao, and M. Lim, *Co-culture of stromal and erythroleukemia cells in a perfused hollow fiber bioreactor system as an in vitro bone marrow model for myeloid leukemia.* Biotechnol Bioeng, 2012. **109**(5): p. 1248-58.
236. Du, Y.A., et al., *Sequential Assembly of Cell-Laden Hydrogel Constructs to Engineer Vascular-Like Microchannels.* Biotechnology and Bioengineering, 2011. **108**(7): p. 1693-1703.
237. McGuigan, A.P. and M.V. Sefton, *Vascularized organoid engineered by modular assembly enables blood perfusion.* Proceedings of the National Academy of Sciences of the United States of America, 2006. **103**(31): p. 11461-11466.

238. Blakely, A.M., et al., *Bio-Pick, Place, and Perfuse: A New Instrument for 3D Tissue Engineering.* Tissue Engineering Part C: Methods, 2014.
239. Miller, J.S., et al., *Rapid casting of patterned vascular networks for perfusable engineered three-dimensional tissues.* Nat Mater, 2012. **11**(9): p. 768-774.
240. Lee, V., et al., *Generation of Multi-scale Vascular Network System Within 3D Hydrogel Using 3D Bio-printing Technology.* Cellular and Molecular Bioengineering, 2014. **7**(3): p. 460-472.
241. Bettahalli, N.M.S., et al., *Development of poly(l-lactic acid) hollow fiber membranes for artificial vasculature in tissue engineering scaffolds.* Journal of Membrane Science, 2011. **371**(1-2): p. 117-126.
242. Loffredo, F. and R.T. Lee, *Therapeutic Vasculogenesis: It Takes Two.* Circulation Research, 2008. **103**(2): p. 128-130.
243. Zheng, X., et al., *Proteomic Analysis for the Assessment of Different Lots of Fetal Bovine Serum as a Raw Material for Cell Culture. Part IV. Application of Proteomics to the Manufacture of Biological Drugs.* Biotechnology Progress, 2006. **22**(5): p. 1294-1300.
244. Chan, R. and V. Chen, *Characterization of protein fouling on membranes: opportunities and challenges.* Journal of Membrane Science, 2004. **242**(1–2): p. 169-188.
245. Cho, C.H., et al., *Oxygen uptake rates and liver-specific functions of hepatocyte and 3T3 fibroblast co-cultures.* Biotechnology and Bioengineering, 2007. **97**(1): p. 188-199.
246. Rafiq, Q., et al., *Culture of human mesenchymal stem cells on microcarriers in a 5 l stirred-tank bioreactor.* Biotechnology Letters, 2013. **35**(8): p. 1233-1245.
247. De Napoli, I.E., et al., *Mesenchymal stem cell culture in convection-enhanced hollow fibre membrane bioreactors for bone tissue engineering.* Journal of Membrane Science, 2011. **379**(1–2): p. 341-352.
248. Lennon, D.P., J.M. Edmison, and A.I. Caplan, *Cultivation of rat marrow-derived mesenchymal stem cells in reduced oxygen tension: Effects on in vitro and in vivo osteochondrogenesis.* Journal of Cellular Physiology, 2001. **187**(3): p. 345-355.
249. Zhang, Q.B., et al., *Effects of hypoxia on proliferation and osteogenic differentiation of periodontal ligament stem cells: an in vitro and in vivo study.* Genet Mol Res, 2014. **13**(4): p. 10204-14.
250. Haque, N., et al., *Hypoxic Culture Conditions as a Solution for Mesenchymal Stem Cell Based Regenerative Therapy.* The Scientific World Journal, 2013. **2013**: p. 12.
251. Hsu, S.-H., C.-T. Chen, and Y.-H. Wei, *Inhibitory Effects of Hypoxia on Metabolic Switch and Osteogenic Differentiation of Human Mesenchymal Stem Cells.* STEM CELLS, 2013. **31**(12): p. 2779-2788.
252. Potier, E., et al., *Hypoxia affects mesenchymal stromal cell osteogenic differentiation and angiogenic factor expression.* Bone, 2007. **40**(4): p. 1078-1087.
253. El Haj, A.J., et al., *Controlling cell biomechanics in orthopaedic tissue engineering and repair.* Pathologie Biologie, 2005. **53**(10): p. 581-589.
254. Bolgen, N., et al., *Three-dimensional ingrowth of bone cells within biodegradable cryogel scaffolds in bioreactors at different regimes.* Tissue Eng Part A, 2008. **14**(10): p. 1743-50.
255. Wexler, S.A., et al., *Adult bone marrow is a rich source of human mesenchymal 'stem' cells but umbilical cord and mobilized adult blood are not.* British Journal of Haematology, 2003. **121**(2): p. 368-374.